Insights into DNA intercalation using combined optical tweezers and fluorescence microscopy

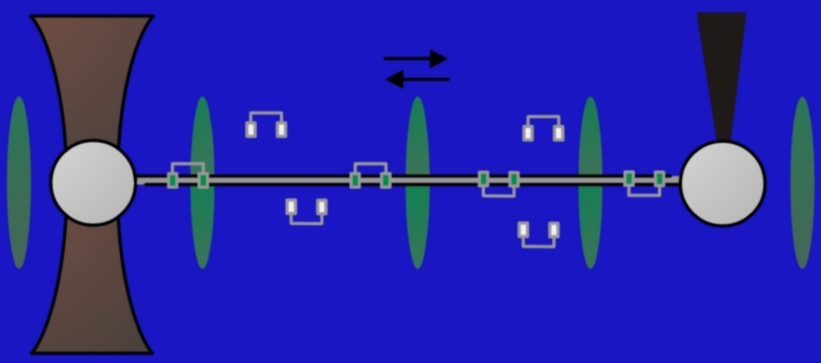

Chandrashekhar Uttamrao Murade

Insights into DNA intercalation using combined optical tweezers and fluorescence microscopy

Chandrashekhar Uttamrao Murade

Thesis committee members

Prof. Dr. G. van der Steenhoven	University of Twente (chairman)
Prof. Dr. V. Subramaniam	University of Twente (thesis advisor)
Dr. ir. M. L. Bennink	University of Twente (assistant advisor)
Dr. C. Otto	University of Twente (assistant advisor)
Prof. Dr. D. Anselmetti	University Bielefeld
Dr. ir. E. J. G. Peterman	VU University Amsterdam
Prof. Dr. F. G. Mugele	University of Twente
Prof. Dr. J. L. Herek	University of Twente

The research described in this thesis was carried out at the Biophysical Engineering Group and MESA+ Institute for Nanotechnology and Faculty of Science and Technology, University of Twente, P.O. Box 217, 7500 AE Enschede, The Netherlands.

The research has been financially supported by 'Stichting voor Fundamenteel Onderzoek der Materie (FOM)', which is financially supported by the 'Nederlandse Organisatie voor Wetenschappelijk Onderzoek (NOW)'.

Printed by: Gildeprint, Enschede

ISBN: 978-90-365-3046-0
DOI: 10.3990/1.9789036530460

INSIGHTS INTO DNA INTERCALATION USING COMBINED OPTICAL TWEEZERS AND FLUORESCENCE MICROSCOPY

DISSERTATION

to obtain
the degree of doctor at the University of Twente,
on the authority of the rector magnificus,
prof. dr. H. Brinksma,
on account of the decision of the graduation committee
to be publicly defended
on Friday, June 4th, 2010, at 13.15 hrs

by
Chandrashekhar Uttamrao Murade
born on August 29th, 1980
in Hiwara Murade, India

This dissertation has been approved by:
Prof. Dr. V. Subramaniam (Promotor)
Dr. ir. M. L. Bennink (Assistant Promotor)
Dr. C. Otto (Assistant Promotor)

To my Mother, Father, Meenakshi and Teachers

Summary

The functioning of a single cell, and indirectly that of complete organism, is due to a large number of interlocking biological processes. These processes essentially comprise of a large number of highly specific interactions between different individual biomolecules, such as nucleic acids, proteins, lipids and other small organic molecules. One of the most important interactions within the cell is the interaction of protein molecules with deoxyribonucleic acid (DNA). DNA contains the genetic information of an organism and by duplicating itself very accurately before cell division, it is responsible for the transfer of this information from one cell to the next. Another central role of the DNA in the living cell is its involvement in the process of transcription and translation, which are the essential steps towards the synthesis of proteins.

Many technologies have been developed that are able to measure biomolecular interactions, but they are limited to measurements on large number of interactions (ensemble measurements). During the past 20 years we have witnessed the development of different single molecule techniques such as magnetic tweezers, atomic force microscopy, fluorescence microscopy and optical tweezers, that allow the measurement of one molecule at a time, or the interactions between a small number of molecules. This '*single molecule*' approach provides detailed information about the interactions that cannot be retrieved using bulk techniques, because the effects would be averaged and therefore not observable.

In this thesis we set out to develop an instrument which is capable of probing the change in the mechanical properties of a single double-stranded DNA molecule as it is interacting with protein molecules, having the capability to detect the number and location of the protein molecules on the DNA simultaneously. This allows us to directly correlate the effect of protein binding on the mechanical properties of the DNA on a single molecule level.

Starting from an existing single-beam optical tweezers set-up, we have successfully integrated line scanning fluorescence microscopy. Single dsDNA molecules have been stretched and relaxed resulting in force extension curves, clearly demonstrating the ability of this instrument to perform the single molecule force spectroscopy. Furthermore we have tested the fluorescence microscopy modality, by imaging a single quantum dot and a single fluorescently labeled protein molecule attached to the dsDNA. Simultaneous operation of both modalities was demonstrated by stretching a single dsDNA molecule in the presence of the dsDNA intercalating dye YO-1.

In a first set of experiments we studied the interaction of YO-1 and YOYO-1 with dsDNA at various concentrations of YO-1 and YOYO-1. These dye molecules are binding

to dsDNA by intercalation, and strongly emit fluorescence when bound. The recorded force extension curves clearly reveal that these molecules affect the mechanical properties of the dsDNA depending on the concentration of dye used. Using the simultaneously recorded fluorescence intensity, it was possible to correlate this with the number of dye molecules bound to the dsDNA. The data clearly indicates that, the interaction of YO-1 with dsDNA is different from that of YOYO-1. The force extension curves clearly showed that the dsDNA-YO-1 complex is always in the equilibrium during the stretching and relaxation of the dsDNA molecule in contrast to the dsDNA-YOYO-1. A model describing the kinetics is presented to explain the observed differences, in which it is assumed that the linker in the YOYO-1 (bis intercalating) molecules interact strongly with the backbone of the dsDNA, which gave rise to the relative slow interaction of the YOYO-1 molecules with the dsDNA. This model is thought to be more generally applicable for bis-intercalating molecules.

Simultaneous force spectroscopy and fluorescence microscopy of the dsDNA-YO-1 and YOYO-1 complex revealed that the fluorescence intensity of the complex increases as force on the complex increases. In other words, the binding constant of YO-1 and YOYO-1 to the dsDNA is force dependent. Fitting the data with an appropriate model that takes into account the binding constant and a certain binding site size of the dye on the dsDNA, the binding constant was found to increase monotonically for YOYO-1 and YO-1 as function of force. The binding site size decreased as a function of force for YO-1. For YOYO-1 this binding site did not change significantly. We explain this discrepancy by assuming that YOYO-1 molecules bind to the dsDNA following a different pathway than YO-1 molecules do.

The structure of the dsDNA in the overstretching region has been a subject of intense debate for the past 15 years. One model assumes that the structure of the dsDNA goes through a phase change from having a B-DNA helical form to a stretched conformation, known as S-DNA. The second model explains the overstretching of dsDNA at 65 pN as a force-induced melting process of the dsDNA. We used YOYO-1 molecules as probe molecules to investigate the structure of the dsDNA in the overstretching region, because YOYO-1 molecules emit fluorescence only when bound to the dsDNA. Using the optical tweezers setup with integrated line scanning polarization-sensitive fluorescence microscopy we were able to measure the fluorescence intensity and orientation of the dye (base pair) molecules as function of force. The results show that during the overstretching of dsDNA the angle of the basepairs within the DNA structure is not affected significantly. Furthermore a reduction of fluorescence intensity was observed as the molecule was stretched, which was explained with the conversion of DNA from double-stranded to single-stranded. Both observations suggest that the dsDNA is indeed melting under the influence of the applied force in the overstretching region.

In another study we characterized the interaction of Lys-Trp-Lys molecules with the dsDNA to probe the role of aromatic amino acids molecules in the dsDNA-protein interaction. The binding constant of Lys-Trp-Lys molecules with the dsDNA in physiological conditions was found to be very low. When DNA-denaturing buffer conditions were used, the binding constant of Lys-Trp-Lys to DNA increased. At these denaturing conditions the binding constant of Lys-Trp-Lys molecules was found to increase as function of applied force. This suggests that, Lys-Trp-Lys molecules have greater affinity towards the denatured dsDNA than intact dsDNA. Furthermore these experiments suggested that, the aromatic amino acids guide (help) the protein molecules to detect denatured sites on the dsDNA.

The final chapter of this thesis is a summary of the main conclusions of this work, with some suggestions for improvements on the constructed instrument. The combined optical tweezers and line scanning fluorescence microscopy instrument along with the suggested improvements will in the future allow us to address new challenging research questions in the field of single molecule biophysics.

Samenvatting

Het functioneren van de levende cel en daarmee indirect dat van het organisme waar het deel van uitmaakt, is het gevolg van een groot aantal biologische processen die heel precies in elkaar grijpen. Deze processen bestaan uit zeer specifieke interacties tussen een groot aantal individuele biomoleculen zoals nucleïnezuren (DNA, RNA), eiwitten, vetzuren en andere kleine organische moleculen. Een van de belangrijkste interacties in de cel is die tussen eiwitmoleculen en DNA. Het DNA bevat de genetische informatie en door zichzelf nauwkeurig te dupliceren voor de celdeling, is het verantwoordelijk voor het overdragen van deze informatie van de ene cel naar de volgende. Een andere belangrijke functie van het DNA in de levende cel is de rol in transcriptie en translatie, de twee processen die uiteindelijk nodig zijn voor het produceren van eiwitten.

Er zijn technieken en technologieën ontwikkeld die in staat zijn om interacties tussen biomoleculen nauwkeurig te meten, maar deze zijn beperkt tot metingen aan zeer grote aantallen van moleculen en interacties ('ensemble' metingen). Gedurende de laatste 20 jaar heeft de ontwikkeling van nieuwe 'single-molecule' technologieën een hoge vlucht genomen. Voorbeelden hiervan zijn de ontwikkeling van magnetic tweezers, atomic force microscopy (AFM), fluorescentie microscopie en de optische trap, die allen in staat zijn om aan een molecuul tegelijk te meten, of aan een enkele interactie tussen bijvoorbeeld twee biomoleculen. Deze manier van meten laat toe om zeer gedetailleerde informatie te verkrijgen, die niet verkregen kan worden met behulp van 'ensemble' technieken, omdat bij deze metingen effecten uitgemiddeld worden.

In dit proefschrift is de doelstelling om een instrument te ontwikkelen dat in staat is om een verandering in de mechanische eigenschappen van een enkel DNA molecuul te meten, terwijl eiwitten eraan binden. Het instrument moet in staat zijn om zowel het aantal eiwitten als ook de positie waar het op het DNA bindt, nauwkeurig te bepalen. Op deze wijze is het mogelijk om het effect van eiwitbinding op de mechanische eigenschappen van DNA op enkel molecuul niveau te meten.

Een bestaande optical trap opstelling is op succesvolle wijze geïntegreerd met een fluorescentie microscoop waarbij het sample met een scannend lijnprofiel wordt belicht. Een enkel DNA molecuul is met aan beide uiteinden vastgezet aan een bolletje. Door nu met de optische trap de ene bol van de andere te verwijderen, is het mogelijk om een individueel DNA molecuul uit te rekken en te meten hoeveel kracht hiervoor nodig is. De fluorescentie is getest met het meten van een quantum dot en een enkel fluorescent gelabeld eiwit dat gebonden zat aan het DNA. De combinatie van krachtmetingen en het afbeelden van de fluorescentie is gedemonstreerd met een het strekken van een DNA molecuul in de aanwezigheid van de YO-1.

In een eerste set experimenten is gekeken naar de interactie van de fluorescente moleculen YO-1 en YOYO-1 en DNA bij verschillende concentraties. Deze fluorescente moleculen binden aan DNA door tussen de baseparen te gaan zitten, en hebben een sterk fluorescentie signaal wanneer ze gebonden zijn. De gemeten kracht-extensie karakteristieken laten duidelijk zien dat het binden van deze moleculen aan het DNA een effect heeft op de mechanische eigenschappen van het DNA afhankelijk van de concentratie die gebruikt is. Door tegelijkertijd de hoeveelheid fluorescentie te meten, is het nu mogelijk om dit te correleren met het aantal gebonden fluorescente moleculen. De data laat duidelijk zien, dat de interactie van YO-1 met DNA anders is dan die van YOYO-1. Uit de data volgt dat het complex van DNA en YO-1 continu in evenwicht is gedurende het experiment, terwijl dit voor DNA en YOYO-1 niet het geval is. Een model dat de kinetiek beschrijft, wordt gepresenteerd om de verschillen te verklaren. Hierin wordt aangenomen dat de linker in YOYO-1 een sterke interactie aangaat met het DNA. Dit resulteert dan in een relatieve langzame interactie-kinetiek, die het experiment laat zien.

De metingen aan het DNA molecuul in de aanwezigheid van de fluorescente moleculen YO-1 en YOYO-1 laten zien dat de hoeveelheid fluorescentie van het gevormde complex toeneemt als de kracht op het complex toeneemt. Met andere woorden, de bindingsconstante van YO-1 en YOYO-1 is krachtsafhankelijk. Door de data bij verschillende krachten te fitten met een model dat een zekere bindingsconstante en een zekere grootte van de bindingsplaats aanneemt, is gevonden dat de bindingsconstante monotoon toeneemt voor beide moleculen als functie van de kracht. The grootte van de bindingsplaats voor YO-1 neemt af, terwijl deze voor YOYO-1 nauwelijks verandert. Hieruit leiden we af dat de beide moleculen volgens een ander mechanisme binden aan het DNA.

Als DNA wordt uitgerekt tot een kracht van circa 65 pN wordt het DNA met een zeer geringe krachtstoename ongeveer 70% langer, als gevolg van een verandering in de structuur van het molecuul. Eén model beschrijft deze overgang als een waarin de structuur van het B-DNA overgaat in een structuur waarin de baseparen een kleinere hoek maken met de as van het molecuul. Deze structuur wordt ook wel S-DNA genoemd. Een ander model beschrijft de overgang als het gevolg van de conversie van dubbelstrengs DNA in enkelstrengs DNA (‘melting’) als gevolg van de aangelegde kracht. In deze experimenten hebben we YOYO-1 moleculen gebruikt als markers, die lokaal de structuur van het DNA weergeven, gedurende deze overgang bij 65 pN. Door gebruik te maken van de optische tweezers om het molecuul te strekken en tegelijkertijd de fluorescentie polarizatie-gevoelig te meten, was het mogelijk om lokaal de orientatie van de baseparen in de structuur te meten. De meting gaf aan dat de hoek die de baseparen maken met de helische as niet significant veranderde gedurende de conversie van de structuur. Daarnaast nam de totale

hoeveelheid fluorescentie af naarmate het DNA molecuul verder gerekt werd. Dit kan verklaard worden met een conversie van het DNA van een dubbelstrengs naar een enkelstrengs structuur. Beide observaties wijzen uit dat het DNA inderdaad 'melt' als gevolg van de aangelegde kracht op het molecuul.

In een andere studie hebben we de interactie tussen Lys-Trp-Lys en DNA gekarakteriseerd om meer inzicht te verkrijgen in de rol van aromatische aminozuren in DNA-eiwit interacties. Onder fysiologische condities bleek de bindingsconstante zeer laag te zijn, en was nauwelijks enige binding waarneembaar. Pas onder DNA-denaturerende condities (laag zoutgehalte) begon het Lys-Trp-Lys te binden. Onder deze condities zijn de bindingskarakteristieken bepaald als functie van de concentratie Lys-Trp-Lys als functie van de kracht op het DNA molecuul. Ook hier bleek dat de bindingsconstante toenam met de kracht op het molecuul. Dit suggereert dat Lys-Trp-Lys een hogere affiniteit vertoont voor gedenatureerd DNA en dat de aromatische aminozuren een rol spelen in de binding van eiwitten aan het DNA.

Het laatste hoofdstuk in dit proefschrift is een samenvatting van de belangrijkste conclusies van dit werk, aangevuld met wat suggesties voor technische verbeteringen wat betreft het instrument. Met dit instrument zal het in de nabije toekomst mogelijk worden om nieuwe en uitdagende vraagstukken op te lossen in het veld van de biofysica.

Contents

Chapter 1

Introduction

Abstract

Deoxyribonucleic acid (DNA) contains the genetic information used in the development and functioning of all known organisms. Quantitatively measuring the interaction of protein molecules with DNA is important to understand the various processes within a single cell, where force generating molecular motors are of vital importance. In this chapter we describe the motivation to build a new instrument, a combined optical tweezers and line-scanning fluorescence microscope, to measure these DNA-protein interactions. This instrument allows mechanical stretching of an individual DNA molecule, providing information on the mechanical properties, and at the same time is able to record fluorescent images of the labeled DNA or proteins bound to it, allowing the accurate determination of the concentration of proteins bound or their positions on the DNA molecule.

1.1
Introduction

The functioning of a single cell, and indirectly that of a complete organism, is due to a large number of interlocking biological processes. These processes are essentially a discrete number of highly specific interactions between different biomolecules, such as nucleic acids, proteins, lipids and other small organic molecules. Many conventional technologies have been developed to measure these biomolecular interactions, but are limited to ensemble measurements of large numbers of interactions. Single-molecule technologies however are developed to measure one molecule at a time, or the interactions between a small number of molecules. This approach provides detailed information on the interactions that cannot be retrieved using bulk techniques, because the effects would be averaged and therefore not observable.

1.2
DNA protein interactions

One of the most important interactions within the living cell is the interaction of protein molecules with deoxyribonucleic acid (DNA). DNA is a biomolecule that contains the genetic information of the organism and by duplicating itself very accurately before cell division, is responsible for the transfer of this information from one cell to the next. Next to duplication, a central role of DNA is its involvement in the process of transcription and translation, which are the steps towards the synthesis of proteins (1-3).

These cellular processes are fundamentally a highly organized interplay of the DNA molecule and a number of protein molecules. For example in the case of transcription a specific sequence of the DNA (i.e. gene) is being copied into a messenger RNA (another nucleic acid) by the action of the protein RNA polymerase in combination with a number of other proteins (4). Another example of DNA-protein interactions is in the formation of chromatin. The length of the DNA within a single human cell is approximately 2 meters, and the typical dimension of the cell nucleus (where the DNA is located) is one micrometer (10^{-6} meter). To physically fit the DNA into the nuclear compartment, the 2 meter long DNA is compacted by the action of histone proteins (5-7). These protein molecules form an octamer around which the DNA wraps itself 1.7 times (146 basepairs). These structures are known as nucleosomes (size is 11 nm), which is the first step of DNA compaction (8-9). From its appearance in the electron microscope, this structure is known as the beads-on-a-string structure. In a next level of compaction these nucleosomes start to stack and form the so-called 30 nm fiber (10). After this level the 30-nm fiber is organized in loops, eventually leading to the observed compaction. One of the main outstanding questions in biophysics nowadays is how proteins involved in, for example, transcription, replication

and repair gain access to the DNA while it is tightly bound to the histone proteins. In recent research it becomes more and more evident that the proteins involved in forming the structure of chromatin are not only responsible for the enormous compaction, but that they also play an active role and are integral part in the processes of transcription and replication (11).

Interactions of protein molecules with DNA can be categorized into non-specific and specific ones (12). In the case of non-specific interactions, protein molecules are attracted to the DNA due to Coulombic interaction. DNA is a negatively charged polymer to which a positively charged protein can bind in a non-specific way. In the case of specific interactions, protein molecules bind to very specific sites on the DNA that allow a protein to bind via multiple interactions (hydrogen bonds, electrostatic interactions, hydrophobic interactions). The arrangement of these interactions in space is exactly matching with that of the protein making it specific, i.e. only that protein will bind at that position (13-14). For example single strand binding proteins will selectively bind to single-stranded DNA and not to the double-stranded DNA.

1.3
Single molecule techniques

DNA-protein interactions have been studied by bulk techniques such as absorption and fluorescence spectroscopy, chromatography and NMR (15). However these techniques extract parameters from a large population of molecules, and are therefore insensitive for heterogeneities and only provide averaged values. In the last twenty years there has been a tremendous development in single-molecule manipulation techniques such as magnetic tweezers, atomic force microscopy and optical tweezers (16). These techniques are nowadays routinely used to study various biological processes at the single molecule level.

Optical tweezers is an optical technique that can be used to exert piconewton forces on individual polymer molecules, such as DNA. Having this molecule attached between two micron-sized beads, one which is immobilized on a glass micropipette and the second one held in an force-measuring optical tweezers, enables the stretching and simultaneously recording of the force that is needed to do so (17). Many studies have been reported in which the mechanical properties of DNA are studied while other molecules are interacting with the DNA (18-22). A major drawback in all these studies is that while the effect of the interaction on the DNA can be measured, it is not possible to directly observe the exact spatial location of the protein or molecule as it is bound on the DNA.

Fluorescence microscopy is a widely spread technique used extensively for imaging in bulk as well as for single molecule detection and localization. Integration of these two techniques potentially enables one to determine the mechanical properties of DNA and at the same time visualize the distribution of molecules that are bound to the DNA.

1.4
Combining optical tweezers and fluorescence microscopy

The combination of optical tweezers and fluorescence microscopy has been used in various disciplines of science (23). In most cases, one of these techniques was used as a immobilization or visualization tool and complementary technique for quantitative data collection. An example of this is the trapping of an individual cell within a flowcell while recording the fluorescence response of the cell as the buffer around it is changed (24). In this section we would like to limit ourselves to single-molecule studies performed by combined optical tweezers and fluorescence microscopy.

The first single-molecule experiment using a combined optical tweezers and fluorescence microscope set-up was performed in 1994 by Thomas Perkins and Steven Chu (25-26) where single YOYO-1 stained dsDNA molecules were attached to optically trapped beads, which were visualized with fluorescence microscopy. They observed tube-like motion of the polymer (dsDNA) in a dense solution of unstained dsDNA, and also observed the relaxation of the dsDNA as a function of dsDNA extension. In this study optical tweezers were utilized as a tool to hold the DNA and fluorescence microscopy was used for the quantitative analysis. On the other hand Nishizaka *et al*. (27) used optical tweezers for quantitative analysis to study unbinding of a single motor molecule. Ishijima *et al.* (28) used both optical tweezers and fluorescence microscopy quantitatively to study the interaction of single myosin molecules with actin molecules. Hohng *et al.* studied the two dimensional reaction landscape of the Holliday junction (29), while van Mameren *et al.* studied the elastic heterogeneity along the single DNA molecule arising due to heterogeneous distribution of the Rad51 molecules (30).

We highlight two specific studies that utilized combined optical tweezers and fluorescence microscopy. The first study, by Bennink *et al.* (17), used optical tweezers and fluorescence polarization microscopy to determine the orientation of the transition dipole moment of YOYO-1 with respective to the helix axis of the dsDNA. Fig. 1 presents the 4 images obtained at various polarizer and analyzer settings. The determined dipole orientation was 69º±3º, which was in good agreement with values reported for other intercalating molecules such as TOTO-1, measured by other techniques. This is the first

study which shed some light on the orientation of molecules as they are bound to the dsDNA measured with optical tweezers and polarization fluorescence microscopy.

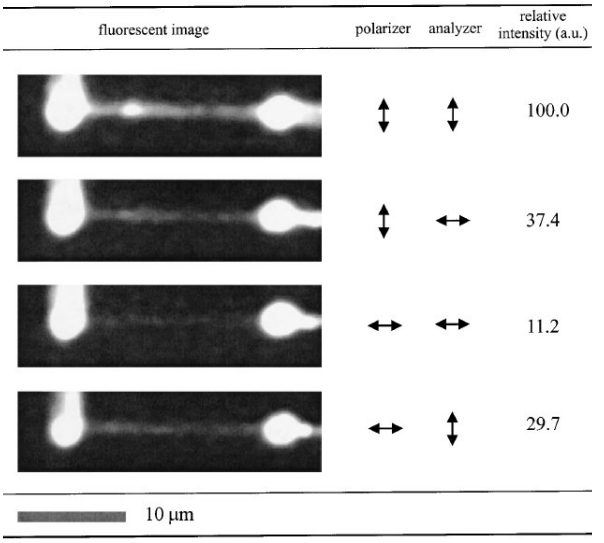

Fig. 1
Fluorescence images of a dsDNA-YOYO-1 complex using different settings for the polarizer and analyzer plates. For each setting of polarizer and analyzer the fluorescence intensity of the complex is indicated in the last column. (Adapted from Bennink *et al*. with kind permission from John Wiley and Sons.)

The second highlight is the development of coincident optical trapping and single molecule fluorescence by Lang *et al*. (31-32). In all the studies described in the previous sections of this chapter, the optical tweezers and fluorescence microscopy are physically separated from each other, that is, fluorescence signals are not acquired from the region covered by the optical tweezers. The instrument developed by Lang *et al.* is a unique instrument where the optical trapping and fluorescence imaging were coincident, that is, the fluorescence signals were acquired from the region which was shared by the optical trapping. Fig. 2 presents the schematics of the coincident optical trapping and fluorescence microscopy. Three different lasers were used in this instrument, including a trapping laser, a detection laser to detect the displacement of the bead within the trap to determine the force, and an excitation laser to excite the fluorophores. Total internal reflection fluorescence microscopy (TIRF) was used to excite the fluorophores. Using this unique instrument Lang *et al.* studied the unzipping of dsDNA. Tetramethylrhodamine (red dots in Fig. 2A) dye was attached to the two strands of the dsDNA. As long as they are close to each other the fluorescence of these dyes is quenched. As soon as the two strands are

separated at force of 9 pN (red curve in Fig. 2 B) the dye is unquenched upon unzipping (blue curve in Fig. 2 B).

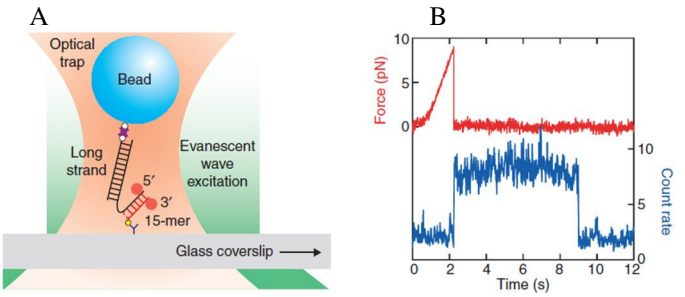

Fig. 2

A combined optical trapping and fluorescence experiment in order to study DNA unzipping. (A) A simplified cartoon of the experimental geometry. A bead was tethered by digoxygenin based linkage (blue and yellow) to the coverglass surface through a DNA molecule, consisting of a long segment (black) joined to a shorter 15 base pair strand that forms a duplex region (red). The bead (blue) was captured by the optical trap and force was applied to unzip the short duplex. Tetramethylrhodamine (TAMRA) dyes attached at the ends of the DNA strands provide a fluorescence signal (red dot). (B) Simultaneous recording of force (red trace) and fluorescence, measured as the photon count rate (blue trace). Rupture occurred as t = 2 sec at an unzipping force of 9 pN. The dye unquenched at the point of rupture, and later bleached at t= 9 sec. (Adapted from Lang *et al.*)

1.5
Outline of the thesis

This thesis describes the design, construction and use of a combined optical tweezers and line-scanning fluorescence microscope for the study of the interaction between DNA and proteins or intercalating molecules.

Chapter 2 describes the basic principles of optical tweezers and fluorescence microscopy. The challenges involved in combining these two techniques are discussed, such as (i) the selection of appropriate light source for trapping and fluorescence excitation, (ii) the selection of optical components and (iii) which excitation mode for fluorescence microscopy is to be used. Furthermore the methods used for the calibration of the optical tweezers as a force transducer are presented. Development of the hardware and software to control and collect the force spectroscopy and fluorescence data is described. Finally the performance of the instrument was determined. Results of imaging dsDNA-YOYO-1 complexes, and single proteins on the dsDNA are presented. Finally we present simultaneous force spectroscopy and fluorescence microscopy of dsDNA-YO-1 complex.

Chapter 3 reports the results obtained upon studying the interaction of dsDNA with mono and bis intercalating molecules (100 nM YO-1 /YOYO-1 in buffer), using the combined optical tweezers and fluorescence microscope. The results reveal that the amount of dye molecules bound to the dsDNA increases as a function of force. The mechanical response of the dsDNA in the presence of YOYO-1 is different from that in the presence of YO-1. The dsDNA-YOYO-1 complex is not in equilibrium while performing force spectroscopy whereas the dsDNA-YO-1 complex is in equilibrium. A model is presented to explain the observed difference in the interaction of mono and bis intercalating molecules with the dsDNA.

In chapter 4 YOYO-1 molecules are used as a marker to report on the structure of the dsDNA in the overstretching region. 10 nM YOYO-1 was chosen as the concentration of YOYO-1 to study the structure of dsDNA in the overstretching region because it was shown to hardly affect the force extension curve. Simultaneous force spectroscopy and fluorescence microscopy along with the polarization fluorescence microscopy revealed that the orientation of the YOYO-1 molecules attached to the dsDNA did not change orientation during the overstretching process. Furthermore it was shown that the amount of fluorescence decreased as a result of the melting of the dsDNA into ssDNA fragments.

In chapter 5 the force extension curves recorded at various concentrations of YOYO-1 and YO-1 (10-1000 nM) were used to extract the binding constant and binding site size of YOYO-1 and YO-1 as a function of applied force. From the force extension

data, the fractional elongation of the complex for each concentration at various forces was determined. From this fractional elongation, the binding density was calculated and these data were curve-fitted with the McGhee-von Hippel binding isotherm to determine the above-mentioned parameters.

As a first step towards protein binding to dsDNA the interaction with Lys-Trp-Lys at various concentrations was measured in chapter 6. At 150 mM NaCl there was almost no detectable interaction. At 10 mM NaCl however, interaction between Lys-Trp-Lys and the dsDNA was observed. This points out that the Lys-Trp-Lys preferably interacts with structurally destabilized dsDNA as opposed to intact dsDNA. The force spectroscopy data obtained at various Lys-Trp-Lys concentrations were used to determine the force dependent binding constant and binding site size.

In the last chapter a summary of the thesis is presented, together with some suggestions for improvements in the existing instrument, and for new experiments which can be performed using the combined optical tweezers and line-scanning fluorescence microscopy.

1.6
References

1. Calladine, C. R. 2004. Understanding DNA the molecule & how it works. Elsevier Academic Press, San Diego, CA.
2. Lehninger, A. L., D. L. Nelson, and M. M. Cox. 1993. Principles of biochemistry. Worth Publishers, New York, NY.
3. Berg, J. M., J. L. Tymoczko, and L. Stryer. 2007. Biochemistry. W.H. Freeman, New York.
4. Hausner, W., and M. Thomm. 2001. Events during initiation of archaeal transcription: open complex formation and DNA-protein interactions. Journal of Bacteriology 183:3025-3031.
5. Van Holde, K. E. 1989. Chromatin. Springer-Verlag, New York.
6. Elgin, S. C. R., and J. L. Workman. 2000. Chromatin structure and gene expression. Oxford University Press, Oxford ; New York.
7. Luger, K., A. W. Mader, R. K. Richmond, D. F. Sargent, and T. J. Richmond. 1997. Crystal structure of the nucleosome core particle at 2.8 angstrom resolution. Nature 389:251-260.
8. Kornberg, R. D., and Y. L. Lorch. 1999. Twenty-five years of the nucleosome, fundamental particle of the eukaryote chromosome. Cell 98:285-294.
9. Bennink, M. L., S. H. Leuba, G. H. Leno, J. Zlatanova, B. G. de Grooth, and J. Greve. 2001. Unfolding individual nucleosomes by stretching single chromatin fibers with optical tweezers. Nature Structural Biology 8:606-610.
10. Carruthers, L. M., and J. C. Hansen. 2000. The core histone N termini function independently of linker histones during chromatin condensation. Journal of Biological Chemistry 275:37285-37290.
11. Sera, T., and A. P. Wolffe. 1998. Role of histone H1 as an architectural determinant of chromatin structure and as a specific repressor of transcription on Xenopus oocyte 5S rRNA genes. Molecular and Cellular Biology 18:3668-3680.
12. Tjong, H., and H. X. Zhou. 2007. DISPLAR: an accurate method for predicting DNA-binding sites on protein surfaces. Nucleic Acids Research 35:1465-1477.
13. Werner, M. H., A. M. Gronenborn, and G. M. Clore. 1996. Intercalation, DNA kinking, and the control of transcription. Science 271:778-784.
14. Leger, J. F., J. Robert, L. Bourdieu, D. Chatenay, and J. F. Marko. 1998. RecA binding to a single double-stranded DNA molecule: a possible role of DNA conformational fluctuations. Proc Natl Acad Sci U S A 95:12295-12299.
15. Kuznetsov, S. V., S. Sugimura, P. Vivas, D. M. Crothers, and A. Ansari. 2006. Direct observation of DNA bending/unbending kinetics in complex with DNA-bending protein IHF. Proc Natl Acad Sci U S A 103:18515-18520.
16. Neuman, K. C., and A. Nagy. 2008. Single-molecule force spectroscopy: optical tweezers, magnetic tweezers and atomic force microscopy. Nature Methods 5:491-505.
17. Bennink, M. L., O. D. Scharer, R. Kanaar, K. Sakata-Sogawa, J. M. Schins, J. S. Kanger, B. G. de Grooth, and J. Greve. 1999. Single-molecule manipulation of double-stranded DNA using optical tweezers: interaction studies of DNA with RecA and YOYO-1. Cytometry 36:200-208.

18. Kleimann, C., A. Sischka, A. Spiering, K. Tonsing, N. Sewald, U. Diederichsen, and D. Anselmetti. 2009. Binding Kinetics of Bisintercalator Triostin A with Optical Tweezers Force Mechanics. Biophysical Journal 97:2780-2784.
19. Husale, S., W. Grange, M. Karle, S. Burgi, and M. Hegner. 2008. Interaction of cationic surfactants with DNA: a single-molecule study. Nucleic Acids Research 36:1443-1449.
20. Sischka, A., K. Toensing, R. Eckel, S. D. Wilking, N. Sewald, R. Ros, and D. Anselmetti. 2005. Molecular mechanisms and kinetics between DNA and DNA binding ligands. Biophysical Journal 88:404-411.
21. Vladescu, I. D., M. J. McCauley, I. Rouzina, and M. C. Williams. 2005. Mapping the phase diagram of single DNA molecule force-induced melting in the presence of ethidium. Physical Review Letters 95:-.
22. Vladescu, I. D., M. J. McCauley, M. E. Nunez, I. Rouzina, and M. C. Williams. 2007. Quantifying force-dependent and zero-force DNA intercalation by single-molecule stretching. Nature Methods 4:517-522.
23. Svoboda, K., and S. M. Block. 1994. Biological Applications of Optical Forces. Annual Review of Biophysics and Biomolecular Structure 23:247-285.
24. Eriksson, E., J. Enger, B. Nordlander, N. Erjavec, K. Ramser, M. Goksor, S. Hohmann, T. Nystrom, and D. Hanstorp. 2007. A microfluidic system in combination with optical tweezers for analyzing rapid and reversible cytological alterations in single cells upon environmental changes. Lab on a Chip 7:71-76.
25. Perkins, T. T., S. R. Quake, D. E. Smith, and S. Chu. 1994. Relaxation of a Single DNA Molecule Observed by Optical Microscopy. Science 264:822-826.
26. Perkins, T. T., D. E. Smith, and S. Chu. 1994. Direct Observation of Tube-Like Motion of a Single Polymer-Chain. Science 264:819-822.
27. Nishizaka, T., H. Miyata, H. Yoshikawa, S. Ishiwata, and K. Kinosita. 1995. Unbinding Force of a Single Motor Molecule of Muscle Measured Using Optical Tweezers. Nature 377:251-254.
28. Ishijima, A., H. Kojima, T. Funatsu, M. Tokunaga, H. Higuchi, H. Tanaka, and T. Yanagida. 1998. Simultaneous observation of individual ATPase and mechanical events by a single myosin molecule during interaction with actin. Cell 92:161-171.
29. Hohng, S., R. B. Zhou, M. K. Nahas, J. Yu, K. Schulten, D. M. J. Lilley, and T. J. Ha. 2007. Fluorescence-force spectroscopy maps two-dimensional reaction landscape of the Holliday junction. Science 318:279-283.
30. van Mameren, J., M. Modesti, R. Kanaar, C. Wyman, G. J. L. Wuite, and E. J. G. Peterman. 2006. Dissecting elastic heterogeneity along DNA molecules coated partly with Rad51 using concurrent fluorescence microscopy and optical tweezers. Biophysical Journal 91:L78-L80.
31. Lang, M. J., P. M. Fordyce, and S. M. Block. 2003. Combined optical trapping and single-molecule fluorescence. J Biol 2:6.
32. Lang, M. J., P. M. Fordyce, A. M. Engh, K. C. Neuman, and S. M. Block. 2004. Simultaneous, coincident optical trapping and single-molecule fluorescence. Nature Methods 1:133-139.

Chapter 2

Development of an optical tweezers instrument with integrated line-scanning fluorescence microscopy

Abstract

This chapter describes the integration of two powerful single molecule techniques namely optical tweezers and line-scanning fluorescence microscopy with single molecule sensitivity. After an introduction of these techniques, the different challenges encountered during the integration process are discussed in detail. The successful integration is demonstrated by a number of experiments. Force extension and relaxation curves of dsDNA interacting with the oxazole yellow dye YO-1 have been recorded. During these stretching experiments, the fluorescence of the complex formed was imaged and quantified simultaneously. The sensitivity for detecting individual fluorescently labeled protein molecules was demonstrated by imaging a single EcoRI protein as it interacted with the suspended dsDNA.

2.1
Introduction

Single molecule techniques such as atomic force microscopy (1-4), optical tweezers (5-8) and fluorescence microscopy (9-11) have revolutionized our understanding about biological processes at the level of individual molecules. Each technique provides different data about the system under study. Atomic force microscopy offers data on the topography and the mechanical properties of the biomolecules when they are deposited onto a solid supporting surface. Optical tweezers (8) on the other hand does not give any topographical information, but yields high-resolution force data representing the mechanical properties of the biomolecules when suspended within the medium (no surface). Fluorescence microscopy is a technique used to directly image and visualize single molecules. In this project we set out to develop a method to measure the change in the mechanical properties of individual dsDNA molecules as they are interacting with proteins and at the same time to localize the interacting protein molecules along this dsDNA with high accuracy. To this end the optical tweezers were integrated with fluorescence microscopy (12-15).

This chapter starts with the fundamentals of optical tweezers and fluorescence microscopy. This brief introduction is followed by a discussion of the different challenges (choice of light source, fluorescence illumination and selection of optical components) encountered in the integration of these two techniques. The successful operation of the integrated line-scanning fluorescence microscope with the optical tweezers instrument was demonstrated by the measurement of the force-dependent interaction of the oxazole yellow dye YO-1 with the individual dsDNA molecule. Optical tweezers force spectroscopy was performed on the dsDNA in the presence of 100 nM YO-1, while fluorescence images of the complex were captured with the help of line-scanning fluorescence microscopy. This enabled the direct correlation of the change in the mechanical properties of dsDNA and the total number of YO-1 molecules bound to the dsDNA. The sensitivity of the instrument to detect individual protein molecules using fluorescence was demonstrated by measuring the interaction between a single EcoRI protein and the dsDNA.

2.2
Optical tweezers

The effects of radiation pressure has been known for centuries. Johannes Kepler observed that the tail of the comet is always pointing away from the sun, which is due to the radiation pressure of the sun experienced by the comet. Arthur Ashkin in the early 1970s demonstrated the use of radiation pressure to levitate dielectric particles (16). In 1986 Ashkin and coworkers succeeded in trapping 10 µm to 40 µm particles using a single-beam optical tweezers configuration (17). Ashkin furthermore demonstrated the trapping of

biological objects such as cells using an infrared laser. Since then optical tweezers has enabled a large number of experiments resulting in significant breakthroughs in the field of single molecule biophysics. Block *et al*. demonstrated the stepping of kinesin as it translocates on a microtubule and measured the stepsize (5). Smith *et al*. and Cluzel *et al*. performed force spectroscopy on a single λ-phage DNA, which clearly revealed the overstretching plateau at a force of 65 pN (18-19). Bennink *et al.* demonstrated the unwinding of single nucleosomes, which are the first level in compaction of dsDNA into chromatin (8), while Kellermayer *et al.* demonstrated the force-induced folding and unfolding of a single titin molecule (20). This and other scientific work clearly reveals the large potential of optical tweezers in the fields of single molecule biophysics, soft condensed matter physics, and physical chemistry (21-23).

2.2.1
The physics of optical force

Light has the ability to interact with matter and as a result to exert forces on it. This effect is expressed as radiation pressure, which is defined as the force per unit area on an object due to the change in momentum of light. Light consists of photons, each having a momentum P. For light of wavelength λ, the magnitude of the momentum of a single photon is given by:

$$\left|\vec{P}\right| = \frac{h}{\lambda} \tag{1}$$

The intensity of the light is determined by the number of photons passing through a given area per unit time. The momentum flux of photons from light of given intensity is expressed by the Poynting vector $\vec{S}$.

$$(d\vec{P}/dt) = (n/c)\vec{S}A \tag{2}$$

where n is the refractive index, c is the speed of light, and A is the area normal to S. Since the force on a dielectric object is given by the change in momentum of light induced due to refraction of the light by the object, the total force on the object is the difference between the momentum flux entering the object and that leaving the object. The total force on an object due to refraction of light is therefore

$$\vec{F} = d\vec{P}_{in}/dt - dP_{out}/dt = (n/c)\iint\left(\vec{S}_{in} - \vec{S}_{out}\right)dA \tag{3}$$

Thus, if the light, upon interacting with a dielectric object in a medium of index n, is deflected, and thus changing the direction of the Poynting vector S, there is a finite force exerted on the object by the light.

2.2.2
Working principle of optical tweezers

In order to optically trap an object with a Gaussian beam, the reflective index of the object to be trapped must be higher than that of surrounding medium; for example a polystyrene bead (n=1.58) in water (n=1.33). The basic principle of optical trapping results directly from the momentum transfer of all photons that interact with the trapped object. For particles that have diameters much larger than the wavelength used for optical trapping, Mie theory can be used to explain the effect of optical trapping. Within this regime simple ray optics can be used to determine the momentum on the trapped object.

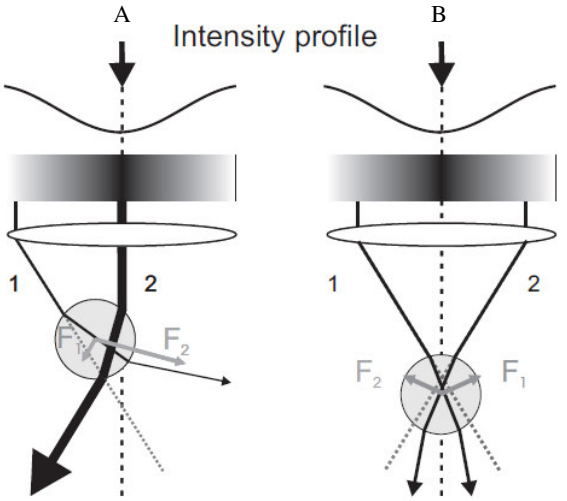

Fig. 1
A ray optics picture of the forces acting on a dielectric particle (bead). The scattering forces due to the reflection are not shown. In (A) the bead is located between the objective and the focus of the laser beam. The situation where the bead is behind the focus is shown in (B). (adapted from Huisstede (24)).

In essence, a laser beam with a Gaussian beam profile is expanded and focused by a high NA objective. When this electromagnetic field interacts with a bead, the bead experiences the radiation pressure (force) dependent on its position with respect to the focal point (Fig. 1). Radiation forces can be decomposed into a gradient force pointing in the direction of the intensity gradient of the light tending to pull the particle towards the focus,

and into a scattering force as result of reflections directed along the optical axis, having a tendency to push the bead away from the focus. In Fig. 1A the situation is sketched for a bead located between the objective and the focal plane. Here two rays as they propagate through the bead are drawn and the force resulting from these is indicated. These two rays differ in intensity since they are representing different parts of the beam, and the momentum change resulting from each ray is proportional to its intensity. The total momentum change causes a net force on the bead which points in the direction of the highest intensity. In Fig. 1B the bead is located behind the focal point (the focal point is indicated by the crossover point of the grey dotted lines showing the direction of the rays if they were not refracted by the bead). Here the resulting force is pointed in an upward direction, causing the bead to be pulled upstream towards the point of highest intensity (i.e. the focus). In these examples the reflections are not shown, which result in a scattering force giving the force an offset in the propagation direction of the incident light. This scattering force results in the bead to be stably trapped slightly behind the focal point where this force is compensated by the gradient force.

For particles with diameters smaller than the wavelength of the light (Rayleigh regime) the phenomenon of optical trapping can be explained by treating the trapped object as a Rayleigh scatterer with a polarizability α. Within an electric field with strength E, a dipole moment αE is induced in the object which therefore experiences a force $\vec{F} = \alpha/2 \nabla \vec{E} \bullet \vec{E}$ effectively attracting it to the focus of the light. Since the polarizability α is proportional to the particle volume, the force holding the particle in the trap is proportional to the particle size, as well as the beam intensity gradient.

2.2.3
Optical tweezers as force transducer

Initially optical tweezers were used as tool to manipulate viruses, bacteria and complete cells. However when trapping spherical beads, it was shown that a single beam gradient trap could be used to accurately exert forces in the range of piconewtons. When the spherical bead is in the centre of the optical trap all optical forces exerted by the light are canceled, resulting in zero net force on the bead. When the bead is slightly displaced, a net force is created that tends to drive the bead back to its centre position. The amplitude of this force is linearly proportional to the distance over which the bead is displaced from the trap center. Conceptually this relation can be described as a Hookean spring as indicated in Fig. 2A. The force F needed to displace a trapped bead by a distance ΔX with respect to its centre position is given by:

$$F = k\Delta X \quad (4)$$

where k is the trap stiffness, expressed in pN/µm. From this equation it is clear that in order to measure forces the position of the bead and the trap stiffness must be accurately determined. The stiffness of the trap can be determined using different methods that are discussed later. The position of the bead is acquired by measuring the deflection of the laser trapping light that is transmitted using a position-sensitive detector (Fig. 2B) or by analysis of the images of the bead recorded by video microscopy. With a typical bead size of 2.6 µm and a trapping laser power of 0.1 – 2 W at the back aperture of the objective, the trap stiffness is in the order of 50 – 500 pN/µm and can be controlled by changing the laser power. Coupling a biopolymer at both its extremities to the trapped bead and another bead which is immobilized on a glass micropipette, enables the application and measurement of a force on the individual molecule (for example dsDNA, RNA or chromatin) (Fig. 2B).

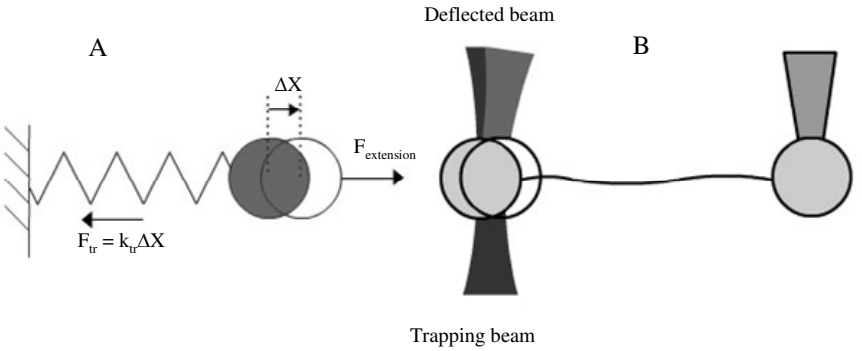

Fig. 2

Force-measuring optical tweezers. (A) When an external force F is applied to the bead the bead moves away from its trap center position over a distance (ΔX) to a position in which the external force is balanced with a counteracting trapping force F_{tr}. (B) A single dsDNA molecule (λ-DNA, contour length= 16.4 µm) has been attached between the trapped bead (d=2.6 µm) and a bead immobilized on a glass micropipette. The force in the molecule and thus upon the trapped bead can be measured accurately by measuring the deflection of the transmitted laser light.

2.3
Fluorescence microscopy

In 1852, 'fluorescence' was first introduced by George Stokes; he proposed that fluorescent dyes can be used for the detection of organic substances. The first detected single molecule attached with multiple fluorophores in a liquid was reported by Hirschfeld (25) in 1976. Nowadays fluorescence microscopy is a tool available in almost every lab. Fluorescence microscopy not only allows the detection of single molecules within a microscopic image, but can furthermore be used to determine the distance between the two molecules on a nanometer scale using fluorescence resonance energy transfer (FRET). To detect the orientation of the individual molecules, fluorescence polarization microscopy can be applied, in which the fluorophores are excited with polarized light, and in which the polarization of the emission light is detected.

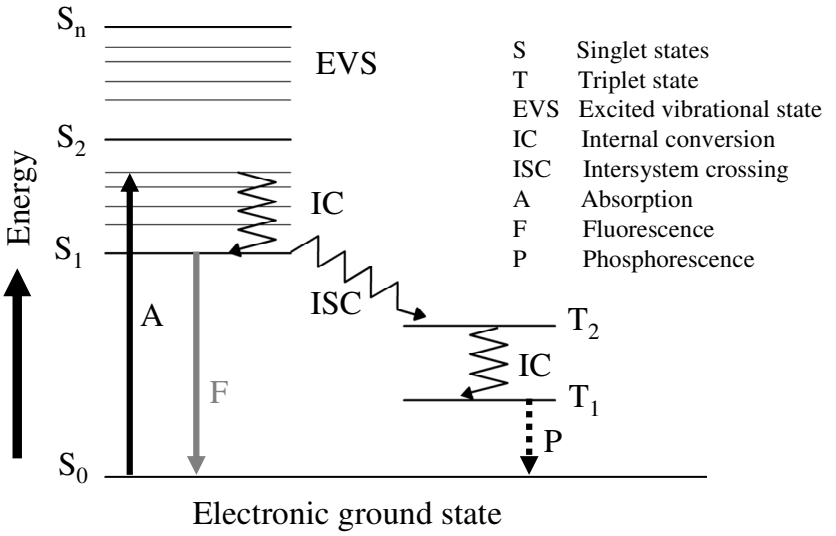

Fig. 3
Schematic presentation of Jablonski diagram.

The fundamental process of fluorescence can be explained with the Jablonski diagram (Fig. 3). After a fluorophore has absorbed a photon with sufficient energy, the molecule is excited from its ground state (S_0) to an excited state. The initial excited state is one of the vibrational states of the excited states (S_1, S_2, …). Immediately following excitation the molecule vibrationally relaxes to the lowest vibrational energy level of the first excited state ($\Delta t=10^{-12}$ s). If it is excited to a higher excited state, it furthermore internally converts to the first excited state (S_1). Once in this state there are a number of

routes to return to the ground state (S_0). The first route is the direct return to the ground state, with the emission of a photon. The wavelength of the emitted photon corresponds with the energy difference between the S_1 and S_0 state (gray line in Fig. 3). This route is defined as fluorescence. The lifetime of the excited state is very short (10^{-5} - 10^{-8} s). A second route is a transition from the excited state to a triplet state, which has a different spin state. The transition is referred to as intersystem crossing. From this triplet state it is also possible to go to the ground state (dotted line in Fig. 3), with the emission of a photon. The lifetime of the triplet state however is much longer than that of the singlet excited state (10^{-4} s to minutes or even hours). This phenomenon is known as phosphorescence.

Fig. 4A presents schematically the basic instrumental set-up that is used for fluorescence microscopy. The objective lens is used to focus the excitation light and to collect the emitted light (emission) from the fluorophores. In order to detect the emission light, which is orders of magnitude lower in intensity than the excitation light, dichroic mirrors that are able to separate the excitation and emission beams based on the difference in wavelength are used. Fig. 4B shows the excitation and emission spectra of YOYO-1 when bound to dsDNA. In many cases an additional band pass filter is applied in the emission path to block off any remaining excitation light that might have leaked through the dichroic mirror. The emission light is then captured using a low temperature CCD camera, a photomultiplier tube or an avalanche photo diode (APD).

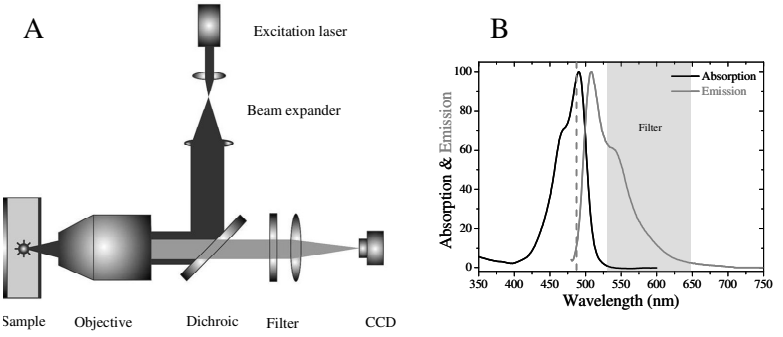

Fig. 4

(A) Basic instrumentation for fluorescence microscopy. (B) Presents the absorption and emission spectra of YOYO-1 bound to dsDNA. The dotted line indicates the excitation wavelength (488 nm) used in this study. The gray area presented in this figure presents the spectral range of light that is transmitted by the band pass filter.

2.4
Instrumental design

2.4.1
Existing optical tweezers setup

The combined optical tweezers and line-scanning fluorescence microscopy instrument described in this chapter has been built from an existing optical tweezers set-up (Fig. 5).

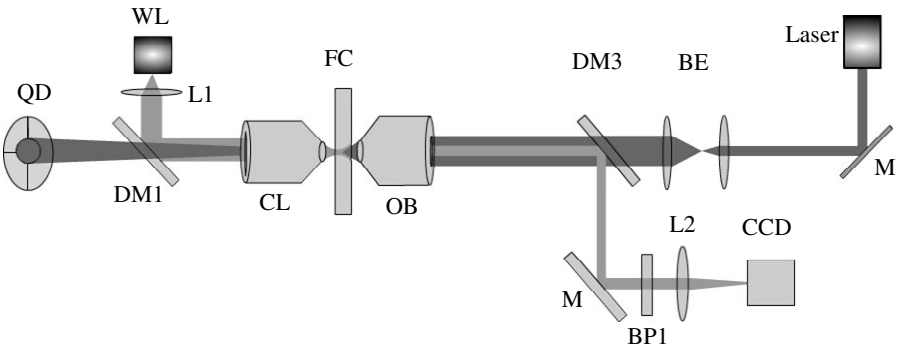

Fig. 5
Single-beam optical tweezers set-up. Description of its operation can be found in the main text. Various parts of the instrument are quadrant detector (QD), white light (WL), dichroic mirror (DM), condenser lens (CL), flowcell (FC), objective (OB), mirror (M), lens (L), band pass filter (BP), beam expander (BE), charge coupled device (CCD).

A Nd:VO_4 laser (Coherent Inc., Santa Clara, CA, USA) with a maximum output power of 2 W at λ = 1064 nm (TEM_{00}) serves as the trapping laser. A beam expander (BE) (Thorlabs, Newton, NJ, USA) is used to overfill the back aperture of the objective (OB) in order to optimize the optical trapping efficiency. A 100x, infinity-corrected, water immersion objective (Leica, NPLAN) with a NA of 1.20 is used to focus the trapping laser light at a position of about 50 µm deep into the flowcell (FC). The same objective is also used to make a microscopic image of the area around the focus with the help of lens L2 and band pass filter (BP – transmits only in visible range). Microscopic white light images are recorded with the CCD camera. In order to get sufficient brightness in the microscopic image, a white light (WL) source was added. Dichroic mirrors DM1 and DM3 transmit 1064 nm and reflect in the visible range. Micrometer sized polystyrene beads (Bangs Laboratories, Fishers, IN, USA) can be trapped just behind the focal point of the laser light,

which is about 50 µm within the flow chamber. The laser light transmitted through the bead is collected by a condenser lens (CL) (NA 0.9). This light is then focused onto a quadrant detector (QD), which is placed just behind the conjugate back focal plane of the condenser. Light falling on the quadrant detector gives rise to the current which is converted into an electrical signal (voltage). When the bead moves with respect to the trap position, the transmitted laser light deflects and will result in a signal of the quadrant detector.

2.4.2
Modification of the existing optical tweezers setup

In the existing optical tweezers set-up a white light source is used to illuminate the area in the flowcell. The spectrum of the white light ranges from 400 nm to 700 nm, and clearly has a considerable overlap with the fluorescence emission wavelength of typical fluorophores. For that reason the white light source was replaced by an 850 nm LED (SMT850-23 ,Roithner Lasertechnik, Vienna, Austria), which has a very narrow spectrum, outside the spectral range of the emission of most fluorophores, and sufficiently different from the 1064 nm wavelength of the laser used for trapping. This is important to block off any remaining laser light for the microscopic imaging. The dichroic mirror used in the existing optical tweezers was designed to transmit 1064 nm and reflect some of the white light. With the introduction of the 850-nm LED, the dichroic mirrors needed to be replaced. The existing dichroic mirrors were replaced by ones that reflect up till 900 nm and transmit 1064nm (Chroma Technology, Bellows Falls, VT, USA). Although the dichroic mirror was designed to transmit 1064 nm, the intensity of this trapping laser beam and of the scattered light in the backward direction is so intense that an additional band pass filter was needed in front of the CCD camera (D850/20m, Chroma Technology) to completely remove the reflected 1064-nm laser light coming from the trapped bead.

2.4.3
The choice of fluorescence microscopy configuration

We considered different possible experimental configurations of the fluorescence microscope. The first one is the confocal fluorescence microscope. In this configuration a diffraction-limited spot is used to scan the sample or the sample is moved with respect to this spot (26) in order to build up the image. This configuration furthermore has a pinhole in the conjugate plane in front of the detector, which significantly reduces the amount of fluorescence coming from fluorophores that are outside the focal volume. For this reason confocal fluorescence microscopy has a very high S/N ratio (27-28). The second experimental configuration is wide-field fluorescence microscopy. In this configuration the total field of view is illuminated and detected by a CCD camera. This may lead to some undesired exposure of the sample outside the area of interest which may lead to bleaching

of that part of the sample. Since this configuration is neither confocal in excitation nor in detection, the S/N ratio is lower than that of confocal microscopy (28). The third experimental configuration is line-scanning fluorescence microscopy. In this mode a sample is illuminated with a line-shaped profile with dimensions of a few tens of µm in one direction and a diffraction-limited spot-size in the second direction. In order to create a full image of the sample, the line-shaped beam is scanned back and forth over the sample. When compared to wide-field illumination this experimental configuration has the advantages that it illuminates only a specific part of the sample at a time, which creates confocality in the excitation. An additional slit needs to be added in the conjugate plane to also ensure confocality in detection.

For the application of detecting individual protein molecules while they are interacting with a single dsDNA molecule that is suspended between two polystyrene beads, the third experimental configuration was selected. The line-shaped beam profile was chosen to be orthogonal to the axis of the dsDNA. In this configuration there was full control of the illumination intensity along the length of the dsDNA molecule. This allowed for example to only excite a particular part of the dsDNA, or to illuminate the dsDNA with a more complex intensity pattern.

2.4.4
Line-scanning fluorescence microscopy setup

Most line-scanning fluorescence microscopy systems create the line-shaped excitation beam by using either a slit (29) or a cylindrical lens (30). The other key component is a scanning mirror to scan the excitation line across the field of view. If confocality in detection is to be realized, a second scanning mirror needs to be added which scans in phase with the first one. By having a slit hole in the conjugate image plane the confocal effect can be exploited, leading to an enhanced S/N ratio. In this setup we chose not to use a second mirror and an additional slit in the detection path. The beam is scanned once back and forth per acquired image.

Fig. 6 shows schematically the experimental layout of the line-scanning fluorescence microscope. The light source used for the excitation of the fluorophores is a 488-nm laser (model 161C-01; Spectra Physics, Mountain View CA, USA) with a maximum power of 10 mW. To create a line-shaped excitation pattern a cylindrical lens (CL) was used (f = 40 mm) (LJ1402L1-A, Thorlabs, Thorlabs, Newton, NJ, USA). This beam is then expanded using a beam expander system consisting of lenses L3 and L4 (40 mm and 250 mm respectively) (CAN254-040-A, ACN254-250-A, Thorlabs, Newton NJ, USA), such that the back aperture of the objective is filled. The combination of lenses L3 and L4 do not just act as the beam expander but also image the center of the scanning

mirror (SM) at the back aperture of the objective. This is achieved by positioning the scanning mirror (SM: General Scanning INC, Watertown, MA, USA) in the focal plane of L3 and the objective in the focal plane of L4 with a distance between the two lenses of 290 mm (which is the sum of the two focal lengths). This complete system acts as a 4f system (31). As the centre of the scanning mirror is imaged at the back aperture of the objective, the beam is always at the same position at the back aperture independent of the position of the scanning mirror. What does change is the angle at which the light is coming to this plane. Next to a 4f system ensuring that the beam is always at the back aperture of the objective, the lens combination L3 and L4 furthermore acts as a beam expander. This system also reduces the mechanical noise induced by the scanning mirror (if any) into the light beam by factor of 6.25 at the back aperture of the objective.

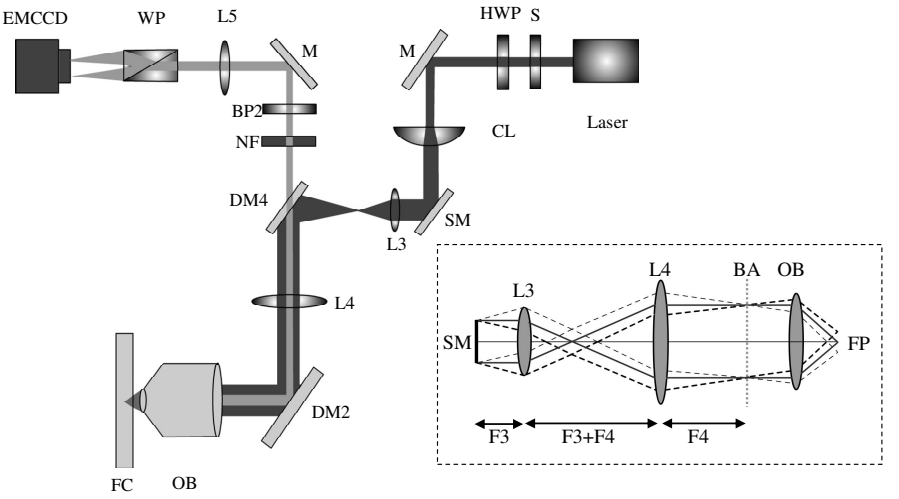

Fig. 6

Schematic representation of the line-scanning fluorescence microscope, and 4f system (Fig. in dotted square box). Flowcell (FC), objective (OB), dichroic mirror (DM), lens (L), Scanning mirror (SM), cylindrical lens (CL), half waveplate (HWP), shutter (S), notch filter (NF), band pass filter (BP), Wollaston prism (WP), electron multiplying charge coupled device (EMCCD).

The relation between the angle of incidence of the laser beam at the back aperture of the objective to the deflection of focal spot in the focal plane of the objective is given by Eq. 5 (31)

$$r = f_{EFL}\theta \quad (5)$$

Where r is the deflection of focal spot in the focal plane of the objective (~ 40 µm), f_{EFL} is the effective focal length of the objective (2.2 mm) and the θ is the angle of incidence of the laser beam at back aperture of the objective in radians (~ 0.018 radian).

2.4.5
Detection system

The emitted photons from the fluorophores are collected by the same objective (OB) which is used for the focusing the excitation laser light. The emitted and excitation light are separated from the trapping laser (1064 nm) and illumination source (850 nm LED) by a dichroic mirror (DM2, NT43-959, Edmund optics, Lysander Close, York, UK). The excitation light is separated from the emitted light by using a second dichroic mirror (DM4, reflects up to 490nm transmit above 505, Q505LP, Chroma Technology, Bellows Falls, VT, USA). A notch filter in the fluorescence emission path (NF-488 nm, NF03-488 E-25, Semrock, Rochester, NY, USA) is used to block the back reflection of the fluorescence excitation laser light. An additional band pass filter (BP2) (transmission from 510 to 680 nm, Chroma Technology, Bellows Falls, VT, USA) is used to transmit the emitted light and block all other light sources. The fluorescence image is formed by inserting an additional lens (L5). The image is then projected onto the EMCCD camera (iXon DV887-BV; Andor, Belfast, Northern Ireland). The entire set-up is enclosed in a black box to reduce the background noise in the fluorescence image.

2.4.6
Incorporation of polarized fluorescence microscopy

In the present line-scanning fluorescence microscopy system fluorescence polarization microscopy has been implemented. The 488-nm laser that is used for fluorescence excitation has a polarization direction which is vertical (i.e. perpendicular with respect to the optical bench). To allow excitation of the sample with the other polarization direction, a rotation of the polarization of 90º is needed.

To this end a half wave plate (HWP, Fig. 6A, WPH05M, Thorlabs, Newton NJ, USA) was inserted in the excitation path between the laser source and the cylindrical lens. To allow polarization sensitive detection in the fluorescence emission, a Wollaston prism (WP:WSP9015, FOCtek Photonics, Fujian, China) was added into the detection path between the imaging lens and the EMCCD camera. This prism separates the two polarized signals from each other and creates two separate images for each polarization, which are slightly displaced from one another.

It is essential to take into account the transmission efficiency of different optical components as a function of the polarization state of the light. The 488-nm laser intensity was therefore measured at the back aperture of the objective in both polarization states, that is without the half wave plate for vertical polarization (100%) and with the half wave plate inserted for horizontal polarization (83%). This difference in intensity was compensated for by using a higher intensity of the excitation beam with horizontal polarization. In order to allow comparison of the detection light in the two polarization states, the transmission efficiency of the dichroic mirror (DM4) was measured using a spectrometer. Fig. 7 presents the response of dichroic mirror to the light perpendicular and parallel to the optical table. For photons in the wavelength range of 500 to 600 nm, the relative difference is 0.94. This difference was compensated for in the final data extracted from the EMCCD camera.

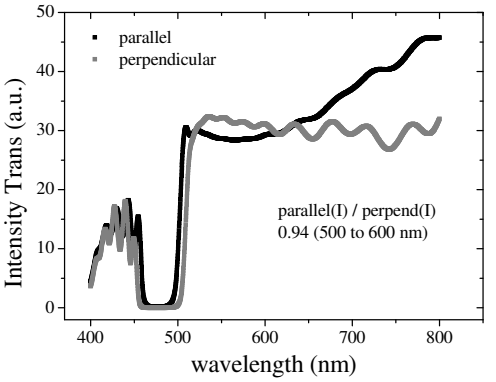

Fig. 7
Transmission spectrum of parallel and perpendicular polarized light through a dichroic mirror oriented at 45° obtained by a spectrometer.

Fig. 8 presents a schematic view of the optical tweezers instrument into which polarization-sensitive line-scanning fluorescence microscopy has been integrated. Fig. 9 shows the transmission spectra of the different filters, dichroic mirrors and light sources used in the instrument. This set of optical components enables a clear separation of the light involved in optical trapping and the light involved in fluorescence excitation or emission.

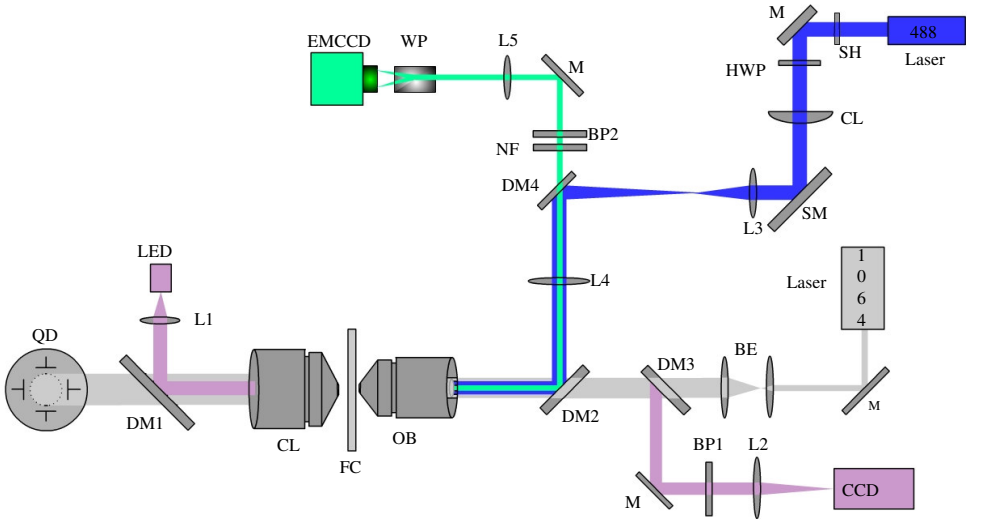

Fig. 8

Set-up of the optical tweezers instrument with integrated polarization-sensitive line-scanning fluorescence microscopy. The instrument is capable of measuring the force (pN), acquiring fluorescence images (single molecule detection), and performing fluorescence polarization microscopy.

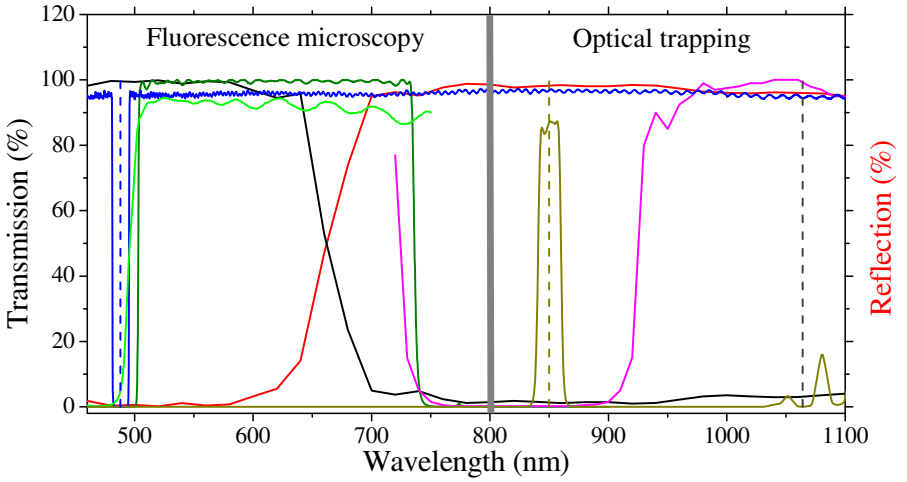

Fig. 9

Transmission spectra of the filters, dichroic mirrors and light sources used in the instrument. (---) dotted blue line indicates excitation laser source (488 nm), (---) dark yellow presents flowcell illumination source (LED 850 nm), (---) black indicates trapping laser (1064 nm). (—) black line presents the dichroic mirror (DM2) placed just behind the objective, which transmits wavelengths above 700 nm and reflects wavelength below 700 nm (—). (—) Bright green present the dichroic mirror (DM4) which reflects below 500 nm and transmits above 505 nm. (—) Dark green line presents the band pass (BP2) filter used in the detection path of fluorescence microscopy. (—) Blue line present notch filter (NF). (—) Dark yellow line present band pass filter (BP1) used to block trapping light in front of CCD camera (normal images). Solid gray line presents the separation between fluorescence microscopy and optical trapping.

2.4.7
Flow cell

In brief the flow cell consists of a channel of ~5 mm width, ~40 mm length and a height of ~200 µm. Two layers of Parafilm ®, with a 5 x 40 mm channel cut out, are sandwiched between a microscope glass slide and a microscope coverslip (170 µm thickness) with the same dimensions (26 x 76 mm). Two 1-mm diameter holes were drilled into the microscope glass slide to provide exit and entry into the flow channel. A square glass capillary with inner diameter of 50x50 μm^2 (VitroCom, Mountain Lakes, NJ, USA) is placed between the coverslip and the parafilm. The assembled flowcell was then heated up to 60°C to partly melt the parafilm which upon cooling provides a waterproof sealing. The flowcell is then clamped onto the holder. A glass micropipette with an end diameter of about 1 µm is pulled using a pipette puller and is inserted through the square capillary into the flowcell with the help of a translation stage and simple microscope. The micropipette is then glued onto the flowcell holder using rapid curing two-component glue. The holder with the sandwiched

flow cell and the inserted micropipette is then attached to the XYZ stage (P-561.3CD, Physik Instrumente, Karlsruhe, Germany) using small cylindrical magnets.

Only a slight modification was added to the custom-made flowcell that has been used for other experiments carried out with the optical tweezers instrument (7). Instead of the clamping strips that kept the inlet and outlet tubes pressed against the glass, a flexible tube (2 mm outer diameter) was glued to the glass. This reduced the occurrence of air bubbles in the flow system dramatically. When the flow cell was positioned in the system, these tubes were connected to the tubes of the flow system (see next section).

2.4.8 Flow system

The flow system used to carry out experiments in this thesis was designed and developed by Bennink *et al.* (7). Fig. 10 presents a schematic scheme of the flow system. The flow system is used to control the exchange of different solutions and the rate of flow within flowcell. The different solutions (buffer, dsDNA, beads, YOYO-1, YO-1 and washing buffer) in the different containers are all connected to a closed air container. Buffer flow is established by increasing the pressure within the air container, such that the different solutions in the containers are pressurized. Thin polystyrene tubing (Intramedic Polyethylene tubing, PE10, ID = 0.28 mm, OD = 0.61 mm Becton Dickinson, Franklin Lakes, NJ, USA) connects each container to a six-way selection valve (Upchurch Scientific, Oak Harbor WA, USA). This selection valve enables selects which container is connected to the main output line going into the flowcell. Changing of one solution to the next is simply achieved by switching the selection valve. All the containers, ranging in volume from 1 ml to 50 ml are plastic disposable screw capped containers, which makes easy plug in of new solution containers possible. The flow rate of the selected buffer can be controlled by changing the pressure on the air container. This pressure is controlled by two solenoid valves, one of which is connected to a high pressure line. Opening of this valve for a short time increases the pressure stepwise. A second solenoid valve is added to restore the pressure to an atmospheric level, causing the flow in the flow cell to stop.

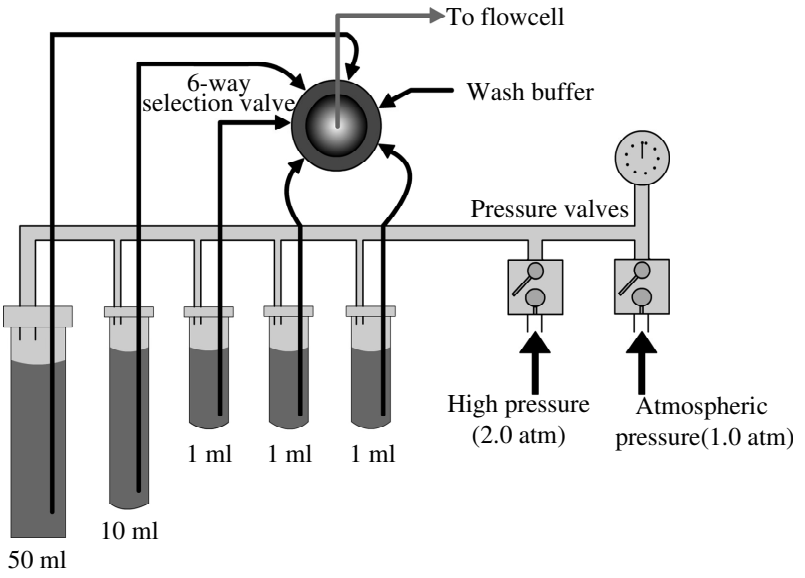

Fig. 10
Schematic of the flow system.

2.4.9
Calibration of Optical tweezers

The optical tweezers is calibrated to determine the relationship between force and displacement of the bead (eq. 4) which means that the spring constant k will be established. To determine the displacement of the bead within the trap and the distance between the two beads while performing force spectroscopy, the image recorded by the CCD camera needs to be calibrated. This was done by imaging a slide containing lines that are spaced 10 µm apart (32). The conversion factor was ~59 nm/pixel for the instrument. The position of the bead is extracted from the images using a centroid method (32).

Determining the position of the bead by video microscopy limits the data rate to 25 Hz. The quadrant detector however is able to get positional information at a much higher rate, but this signal needs to be calibrated. To this end microscopic images (acquired by video microscopy) of the trapped bead and the signal of the position detector were recorded simultaneously at different flow rates. A typical result of this calibration procedure is shown in Fig. 11.

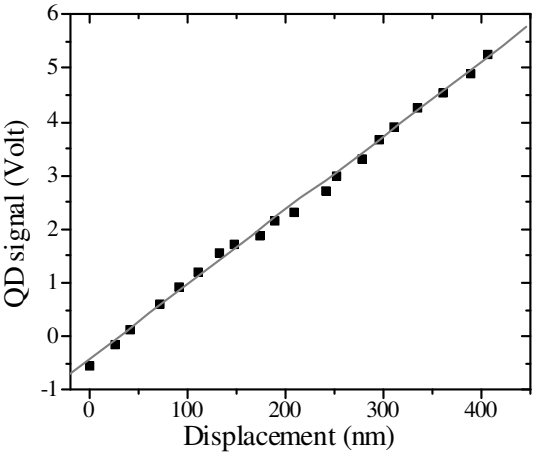

Fig. 11

Signal from the quadrant detector (QD) as function of displacement of bead from the center of trap determined from video images using a centroid method. The slope of the line is fitted to get the calibration factor (V/nm).

To determine the force (F) acting on the bead from its position with respect to the trap center, the trap stiffness (k) needs to be determined. The trap stiffness can be determined by various techniques such as escape force method, the momentum transfer method, the equipartition method, the drag force method and the power spectrum method (32-34). In this study the power spectrum method was used. For beads optically trapped in solution, the fluctuations due to thermal collisions of surrounding molecules can be modeled as the response of the bead in a quadratic potential field that is subjected to a randomly fluctuating thermal force, expressed by the Langevin equation (35). The harmonic oscillator is strongly overdamped due to the viscosity of the surrounding medium, such that the influence of the mass can be neglected. For such a Brownian harmonic oscillator, where motion takes place at small Reynolds number, the power spectral density of the bead position is given by the Lorentzian expression (35).

$$S_x(f) = \frac{k_B T}{\gamma_0 \pi^2 (f_c^2 + f^2)} \tag{6}$$

Where k_B is Boltzmann's constant, T the absolute temperature and *f* the frequency of the positional fluctuation, γ_0 is hydrodynamic coefficient. The units of $S_x(F)$ are nm/√Hz. At low frequencies ($f > f_c$) the power spectral density is approximately constant, given by

$$f = \langle\langle f_c \Rightarrow S_x(0) \approx \frac{k_B T}{\gamma \pi^2 f_c^2} = \frac{4 \gamma k_B T}{k_{tr}^2} \tag{7}$$

The thermal force amplitude is given by S_F (f) = 4 $\gamma k_B T$ and $S_x(0)$ thus reflects the confinement of the bead, which is dependent on the stiffness of the optical trap. For frequencies $f >> f_c$ the power spectra drops as $1/f^2$, indicative of free diffusion. Using this model to fit the recorded power spectral density, the trap stiffness can be deduced from the cut-off frequency (f_c). The trap stiffness k_{tr} is related to this cut-off frequency f_c according to $k_{tr} = 2\pi\gamma f_c$.

Fig. 12 presents a typical power spectrum recorded (i) with the laser turned off, (ii) with laser on, but no bead trapped and (iii) with the laser on and a bead trapped. The power spectral density with the laser turned on, reveals the mechanical vibrations of the instrument, probably originating from vibrations of the building. The power spectral density of the trapped bead was fitted with Eq. (6) to determine the cut-off frequency. Typical trap stiffness obtained in this instrument ranges from 300 pN/µm to 480 pN/µm depending on the power of the laser (1 – 2 W).

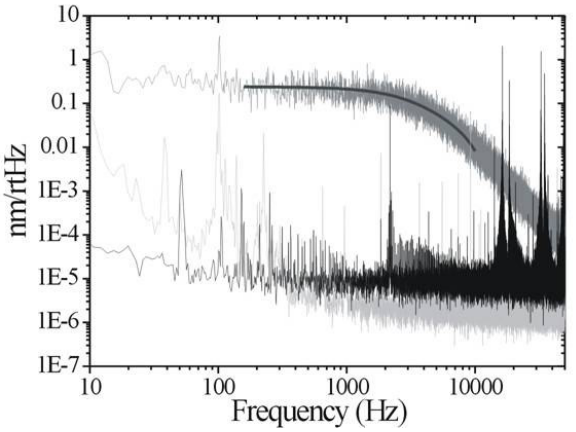

Fig. 12

Power spectral density recorded at various conditions. The black curves has been recorded with the laser turned off and reveals the electronic noise in the QD. The gray has been recorded with the trapping laser turned on, but no bead trapped. This spectrum reveals mainly noise coming from mechanical vibrations of the optical system (most probably induced by external noise sources). The dark gray curve has been recorded with a bead trapped, revealing the thermal motion of the bead in the trap. This curve was fitted with a Lorentzian function (Eq. (6)) to determine the cut-off frequency.

The experiments were performed using polystyrene beads with a diameter of ~2.6 µm. While calibrating the trap stiffness by the determination of the cut-off frequency in the power spectrum, quite a significant spread in the value of the trap stiffness was observed. External factors such as air currents in ambient environment where the laser beam is

propagating can dramatically affect the power spectral density (36) leading to an error in the determination of the cut-off frequency. Fig. 13 shows the cut-off frequency as measured for different beads at the same position within flowcell at the same laser power. For each trapped bead 10 separate power spectra were recorded and fitted. These values for the cut-off frequency for each bead did reveal quite a spread. The standard deviations obtained for beads 1 to 7 are 657, 810, 589, 332, 367, 832 and 437 Hz respectively. This corresponds to a relative error of 25% in force. Because of this large error, in practice the cut-off frequency is determined a number of times and an average value is taken to calculate the trap stiffness. Fig. 14 presents two examples of recorded power spectra recorded consecutively on the same bead, clearly showing that the power spectral density does fluctuate as a function of time.

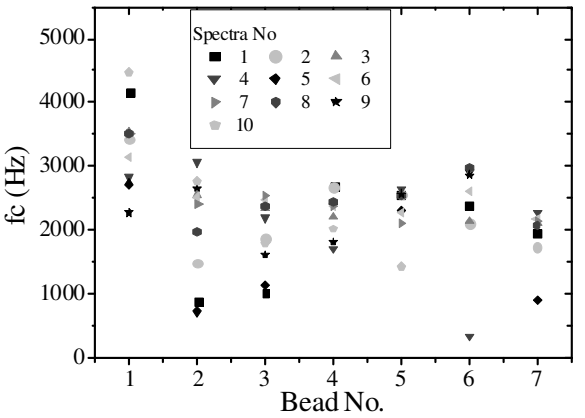

Fig. 13

Various cut-off frequencies determined from the power spectra for 7 beads at a fixed laser power. For each bead 10 spectra are recorded and analyzed.

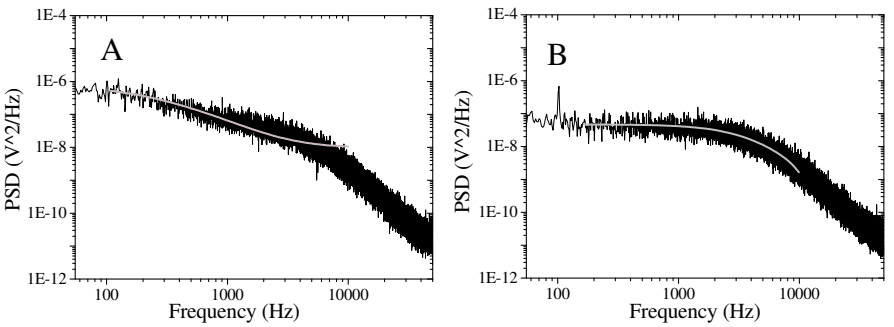

Fig. 14

Examples of consecutively recorded power spectra of a trapped 2.6-µm bead. (A) Distorted spectrum due to unknown reasons, which complicates the determination of the cut-off frequency (f_c = 900 Hz). (B) Noise-free power spectrum, that allows a good fit (f_c = 2273 Hz). Gray line indicates the Lorentzian fit. (PSD – Power Spectral Density).

Another way to calibrate the trap stiffness and the deflection sensitivity of the QD is to stretch a single dsDNA molecule and determine the value of the bead displacement and the QD signal at the point where the dsDNA is overstretching, which is known to occur at a force of 65 pN (in 150 mM NaCl). Fig 15 presents the bead displacement (A) and the QD signal (B) as a function of dsDNA extension.

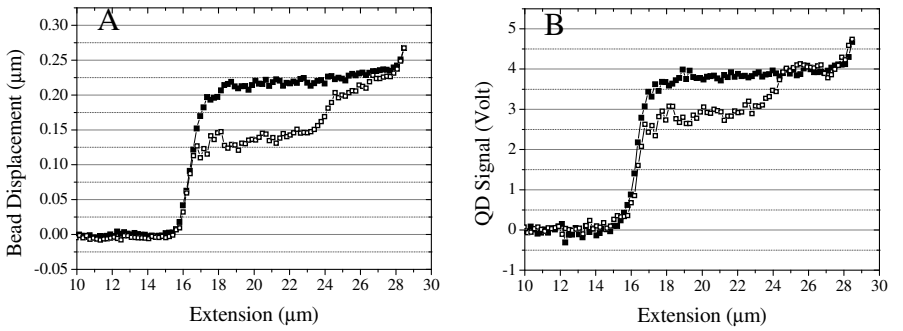

Fig. 15

Bead displacement (A) and QD signal (B) recorded while stretching a single λ-phage DNA molecule. By determining the value of these parameters at the overstretching region of the DNA, both are calibrated, since this plateau is found at 65 pN (in 150 mM NaCl).

This method can be used in case the other methods do not give any or unreliable results, and otherwise validates the earlier determined calibration factors.

2.5
Force spectroscopy of single dsDNA

All the experiments described in this thesis start with the attachment of a single double-stranded λ-phage DNA molecule between two micron-sized (2.6 µm) polystyrene beads. Using this construct we can measure directly the force acting on the dsDNA as a function of dsDNA extension. Attachment of the dsDNA to the polystyrene bead is achieved by using end-biotinylated DNA, and streptavidin-coated polystyrene beads. The protocols for preparing this DNA and the beads and the procedure used to suspend a single molecule between the two beads are described in (7).

A buffer solution (10 mM Tris-HCL, pH 7.5, 1 mM EDTA, supplemented with 150 mM NaCl and 0.01% NaN_3) was used as a main flow buffer for performing force spectroscopy on the single dsDNA molecule. Experiments involving the interaction of YOYO-1 and YO-1 with dsDNA were performed by adding the dye in the above mentioned buffer such as to achieve the desired concentration. These buffers were bubbled with nitrogen gas before use to remove any dissolved oxygen, which is responsible for the enhanced photocleavage of dsDNA molecules (37-38) while performing fluorescence microscopy.

Force spectroscopy of the single dsDNA molecule is performed as follows. The suspended dsDNA molecule was stretched by moving the bead immobilized on the glass micropipette using an XYZ piezo stage, where the data acquisition was synchronized with the applied ramp to the XYZ stage. Due to the resolution of the data acquisition (DAQ) card (12-bits) the ramp was created with steps of 25 nm with the time between each step determined by the pulling speed as set in the software. For each step, the QD signal was acquired at a rate of 100 kHz, and this data was averaged. This displacement data in combination with the voltage obtained from the QD was used to calculate the force extension curve.

Fig. 16 presents a typical force extension and relaxation curve for a single double-stranded λ-phage DNA acquired at 3 μm/s pulling speed. To determine the various mechanical properties of the dsDNA, such as contour length, persistence length and stretch modulus, we fitted the experimental curve with an expression describing the extensible worm like chain model (WLC) (Eq. 8) (39). A custom-made Labview software program was developed to determine the best fit to the data based on visual inspection of the data and the fitted curve and by obtaining the lowest value for χ^2. For the extension part of the curve typical parameters obtained for bare dsDNA are: contour length of 16.4±0.2 μm, persistence length of 52.0±5 nm and a stretch modulus of 1200±200 pN. These values are in agreement with the values presented in the literature (18-19, 40).

$$F = \frac{k_B T}{L_p}\left[\frac{1}{4(1 - x/L_0 - F/S)^2} - \frac{1}{4} + \frac{x}{L_0} - \frac{F}{S}\right] \qquad (8)$$

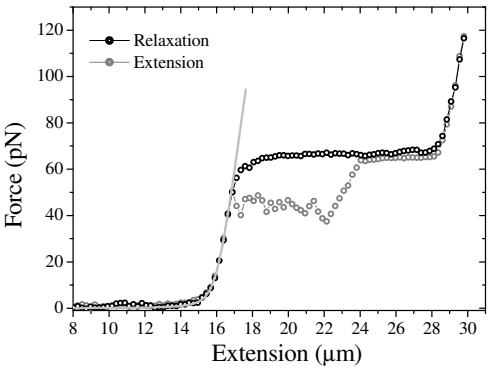

Fig. 16

Force extension and relaxation curve of double-stranded λ-phage DNA. Both the extension (black symbols) as well as the relaxation (gray symbols) of the cycle are shown. The solid gray line is the curve fitted line to the extension part of the curve up to a force of 50 pN with Eq. 7. The DNA was pulled at 3 μm/sec.

2.6
Fluorescence microscopy

An EMCCD camera (iXon DV887-BV; Andor, Belfast, Northern Ireland) was used to acquire the fluorescence images. The pixel size as used in the instrument was 16 x 16 μm, and the array has 512x512 pixels. The CCD array is back-illuminated, has single photon sensitivity, and an EM (Electron Multiplication) gain up to of 1000. The lowest chip temperature achieved was -60ºC. The sample was scanned back and forth at 12.5 Hz. This means that one forward and reverse sweep takes 80 ms. The exposure time of the EMCCD camera was set slightly larger than this (100 ms). All photons emitted from the fluorophores during one sweep were collected and imaged onto the EMCCD chip. Images can be acquired either one at a time or a sequence of the images can be acquired.

Fig. 17A presents a fluorescence image of a YOYO-1-labeled λ-phage DNA molecule with 100 nM YOYO-1 in the surrounding buffer. The complex was scanned at 12.5 Hz and a camera exposure time of 100 ms. The laser power at the back aperture of the objective was 3 μW. Fig 17B presents the intensity profile along a line perpendicular to the helical axis of dsDNA. Fitting this intensity profile with a Gaussian function gives a FWHM of 0.32 μm.

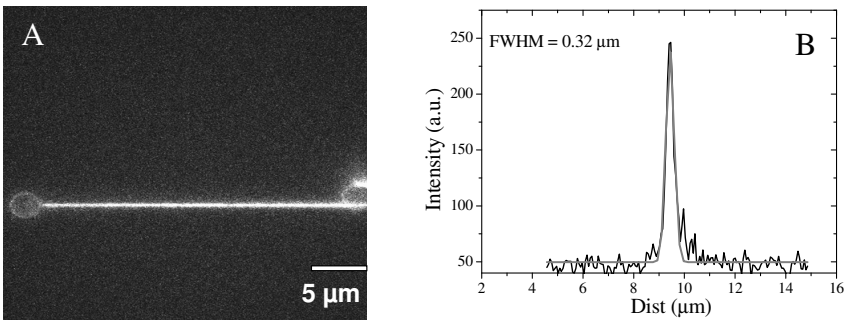

Fig. 17

Fluorescence image of a YOYO-1 labeled λ-phage DNA molecule in 100 nM YOYO-1. The acquisition time was 100 ms, and the scanning frequency was 12.5 Hz. Panel B presents the intensity profile of the dsDNA-YOYO-1 complex along a line drawn perpendicular to the dsDNA helical axis. Gray solid line presents a Gaussian fit to the intensity profile.

2.6.1
Single molecule detection

The ability of the instrument to detect a single dsDNA molecule that is labeled with a large number of dye molecules has been demonstrated in previous section. Here we test the ability of the instrument to detect a single molecule protein that is attached (bound) to the dsDNA. To this end, we have set up two experiments to fluorescently detect a single quantum dot and a single EcoRI protein.

In the first experiment, streptavidin coated quantum dots (Quantum Dot Corp. CA, USA) were used. In contrast to suspending the dsDNA between two beads, only one bead was caught and a single dsDNA molecule was attached to this. The attachment of the dsDNA to the trapped bead was detected by a step-wise increase in the QD signal. Next, a buffer containing the streptavidin-coated quantum dots was flown in. Due to the high affinity of streptavidin and biotin one single quantum dot was able to bind to the end of the dsDNA strand. Fig. 18A presents a fluorescence image of the quantum dot attached to the end of the dsDNA. In the image there are actually two quantum dots visible, which is most probably due to the presence of two dsDNA molecules that are attached to the trapped bead. Fig. 18B presents an intensity profile along a line crossing the intensity peak of the quantum dot. The FWHM of this profile was determined by fitting the intensity profile with a Gaussian function, and equals 0.30 µm.

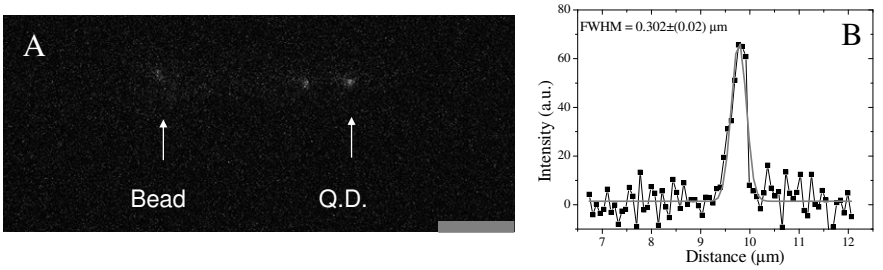

Fig. 18

(A) Fluorescent image of the two quantum dots attached to the end of the dsDNA. Scale bar 5 µm. (B) Intensity profile of the single quantum dot (extreme right). The width of obtained spot (FWHM) obtained by curve fitting data points with Gaussian fit is 0.30 µm.

2.6.2
Single protein detection

To demonstrate the ability of the instrument to detect a single protein molecule interacting with dsDNA, we studied the interaction of the EcoRI protein with the dsDNA. EcoRI is a restriction enzyme known to specifically bind and cleave dsDNA at the sequence (5' G|AATTC 3'). Fluorescence labeling of EcoRI was achieved by using amine reactive Alexa Fluor succinimidyl esters (Alexa-488, Invitrogen – Molecular Probes, Carlsbad CA, USA) that react with the primary amines ($R\text{-}NH_2$) located on the proteins. The λ-DNA that is used in the experiments contains 5 positions with this sequence. The distance of these five specific binding sites on the λ-DNA starting from one end is 7.22, 8.87, 10.79, 13.32 and 15.29 µm respectively. In the presence of Mg^{2+} ions this protein cleaves the λ-DNA but in the presence of Ca^{2+} ions the EcoRI only binds to the specific cleavage site without cleaving the λ-DNA. Fig. 19A shows the force extension and relaxation curve of an individual dsDNA molecule with a single EcoRI protein bound to it. As anticipated, the mechanical properties of the dsDNA with one single EcoRI protein bound to it is not significantly different from that of bare dsDNA (L_0 = 16.42 µm, L_p = 49 nm, S = 1070 pN). Fig. 19B presents images of dsDNA-EcoRI complexes at various extensions of the dsDNA. The first image is recorded at an extension of ~16.4 µm. The distance of the EcoRI from the trapped bead is 8.63 µm, which is in reasonable agreement with the second binding site (at 8.87 µm). Consecutive images were acquired by stretching the DNA-EcoRI complex further even into the overstretching region, revealing that the EcoRI protein remains bound on the dsDNA. The signal-to-noise ratio in these fluorescence images is 28 (±4).

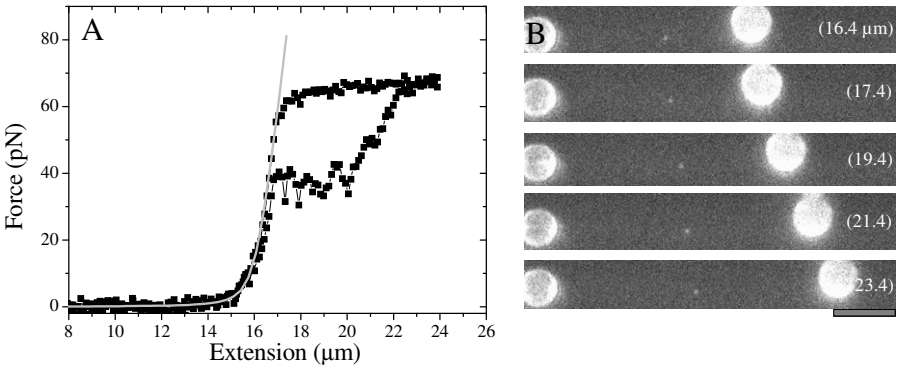

Fig. 19

(A) Force extension relaxation curve of a λ-DNA molecule with an EcoRI protein bound. Gray curve is the curve-fit with an extensible wormlike chain model. (B) Fluorescence images of λ-DNA-EcoRI complex at DNA extensions of 16.4, 17.4, 19.4, 21.4 and 23.4 μm respectively. Scale bar is 5 μm, exposure time is 5 sec and scanning rate is 0.22 Hz.

2.7

Development of software to acquire simultaneous force spectroscopy data and fluorescence images

In order to have simultaneous measurements of the force extension curve and the fluorescence intensity or images, specific software and hardware has been developed in order to synchronize the different parts.

The optical tweezers instrument is run by a custom-made Labview program which controls the movement of the stage and at the same time acquires the data from the QD in order to construct a force extension curve. The EMCCD camera that is used to record the fluorescence images has its own stand-alone software, which controls the mode of acquisition (single frame, or sequence). The scanning mirror (which scans the line-shaped beam) is controlled by a sawtooth signal that is generated by a programmable function generator. In order to make the integrated system work, these three systems need to be connected such that they operate in a synchronized way.

The first step is the synchronization of the scanning mirror and the EMCCD camera. This is realized by a TTL pulse that is generated as soon as the EMCCD starts to acquire an image. The signal is 'high' during the time an image is acquired. This pulse acts as a trigger for the function generator and the shutter which is open for the duration of the TTL pulse (frame acquisition time). The function generator is programmed to generate one period of a triangular wave which is fed into the controller of the scanning mirror. The scanning frequency of the scanning mirror is always set slightly higher than that of image

acquisition frequency, to make sure that a full forward and backward movement of the beam-shaped profile is finished within one frame of the EMCCD camera. Typical numbers are 12.5 Hz for the scanning mirror and 10 Hz for the EMCCD image acquisition rate. The different synchronization signals as a function of time are presented in the Fig. 20.

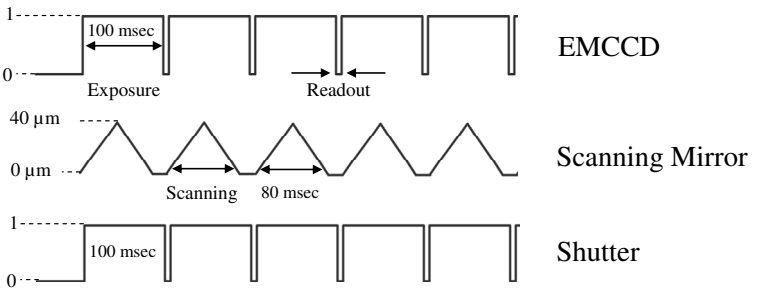

Fig. 20
Various signals used for synchronizing the different components in the line-scanning fluorescence microscopy.

The second step is the synchronization of the force spectroscopy and the acquisition of fluorescence images. This is done by a slight adaptation of the optical tweezers control software. At the moment that a force spectroscopy experiment is starting, the computer generates a TTL pulse that acts as a trigger for the EMCCD camera. As soon as the EMCCD camera starts its operation it will trigger the operation of the scanning mirror and the shutter. As an additional signal the TTL pulse generated by the EMCCD camera is also read by the data acquisition card. This allows the user to count the images and uniquely label each recorded image (with an image number) and relate these with the force extension data. The signal and triggering scheme is presented in Fig. 21.

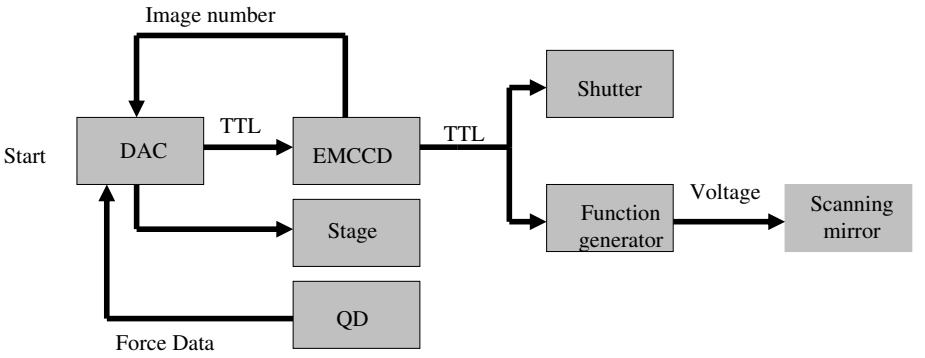

Fig. 21
Schematic presentation of the signals shared between the different components of the combined optical tweezers and line-scanning fluorescence microscopy.

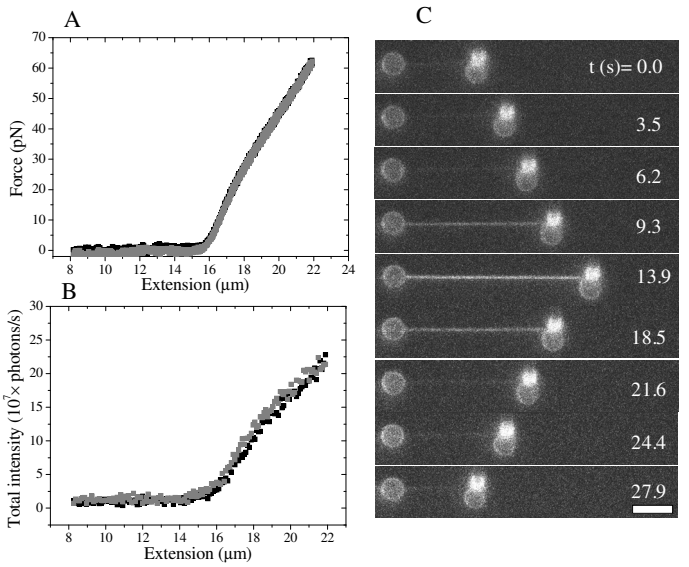

Fig. 22

Data from a simultaneous force spectroscopy and fluorescence microscopy experiment performed on λ-phage DNA in the presence of 100 nM YO-1. (A) Force extension curve (B) Total fluorescence intensity as function of DNA extension. Both curves show extension (black symbols) as well as the relaxation (gray symbols). Pulling speed is 1 µm/s. (C) Selected fluorescence images from the total sequence of images acquired during the experiment. Scale bar is 5 µm.

Fig. 22 shows a force extension and relaxation curve and simultaneously recorded fluorescence images of dsDNA in the presence of 100 nM YO-1. The fluorescence images were acquired at 10 Hz with a 3 µW laser power measured at the back aperture of the objective. From the fluorescent images the total fluorescence intensity was determined and this is plotted as a function of the extension in Fig. 22B. As the complex is stretched, the total fluorescent intensity of the complex increases as function of extension. A more detailed analysis of these results and interpretation is described in chapter 3.

2.8
Conclusions

Successful integration of an optical tweezers instrument and line-scanning fluorescence microscopy has been realized. The various technical challenges have been described and addressing these challenges adequately lead to the combined system. The power spectral density method that was used to determine the trap stiffness was shown to give variable results. Multiple power spectra need to be taken and analyzed in order to get a reliable value for the trap stiffness.

Force spectroscopy on single λ-DNA molecules can be done routinely as shown in Fig. 16. Recording fluorescence images of a suspended dsDNA-YOYO-1 complex with the instrument was demonstrated in Fig. 17. The ability to detect single molecules using fluorescence detection was shown by imaging a single quantum dot attached to the end of the dsDNA (Fig. 18) and by imaging a single EcoRI protein bound to the dsDNA (Fig. 19). Simultaneous force spectroscopy and fluorescence microscopy was performed on a single double-stranded DNA molecule in a buffer containing 100 nM YO-1 (Fig. 22). In conclusion the present instrument is performing as expected and has a great potential in the study of various biophysical problems at the single molecular level such as the interactions between DNA and proteins.

2.9
References

1. Bennink, M. L., D. N. Nikova, K. O. van der Werf, and J. Greve. 2003. Dynamic imaging of single DNA-protein interactions using atomic force microscopy. Analytica Chimica Acta 479:3-15.
2. Bustamante, C., and D. Keller. 1995. Scanning Force Microscopy in Biology. Physics Today 48:32-38.
3. Bahatyrova, S., R. N. Frese, C. A. Siebert, J. D. Olsen, K. O. van der Werf, R. van Grondelle, R. A. Niederman, P. A. Bullough, C. Otto, and C. N. Hunter. 2004. The native architecture of a photosynthetic membrane. Nature 430:1058-1062.
4. van Noort, S. J. T., K. O. van der Werf, A. P. M. Eker, C. Wyman, B. G. de Grooth, N. F. van Hulst, and J. Greve. 1998. Direct visualization of dynamic protein-DNA interactions with a dedicated atomic force microscope. Biophysical Journal 74:2840-2849.
5. Block, S. M., L. S. B. Goldstein, and B. J. Schnapp. 1990. Bead Movement by Single Kinesin Molecules Studied with Optical Tweezers. Nature 348:348-352.
6. Wuite, G. J. L., S. B. Smith, M. Young, D. Keller, and C. Bustamante. 2000. Single-molecule studies of the effect of template tension on T7 DNA polymerase activity. Nature 404:103-106.
7. Bennink, M. L., O. D. Scharer, R. Kanaar, K. Sakata-Sogawa, J. M. Schins, J. S. Kanger, B. G. de Grooth, and J. Greve. 1999. Single-molecule manipulation of double-stranded DNA using optical tweezers: Interaction studies of DNA with RecA and YOYO-1. Cytometry 36:200-208.
8. Bennink, M. L., S. H. Leuba, G. H. Leno, J. Zlatanova, B. G. de Grooth, and J. Greve. 2001. Unfolding individual nucleosomes by stretching single chromatin fibers with optical tweezers. Nature Structural Biology 8:606-610.
9. Kassies, R., A. Lenferink, I. Segers-Nolten, and C. Otto. 2005. Prism-based excitation wavelength selection for multicolor fluorescence coincidence measurements. Applied Optics 44:893-897.
10. Segers-Nolten, G. M., C. Wyman, N. Wijgers, W. Vermeulen, A. T. Lenferink, J. H. Hoeijmakers, J. Greve, and C. Otto. 2002. Scanning confocal fluorescence microscopy for single molecule analysis of nucleotide excision repair complexes. Nucleic Acids Research 30:4720-4727.
11. Zhang, D., H. Lans, W. Vermeulen, A. Lenferink, and C. Otto. 2008. Quantitative fluorescence correlation spectroscopy reveals a 1000-fold increase in lifetime of protein functionality. Biophysical Journal 95:3439-3446.
12. Lang, M. J., P. M. Fordyce, A. M. Engh, K. C. Neuman, and S. M. Block. 2004. Simultaneous, coincident optical trapping and single-molecule fluorescence. Nature Methods 1:133-139.
13. Harada, Y., T. Funatsu, K. Murakami, Y. Nonoyama, A. Ishihama, and T. Yanagida. 1999. Single-molecule imaging of RNA polymerase-DNA interactions in real time. Biophysical Journal 76:709-715.
14. Hohng, S., R. B. Zhou, M. K. Nahas, J. Yu, K. Schulten, D. M. J. Lilley, and T. J. Ha. 2007. Fluorescence-force spectroscopy maps two-dimensional reaction landscape of the Holliday junction. Science 318:279-283.
15. van Mameren, J., E. J. G. Peterman, and G. J. L. Wuite. 2008. See me, feel me: methods to concurrently visualize and manipulate single DNA molecules and associated proteins. Nucleic Acids Research 36:4381-4389.

16. Ashkin, A., and J. M. Dziedzic. 1971. Optical Levitation by Radiation Pressure. Applied Physics Letters 19:283-&.
17. Ashkin, A., J. M. Dziedzic, J. E. Bjorkholm, and S. Chu. 1986. Observation of a Single-Beam Gradient Force Optical Trap for Dielectric Particles. Optics Letters 11:288-290.
18. Smith, S. B., Y. J. Cui, and C. Bustamante. 1996. Overstretching B-DNA: The elastic response of individual double-stranded and single-stranded DNA molecules. Science 271:795-799.
19. Cluzel, P., A. Lebrun, C. Heller, R. Lavery, J. L. Viovy, D. Chatenay, and F. Caron. 1996. DNA: An extensible molecule. Science 271:792-794.
20. Kellermayer, M. S. Z., S. B. Smith, H. L. Granzier, and C. Bustamante. 1997. Folding-unfolding transitions in single titin molecules characterized with laser tweezers. Science 276:1112-1116.
21. Crocker, J. C., and D. G. Grier. 1996. Methods of digital video microscopy for colloidal studies. Journal of Colloid and Interface Science 179:298-310.
22. Dinsmore, A. D., A. G. Yodh, and D. J. Pine. 1996. Entropic control of particle motion using passive surface microstructures. Nature 383:239-242.
23. Rubinsztein-Dunlop, H., T. A. Nieminen, M. E. J. Friese, and N. R. Heckenberg. 1998. Optical trapping of absorbing particles. Advances in Quantum Chemistry, Vol 30 30:469-492.
24. Huisstede, J. H. G. 2006. Scanning probe optical tweezers : a new tool to study DNA-protein interactions. Enschede. 132.
25. Hirschfeld, T. 1976. Optical Microscopic Observation of Single Small Molecules. Applied Optics 15:2965-2966.
26. Kassies, R., K. O. van der Werf, A. Lenferink, C. N. Hunter, J. D. Olsen, V. Subramaniam, and C. Otto. 2005. Combined AFM and confocal fluorescence microscope for applications in bio-nanotechnology. J Microsc 217:109-116.
27. Pawley, J. B. 1995. Handbook of biological confocal microscopy. Plenum Press, New York.
28. Sandison, D. R., and W. W. Webb. 1994. Background Rejection and Signal-to-Noise Optimization in Confocal and Alternative Fluorescence Microscopes. Applied Optics 33:603-615.
29. Sabharwal, Y. S., A. R. Rouse, L. Donaldson, M. F. Hopkins, and A. F. Gmitro. 1999. Slit-scanning confocal microendoscope for high-resolution in vivo imaging. Applied Optics 38:7133-7144.
30. Im, K. B., S. M. Han, H. Park, D. Kim, and B. M. Kim. 2005. Simple high-speed confocal line-scanning microscope. Optics Express 13:5151-5156.
31. Fallman, E., and O. Axner. 1997. Design for fully steerable dual-trap optical tweezers. Applied Optics 36:2107-2113.
32. Huisstede, J. H. G., K. O. van der Werf, M. L. Bennink, and V. Subramaniam. 2005. Force detection in optical tweezers using backscattered light. Optics Express 13:1113-1123.
33. Svoboda, K., and S. M. Block. 1994. Biological Applications of Optical Forces. Annual Review of Biophysics and Biomolecular Structure 23:247-285.
34. Visscher, K., and S. M. Block. 1998. Versatile optical traps with feedback control. Molecular Motors and the Cytoskeleton, Pt B 298:460-489.
35. Gittes, F., and C. F. Schmidt. 1998. Thermal noise limitations on micromechanical experiments. European Biophysics Journal with Biophysics Letters 27:75-81.
36. Moffitt, J. R., Y. R. Chemla, S. B. Smith, and C. Bustamante. 2008. Recent advances in optical tweezers. Annual Review of Biochemistry 77:205-228.

37. Gurrieri, S., K. S. Wells, I. D. Johnson, and C. Bustamante. 1997. Direct visualization of individual DNA molecules by fluorescence microscopy: Characterization of the factors affecting signal/background and optimization of imaging conditions using YOYO. Analytical Biochemistry 249:44-53.
38. Akerman, B., and E. Tuite. 1996. Single- and double-strand photocleavage of DNA by YO, YOYO and TOTO. Nucleic Acids Research 24:1080-1090.
39. Marko, J. F., and E. D. Siggia. 1995. Stretching DNA. Macromolecules 28:8759-8770.
40. Husale, S., W. Grange, M. Karle, S. Burgi, and M. Hegner. 2008. Interaction of cationic surfactants with DNA: a single-molecule study. Nucleic Acids Research 36:1443-1449.

Chapter 3

Interaction of oxazole yellow dyes with dsDNA studied with combined optical tweezers – line scanning fluorescence microscopy

Abstract

We have studied the force extension behavior of individual dsDNA molecules in the presence of 100 nM YOYO-1 and YO-PRO-1 intercalating molecules with the help of combined optical tweezers – fluorescence microscopy. The fluorescence modality was used to record fluorescent images during the stretching and relaxation cycle. In recording the force extension curves, for bare dsDNA the characteristic overstretching transition was not observed in the presence of either dye. Using the wormlike chain model to curve-fit the force extension data revealed a contour length increase of 6% and 30% in the presence of YO-PRO-1 and YOYO-1 respectively. The simultaneously recorded fluorescence images showed that the number of bound dye molecules increased as the dsDNA molecule was stretched and decreased again as the force on the complex was lowered. In the case of dsDNA-YOYO-1 complexes the force extension curves showed hysteresis between the stretching and relaxation cycles, indicative of a kinetics-limited system. The rate of YO-PRO-1 binding and unbinding was found to be 2 orders of magnitude larger than that for YOYO-1. A kinetic model is proposed to explain this observation.

The content of this chapter is based on:
Murade, C. U., V. Subramaniam, C. Otto, M. L. Bennink. 2009. Interaction of oxazole yellow dyes with DNA studied with hybrid optical tweezers and fluorescence microscopy. Biophys. J. 97:835-843.

3.1
Introduction

Intercalation is a binding mode in which small molecules insert their planar aromatic moiety between two adjacent basepairs of double-stranded DNA (dsDNA) (1). As a result of this binding mode the length of the dsDNA molecule increases and this may disturb processes such as transcription, replication and dsDNA repair, which involve specific interactions between proteins and dsDNA (2). Some fluorescent intercalators are used in single dsDNA molecule fluorescence studies. Other intercalators, such as cisplatin, because of their specific property of interfering with dsDNA-protein interactions, are used in anti-cancer drug formulations (3). Understanding the interaction kinetics of these intercalating agents to dsDNA is of utmost importance in the development of more specific and efficient drugs (4).

Absorption spectroscopy, linear dichroism and ^{1}H NMR spectroscopy have been used to characterize the structure, binding mode, optical and photophysical properties of the YOYO-1/YO-1 molecules, both free and bound to dsDNA (5-7). Single molecule techniques such as optical tweezers and atomic force microscopy have probed the mechanical properties of individual dsDNA molecules in interaction with YO-1 and YOYO-1 and other intercalating agents (8-11). These studies show that depending on the intercalator concentration the overstretching plateau, typically observed in stretching bare dsDNA, shortens, tilts and eventually disappears (see Chapter 5). In a recent study by Vladescu et al. (12-13) the mechanical properties of dsDNA in interaction with the mono-intercalator ethidium were studied. It was shown that the binding constant of the ethidium increases from $4.6 \cdot 10^{5}$ M^{-1} at zero force to $5.5 \cdot 10^{7}$ M^{-1} at a force of 80 pN. Furthermore it was found that the size of the binding site of ethidium reduced from 2.4 bp to 1.7 bp.

Here we present a single molecule study using optical tweezers combined with line scanning fluorescence microscopy imaging in which we study the interaction of individual dsDNA molecules with the oxazole yellow dyes YO-1 and YOYO-1. Using combine optical tweezers and fluorescence microscopy, the mechanical properties of individual dsDNA molecules can be directly related to the number of fluorescent molecules bound to the dsDNA and their distribution. Furthermore force relaxation experiments were carried out to get more detailed insight into the kinetics of YO-1 and YOYO-1 binding to dsDNA. The binding and unbinding rate of YOYO-1 was two orders of magnitude lower than for YO-1. We propose a model which describes and explains the interaction kinetics measured for the intercalating oxazole yellow molecules.

3.2
Properties of YO-1 and YOYO-1

The dimer YOYO-1 and monomer YO-PRO-1 (YO-1) are oxazole yellow dyes (5, 14-15), that bind to dsDNA through intercalation (Fig. 1). The YO-1 molecule carries a net positive charge of +2 and has only one single aromatic moiety that intercalates between the basepairs of dsDNA (Fig. 1A). YOYO-1 is a bis-intercalator with two intercalating aromatic moieties connected via a linker and carries a net positive charge of +4 (Fig. 1B). Both moieties intercalate between basepairs leaving one position in between unoccupied (10). The estimated binding constant for YOYO-1 to dsDNA is 10^{10}-10^{12} M^{-1}, while YO-1 has been reported to have a lower affinity (7).

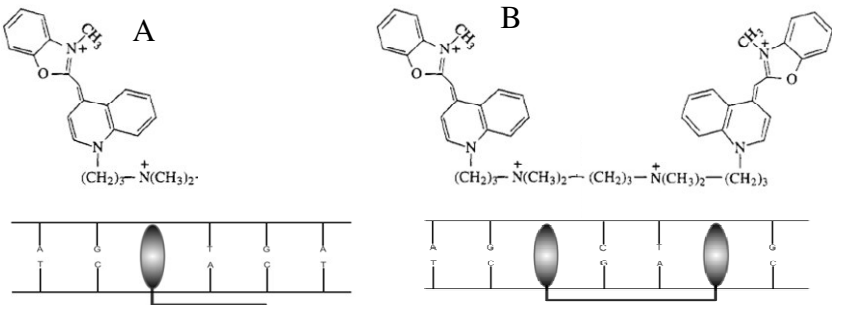

Fig. 1
Chemical structure and schematic representation of (A) YO-1 (mono intercalation) and (B) YOYO-1 (bis intercalation) bound to dsDNA.

The absorption and emission spectra of YO-1 and YOYO-1 bound to dsDNA are identical and is presented in Fig. 2. The absorption has a maximum at 491 nm and the maximum emission is at 509 nm. When not bound to dsDNA both dyes have a fluorescence intensity that is a few orders of magnitude lower. Because of this property these molecules have been used extensively in single molecule dsDNA detection and dsDNA protein interaction studies (6, 16-17). It allows one to achieve very high S/N ratio as the background signal resulting from free dye molecules is negligible. These intercalating molecules also act as photocleavage agents.

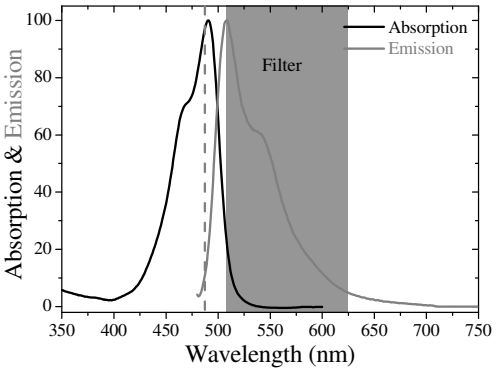

Fig. 2

Absorption and emission spectra of YO-1 and YOYO-1 when complexed with dsDNA. Dotted gray line presents the excitation wavelength used (488 nm) and gray area presents band pass filter used in detection path.

3.3

Materials and Methods

The combined optical tweezers – line scanning fluorescence microcopy instrument used here to study the dsDNA-dye interaction has been described in detail in chapter 2. Attachment of the dsDNA to two polystyrene beads was carried in a specialized flow cell as described in (11). The experiments were performed in a buffer solution containing 10 mM Tris-HCl, pH 7.5, 1 mM ethylenediaminetetraacetic acid (TE) supplemented with 150 mM NaCl and 0.05% NaN_3. After successfully attaching the molecule between two beads, force spectroscopy confirmed the single molecule attachment. Next the previously described buffer containing 100 nM of YOYO-1 or YO-PRO-1(Invitrogen - Molecular Probes, Carlsbad, California, USA) was added to the flowcell. This buffer was bubbled with nitrogen gas for 1 hr to remove dissolved oxygen to reduce quenching and photo damage of the fluorophores which causes the dsDNA to break (18-19).

Force spectroscopy experiments were performed at a rate of 3 μm/s, if no fluorescent images were recorded. In the experiments in which the fluorescence was simultaneously recorded, a rate of 1 μm/s was used. This pulling speed was chosen so as to acquire maximum number of fluorescence images before the dsDNA-dye complex breaks due to photocleavage. Fluorescence images were acquired at 10 Hz. The fluorescence intensities were obtained from the images by integrating for every frame the light intensity in a fixed-width rectangle with a length equal to the dsDNA length. This rectangle completely enclosed the entire DNA molecule at all extensions. An identical rectangle was taken in a dark region, the total integrated intensity of which was used for background-

correction. Fluorescence kymographs were constructed from the sequence of images as described in (20).

3.4
Results

3.4.1
Force spectroscopy of dsDNA-YOYO-1 complex

Force extension curves were recorded on individual dsDNA molecules in the absence and presence of 100 nM YOYO-1 (Fig. 3A). In the absence of dye molecules the overstretching transition was observed at about 65 pN and typical hysteresis was observed between 17 and 24 µm during relaxation. The contour length (16.4 ± 0.2 µm), persistence length (52 ± 4 nm) and stretch modulus (1100 ± 100 pN) were determined from the force extension data with the help of the extensible worm-like chain model (EWLC) (21). These results are in good agreement with published results (22-23).

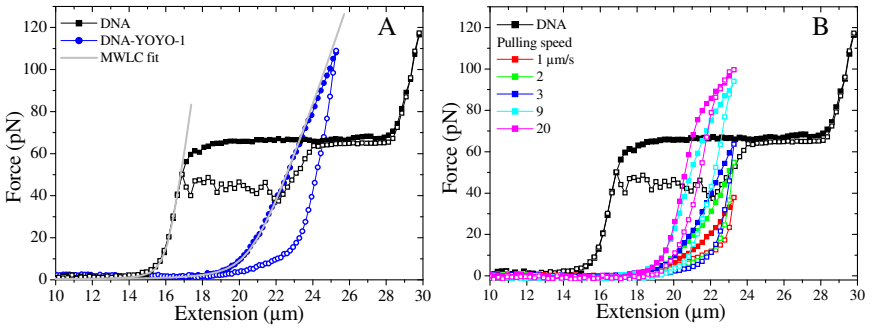

Fig. 3
(A) Force extension curves of the dsDNA in the presence and absence of 100 nM YOYO-1. The gray line presents the EWLC fit to the extension part of the force extension relaxation curves. The pulling speed is 3µm/s. (B) Force extension curves of the dsDNA in presence of 100 nM YOYO-1 obtained at different pulling speeds. For reference the curve obtained with no YOYO-1 is included. Closed and open symbols represent the stretching and relaxation cycle respectively.

In 100 nM YOYO-1 the force extension and relaxation of dsDNA were remarkably different. The overstretching transition was not observed, the contour length was increased by about 30%, the persistence length and the stretch modulus reduced. We also observed hysteresis between the stretching and relaxation cycle, which is entirely different from the one observed for bare dsDNA. These changes were qualitatively similar

to those observed by Sischka *et al.* (10), where a YOYO-1 concentration of 1 µM was used. Fig. 3B shows force extension curves of the dsDNA-YOYO-1 complex when pulled at different pulling speeds to a same extension. Force extension curves were fitted using the EWLC model and the resulting parameters are listed in Table 1. As the pulling speed is increased from 1 to 20 µm/s the maximum force experienced by the complex increases and the contour length decreases. These force extension curves are highly reproducible. The dependence of the force extension curves on the pulling rate and the observed hysteresis suggests that the amount of dye molecules on the suspended dsDNA in 100 nM YOYO-1 is not constant during the stretching experiment and that the binding and unbinding rates are the limiting factor.

Table 1 Resulting parameters from the curve-fit with the EWLC model

Pulling speed µm/s	Persistence length (nm)	Contour length (µm)	Stretch modulus (pN)
1	8.80	22.38	415
2	14.40	21.37	443
3	16.70	21.32	577
9	25.60	20.36	943
20	32.10	20.29	1120

Mechanical and elastic parameters of dsDNA-YOYO-1 complex obtained by curve fitting the extension part by the EWLC model to the force extension of the dsDNA-YOYO-1 complex at 100 nM YOYO-1 pulled at different pulling speeds.

3.4.2 Simultaneous force and fluorescence spectroscopy

The results of the force spectroscopy on the dsDNA-YOYO-1 complex suggested that the amount of YOYO-1 is not constant and that the system is not in equilibrium with the surrounding buffer. To further test this hypothesis we performed simultaneous force and fluorescence experiments as described in the Material and Methods section. Fig. 4A presents nine selected fluorescent images recorded while performing simultaneous force fluorescence spectroscopy. Fig. 4B shows the total fluorescent intensity of the dsDNA-YOYO-1 complex as a function of the force. As the force on the complex increased the total fluorescent intensity of the complex increased. As soon as the force on the complex was reduced again, the total fluorescent intensity also dropped. However this curve showed a significant hysteresis. The total intensity during the relaxation phase is much higher than the total intensity during the stretching phase at equal forces. This further supports the notion that dsDNA-YOYO-1 complex is not in equilibrium with the surrounding buffer. From the sequence of images recorded while performing simultaneous force fluorescence spectroscopy, a kymograph has been created (Fig. 4C).

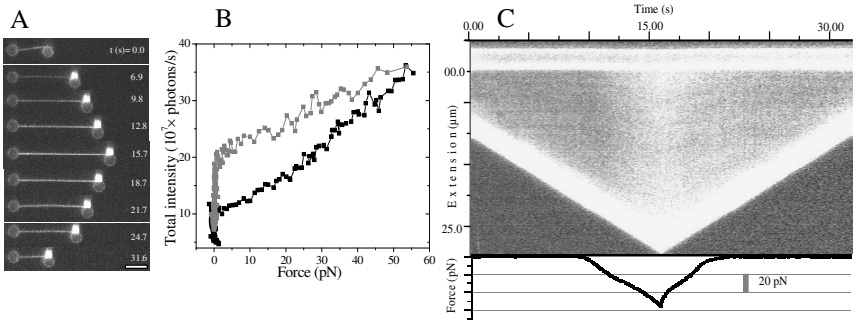

Fig. 4

(A) Fluorescence images taken from a sequence recorded during the extension and relaxation of the dsDNA-YOYO-1 complex in the presence of 100 nM YOYO-1 (Pulling speed is 1 µm/s, scale bar 5 µm). (B) Total fluorescence intensity plotted as a function of force (■ extension, ■ relaxation), (C) Kymograph created from the sequence of images recorded simultaneously while performing force spectroscopy, where the horizontal axis represents time, and the vertical axis is extension. Two extreme bright bands in the kymograph represent the streptavidin coated polystyrene beads at either end of the dsDNA molecules. The force on the complex is plotted as a function of time in the plot below the kymograph.

The fluorescence intensity is linearly proportional to the number of YOYO-1 molecules when one assumes (i) a single, intercalative, binding mode of YOYO-1 with dsDNA which contributes significantly to the fluorescence (24), and (ii) there is no interaction between neighboring dye molecules. Here we showed for the first time using fluorescence microscopy that the number of intercalating molecules bound to the dsDNA increased as the force applied to the dsDNA increased. Vladescu *et al.* (13) recently reported this but based on the measured increase in fractional elongation which was deduced from the force extension curves. The fractional elongation γ due to the intercalation of the molecules into the dsDNA helical structure is defined as: (13)

$$\gamma(F) = \frac{x_{complex}(F) - x_{DNA}(F)}{x_{DNA}(F)} \qquad (1)$$

Here $x_{complex}(F)$ and $x_{DNA}(F)$ represents the length of dsDNA at force F, respectively in the presence and absence of YOYO-1 or YO-1. Performing this analysis on our stretching and relaxation data and plotting the fractional elongation versus the total fluorescence intensity (Fig. 5) revealed a linear relationship between the two parameters, showing that the fractional elongation is indeed proportional to the number of intercalated dye molecules. Since each intercalating YOYO-1 molecule increases the contour length of dsDNA by 0.884 nm (6), one can calculate the number of molecules bound to dsDNA using:

$$n = \frac{x_{complex}(F) - x_{DNA}(F)}{elongation\ per\ intercalator} \qquad (2)$$

From the slope the fluorescence emission per YOYO-1 molecule is calculated to be (41.7 ± 0.8)·10^3 photons/s at 0.4 kW/cm^2 power in the focal plane

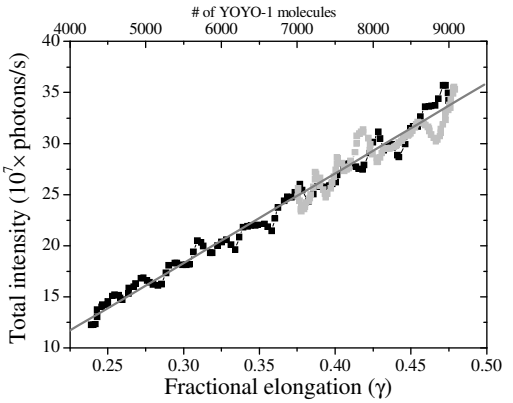

Fig. 5

Total fluorescence intensity versus the fractional elongation obtained during the stretching (■) and relaxation (■) of a dsDNA molecule in 100 nM YOYO-1. The number of YOYO-1 molecules (top x axis) is calculated from the fractional elongation. Solid gray line presents the linear fit to the data.

3.4.3
Constant extension experiments

To acquire more quantitative information on the kinetics of the dsDNA-YOYO-1 interaction, dsDNA was stretched to different preset extensions with a pulling rate of 3 µm/s. Subsequently the force was recorded while the extension remained constant. Fig. 6A shows force relaxation results for different constant extensions (21.5, 22.5, 23.5, 24.5 and 25.5 µm). The force drops exponentially to a lower value. In all cases the force dropped to 58.8 ± 5.0 % of its initial value independent of the absolute value of the initial force. Changes in the pulling rate, however, did have an effect on this relative drop in force. When pulling rates were varied from 1 to 5 µm/s (Fig. 7), this relative drop in force increased linearly as function of the pulling rate. For higher pulling rates this relative drop in force remained constant at 67.8 ± 0.5 % (Fig. 7B). The force towards which the system equilibrated (i.e. equilibrium force) is independent of the pulling speed but depends on the extension to which it has been pulled (Fig. 7A).

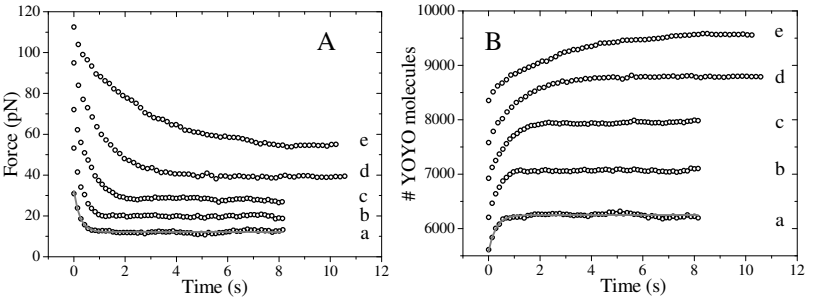

Fig. 6

(A) Force as a function of time recorded as the dsDNA molecule is left to equilibrate after being pulled to different extensions at 3 µm/s pulling speed in the presence of 100 nM YOYO-1. Curves a-e represent constant extension of 21.5, 22.5, 23.5, 24.5, 25.5 µm respectively. (B) The number of YOYO-1 molecules bound to dsDNA as function of time during force relaxation was calculated using Eq. 2. Gray solid line represent the single exponential function curve fitting to the obtained curves a in A and B. The time axis has its original at the point where the complex has been extended to the preset extension.

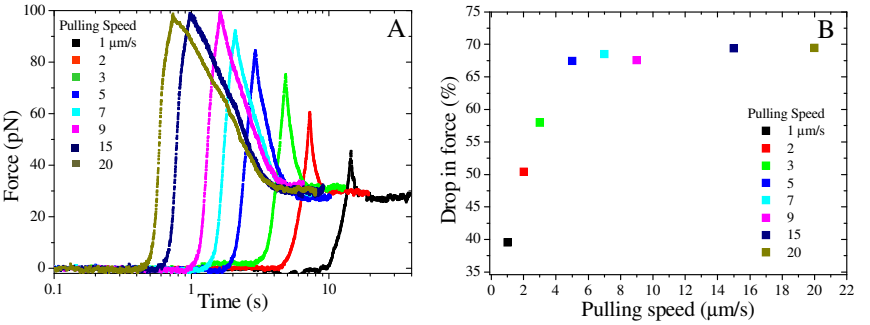

Fig. 7

dsDNA-YOYO-1 complex pulled at different pulling speeds to 23.5 µm extension (A) Force as a function of time recorded during a relaxation experiment (B) Drop in the in force (%) as function of pulling speed.

The data in Fig. 6A is curve fitted with a single exponential function to acquire a characteristic time constant τ_{FR}, which is presented in Table 2. The exponential decrease in force reflects the binding of YOYO-1 molecules in order to restore equilibrium. The larger the extension at which the complex was held, the larger the initial force and the larger the τ_{FR}. We also curve-fitted the data in Fig. 6B with a single exponential function, resulting in similar values for the time constants (Table 2).

Table 2 Characteristic relaxation time constant.

Extension (μm)	Time constant τ_{FR} (s)	Time constant $\tau_{\#YOYO}$ (s)
21.5	0.23	0.25
22.5	0.33	0.35
23.5	0.64	0.66
24.5	1.13	1.18
25.5	2.54	2.63

Characteristic time constant describing the relaxation, obtained from curve-fitting the data in Fig. 6A and 6B

Both the force spectroscopy and constant extension experiments along with simultaneous fluorescence – force spectroscopy clearly illustrates that the dsDNA-YOYO-1 complex is out-of-equilibrium during the force extension and relaxation experiments. The complex requires typically 0.2 to 2.5 seconds to restore equilibrium with its surrounding buffer.

3.4.4
Force spectroscopy of dsDNA-YO-1 complex

Force spectroscopy on dsDNA in the presence of 100 nM YO-1 was performed, and the force extension behavior is presented in Fig. 8(A). The overstretching transition in dsDNA was not observed in the presence of the mono-intercalator YO-1. The curve-fitted contour length was 17.2 (±0.2) μm and the persistence length was 46 ± 4 nm. Between the stretching and relaxation curve no hysteresis was observed. In the enthalpic stretching regime, the force extension curve does reveal a change in slope from 13.9 pN/μm to 9.4 pN/μm at extensions beyond 18 μm. This change of slope can be attributed to a structural change in the dsDNA-YO-1 complex due to applied force. Varying the pulling speed from 1 to 20 μm/s did not lead to significant differences in force extension behavior (Fig. 8B), indicating that the binding of YO-1 to dsDNA is in equilibrium even at the largest pulling speed tested for. From this we conclude that the binding and unbinding rate constants of YO-1 with dsDNA are larger than those for YOYO-1 in interaction with dsDNA.

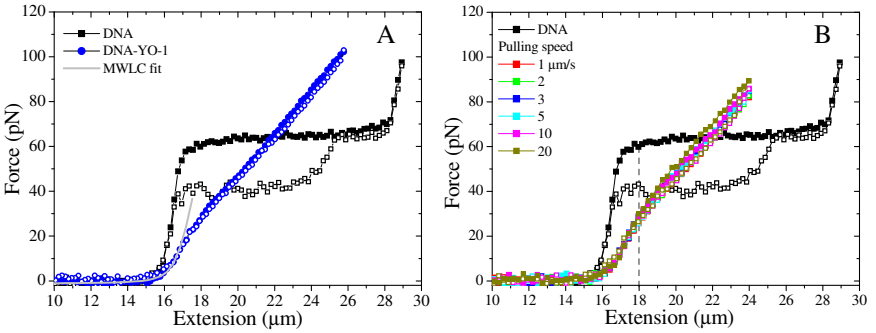

Fig. 8

(A) Force extension curves of dsDNA in the absence and presence of 100 nM YO. The solid gray line presents the EWLC curve fit to the force extension curve of dsDNA-YO-1 complex at forces lower than 20 pN. Pulling speed was 3 µm/s. (B) Force extension curve of dsDNA-YO-1 complex pulled at different pulling speeds. Dotted gray line indicates the change in slope at 18 µm as mentioned in the main text. Closed and open symbols present extension and relaxation respectively.

3.4.5
Simultaneous force and fluorescence spectroscopy of dsDNA-YO-1

As for dsDNA stretching in presence of YOYO-1, fluorescence images were also recorded for dsDNA stretching in 100 nM YO-1. Fig. 9A presents nine fluorescent microscopy images taken from the sequence at different points during the experiment. In Fig. 9B the fluorescence intensity as a function of force is plotted. No significant hysteresis (as was the case for YOYO-1) in the stretching and relaxation cycle was observed. Furthermore Fig. 9C shows the results in a kymograph format, where in we have observed the symmetry in the intensity. As has been observed for YOYO-1 (Fig. 4), the intensity of the dsDNA-YO-1 complex also increases as the force is increased. Although the absolute value of intensity at low forces for YO-1 ($2 \cdot 10^7$ photons/s) is much lower than for YOYO-1 ($8 \cdot 10^7$ photons/s). The fluorescence intensity was 5 times higher at 55 pN compared to the intensity at 5 pN. When the fluorescence intensity is plotted as a function of the extension (Fig. 10B), a slight change in the slope of the curve around an extension of 18 µm was observed, which coincides with the change in slope observed in the force extension curve (Fig. 8).

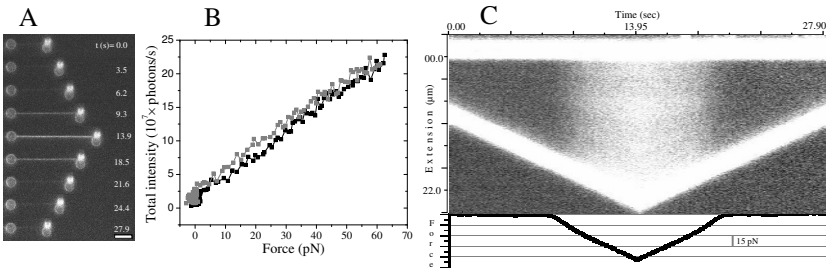

Fig. 9

(A) Fluorescence images taken from a sequence recorded during the extension and relaxation of the dsDNA-YO-1 complex in the presence of 100 nM YO-1, Pulling speed was 1 µm/s. Scale bar 5 µm. (B) Total fluorescence intensity plotted as a function of force (■ extension, ■ relaxation), (C) Kymograph created from a sequence of images recorded simultaneously while performing force spectroscopy, where the horizontal axis represents time, and the vertical axis is extension. The two bright lines in the kymograph represent the streptavidin coated polystyrene beads at either end of the dsDNA molecule. The force on the complex is plotted as a function of time in the plot below the kymograph.

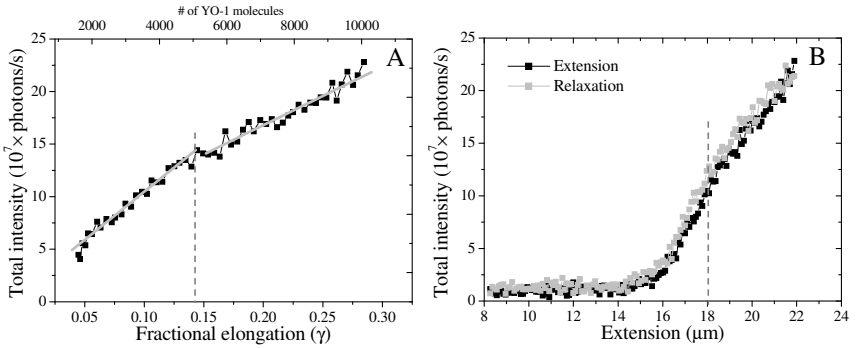

Fig. 10

(A) Total fluorescence intensity (■) versus the fractional elongation obtained during the stretching of a dsDNA molecule in 100 nM YO-1. The number of YO-1 molecules (top x axis) is calculated using Eq. 2. Data below and above a fractional elongation is fitted with two linear functions (gray lines), indicated by the dotted gray line. (B) Total intensity of the dsDNA-YO-1 complex as function of extension (■ extension, ■ relaxation). Dotted gray line at 18 µm indicates where the slope is changing.

Fig. 10A shows the fluorescence intensity as a function of the fractional elongation of the dsDNA-YO-1 complex. Here, again the two distinct regimes can be distinguished, before and after a fractional elongation of 0.14 (corresponds to 18 µm extension). From the slope of a linear fit for data below 0.14, an emission of $(23.2 \pm 0.8) \cdot 10^3$ photons/s per YO-1

molecule was determined. The power of the excitation beam is 0.4 kW/cm^2 power in the focal plane. This is about half the value of YOYO-1 (Fig. 5), which may be expected from the chemical composition of the molecule. However, at an extension beyond 18 µm a reduced slope of (14.5±0.8) $\cdot 10^3$ photons/s per YO-1 molecule was measured, which may be attributed to a force-induced structural transition in the dsDNA-YO-1 complex (for details please refer Chapter 5).

3.4.6
Constant extension experiments

Fig. 11 presents the force as a function of time obtained during constant extension experiments on dsDNA in the presence of 100 nM YO-1. After stretching the molecule to extensions of 18, 20, 22 and 24 µm no relaxation of the force was observed, corroborating the notion that the dsDNA-YO-1 complex is in equilibrium with the surrounding buffer. Assuming an exponential decay in force to reach the equilibrium (as observed for YOYO-1), a maximum characteristic time constant of 8 ms was determined. The number of YO-1 molecules bound to dsDNA is derived from the force extension data using Eq. 2 and plotted as a function of time (Fig. 11B). Here it is clear that the number of YO-1 molecules on the dsDNA remains constant as soon as the preset extension is reached.

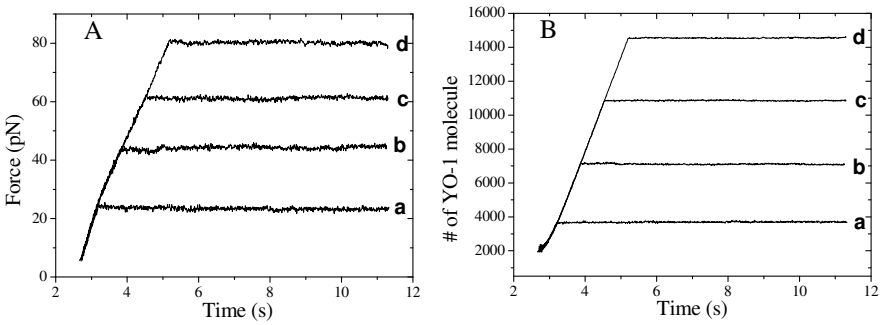

Fig. 11
(A) Force as a function of time recorded as a dsDNA molecule is pulled to preset extensions at 3µm/s pulling speed and then kept at these extensions in the presence of 100 nM YO-1 in the buffer. Curve a-d represents constant extensions of 18, 20, 22, and 24, µm respectively. (B) Number of YO-1 molecules on dsDNA as function of time during the experiment, derived from the force extension data.

3.5
Comparing interaction of YOYO-1 and YO-1 with dsDNA

From this study it is evident that the interaction kinetics of oxazole yellow dyes YO-1 and YOYO-1 with the dsDNA are different. First, we compared the fluorescence intensities at forces below 5 pN. The intensity of the dsDNA-YOYO-1 complex is about 4 times larger than that of dsDNA-YO-1 complex, indicating that twice the amount of dye molecules are bound to dsDNA. This difference is also reflected in the relative increase in contour length measured in the presence of either dye (6% for YO-1 and 30% for YOYO-1). The force extension curves of dsDNA in the presence of YOYO-1 clearly reveal hysteresis which was not observed in the presence of YO-1. This indicates a difference in binding and unbinding rates for the two intercalators. The hysteresis suggests that the YOYO-1 complex is not in equilibrium with its surrounding solution during the stretching and relaxation experiments whereas the dsDNA-YO-1 complex is. In the case of the bis-intercalator YOYO-1, typical times to restore equilibrium are on the order of seconds (see Fig. 6, Table 2). In the case of YO-1 relaxation was not observed with the time resolution of the data acquisition system, demonstrating that for YO-1 the characteristic time is smaller than 0.01 s, which is a difference of 2 orders of magnitude when compared to the bisintercalator YOYO-1.

3.6
Kinetic model

A kinetic model is presented to explain the differences observed in the interaction kinetics of the oxazole yellow mono and bis-intercalator with dsDNA. The long range interaction between positively charged oxazole yellow dyes and negatively charged dsDNA is determined by Coulombic interaction. In Fig. 12 the on- and off-rates of this interaction are described with k_1 and k_{-1}. This step is assumed to be diffusion-controlled and a rate of $1.6 \cdot 10^9$ $M^{-1}s^{-1}$ can be calculated for YOYO-1 using the Smoluchowski equation, indicating that this step is extremely fast with respect to the rate constants found in the results. For YO-1 this rate is slightly higher. In the case of YO-1 the next step in the intercalation process of YO-1 to dsDNA is the actual intercalation, described by the rate constants k_2 and k_{-2}. (Fig. 12A). From the force relaxation experiments the typical relaxation time for reaching equilibrium for YO-1 was found to be smaller than 0.01 s. Considering the fact that k_1 is so high, this measured rate is effectively k_2. The YOYO-1 molecule is a bis-intercalating agent which consists of two identical YO-1 moieties each bearing +2e charge. The proposed model assumes that actual intercalation of YOYO-1 occurs in two steps. In the first step one of the YO moieties intercalate in the dsDNA and in a second step the second YO moiety intercalates. The binding rate k_2 of the first moiety is assumed to be similar to that of YO-1 to dsDNA. With the first YO moiety of YOYO-1 bound to dsDNA, the second YO moiety resides close to the dsDNA molecule and a possible available

binding site (Fig. 12B(iii)). This leads to an increased effective concentration of the YO moiety locally and would result in a binding rate that is even higher than that for binding the first moiety (k_2). This however is not observed. Both the force spectroscopy data as well as the force relaxation measurements show that YOYO-1 binding to dsDNA is much slower than that of YO-1 binding. In order to account for this, an intermediate state is introduced within the model that is relatively stable, and which effectively reduces the intercalation rate for the 2nd YO moiety of a YOYO-1 (Fig. 12B(iii)). The rate converting the intermediate state to the final state k_3 has to be much lower than k_2, which results in an overall reduction of the binding rate from the unintercalated to the bis-intercalated state for YOYO-1. For YOYO-1 it means that k_3 is the rate limiting step (Fig. 12B from (iii) to (iv) state).

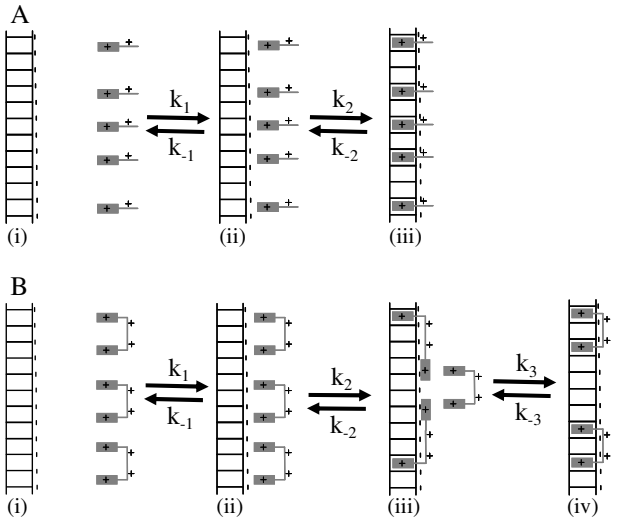

Fig. 12

Schematic illustration of different steps in the interaction of (A) YO-1 and (B) YOYO-1 molecules with dsDNA

Although the results presented in this chapter do not reveal the structure of the intermediate state, we assume that the intermediate state is one in which one YO moiety is intercalated and the second one is close to the dsDNA (Fig. 12B(iii)). It has been proposed that the non-intercalating moiety can strongly interact with the backbone of a dsDNA molecule (25). It is also possible that the non-intercalated YO moiety temporarily blocks some of the neighbouring binding sites effectively reducing the number of available binding sites, and results in a lower effective kinetic on-rate. The length of the linker which connects the two YO moieties is about 1.14 nm (7) and combined with the size of a YO moiety it is possible to cover approximately 5-6 base pairs. In the literature multiple force

spectroscopy studies of single dsDNA molecules in the presence of mono-intercalating and bis-intercalating molecules have been presented, and in most cases the bis-intercalating variant reveals more hysteresis than its mono-intercalating counterpart (10). We therefore hypothesize that the model proposed here is generally applicable to describe the binding of bis-intercalating agents to dsDNA.

To test this hypothesis we furthermore carried out the force extension relaxation experiments on the dsDNA in the presence of 100 nM ethidium (Eth, mono intercalator) and ethidium homo dimer (Eth-D, bis intercalator). Force extension curves are presented in Fig. 13(A). As observed in the case of YOYO-1 and YO-1 we do observe a hysteresis in the dsDNA-ethidium homo dimer complex and no hysteresis in the case of dsDNA-ethidium complex. By performing the force relaxation at constant extension experiments on the dsDNA-ethidium homo dimer complex we have observed that the force exerted by the complex decreased as soon as the present extension is reached Fig. 13(B) similar to YOYO-1 (Fig. 6A).

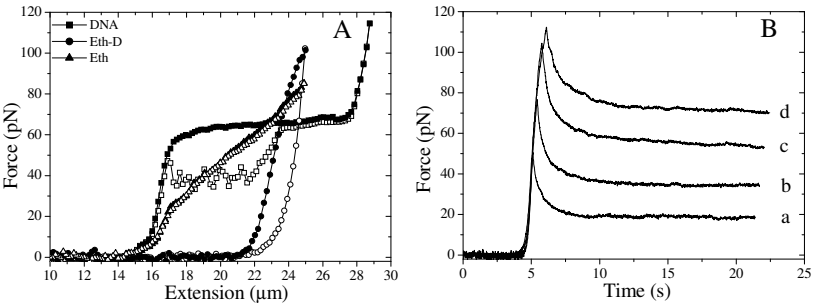

Fig. 13

(A) Force extension curve of bare λ-DNA compared with dsDNA-Eth and dsDNA-Eth-D complex at 100 nM. Closed and open symbols present extension and relaxation respectively. Force extension curves were obtained at 3μm/s pulling speed. (B) Force as a function of time recorded as a dsDNA molecule is pulled to preset extensions at 3μm/s pulling speed and then kept at these extensions in the presence of 100 nM ethidium homo dimmer in the buffer. Curve a-d represent constant extensions of 23, 24, 25 and 26, μm respectively

3.7
Conclusions

Using a combined optical tweezers and fluorescence microscope we have studied the interaction of the monointercalator YO-1 and bisintercalator YOYO-1 with a double-stranded DNA molecule. The contour length of the dsDNA increased upon addition of YO-1 and YOYO-1, which is a direct result of the intercalation of the dye between the basepairs of dsDNA. The number of molecules determined from the increase in contour length was correlated with the fluorescence intensity. For the first time using fluorescence microscopy it was shown that the number of YO-1 and YOYO-1 dye molecules bound to the dsDNA increased as the force applied to the dsDNA increased. Furthermore, from the hysteresis observed in the force extension curve and fluorescence intensity along with the results of the force relaxation experiments, it was concluded that the dsDNA-YOYO-1 complex, as opposed to the dsDNA-YO-1 complex was not in equilibrium with the surrounding medium. Force relaxation experiments at constant extension were performed, to determine the typical relaxation time for the dsDNA-dye complex after being stretched to different constant extensions. In the case of YOYO-1 this characteristic time increased for higher extensions, indicating that the relaxation was slower when initially there are more YOYO-1 molecules already bound to the dsDNA. In the case of YO-1 no significant hysteresis was observed in the force extension curve, suggesting that the characteristic relaxation time is smaller than 0.01 s. To explain this unexpected kinetic behavior, a model was proposed in which the YOYO-1 binding occurs via a relatively stable intermediate step, in which the second intercalation of the second YO-moiety forms the limiting step. This model is thought to be more generally applicable for bis-intercalating molecules.

3.8
References

1. Lerman, L. S. 1963. The structure of the DNA-acridine complex. Proc Natl Acad Sci U S A 49:94-102.
2. Xu, C., M. Losytskyy, V. Kovalska, D. Kryvorotenko, S. Yarmoluk, S. McClelland, and P. Bianco. 2007. Novel, Monomeric Cyanine Dyes as Reporters for DNA Helicase Activity. Journal of Fluorescence 17:671-685.
3. Hurley, L. H. 2002. DNA and its associated processes as targets for cancer therapy. Nat Rev Cancer 2:188-200.
4. Leng, F., W. Priebe, and J. B. Chaires. 1998. Ultratight DNA Binding of a New Bisintercalating Anthracycline Antibiotic†. Biochemistry 37:1743-1753.
5. Carlsson, C., A. Larsson, M. Jonsson, B. Albinsson, and B. Norden. 1994. Optical and Photophysical Properties of the Oxazole Yellow DNA Probes YO and YOYO. The Journal of Physical Chemistry 98:10313-10321.
6. Johansen, F., and J. P. Jacobsen. 1998. H-1 NMR studies of the bis-intercalation of a homodimeric oxazole yellow dye in DNA oligonucleotides. J Biomol Struct Dyn 16:205-222.
7. Larsson, A., C. Carlsson, M. Jonsson, and B. Albinsson. 1994. Characterization of the Binding of the Fluorescent Dyes Yo and Yoyo to DNA by Polarized-Light Spectroscopy. J Am Chem Soc 116:8459-8465.
8. Eckel, R., R. Ros, A. Ros, S. D. Wilking, N. Sewald, and D. Anselmetti. 2003. Identification of binding mechanisms in single molecule-DNA complexes. Biophys J 85:1968-1973.
9. Krautbauer, R., S. Fischerlander, S. Allen, and H. E. Gaub. 2002. Mechanical fingerprints of DNA drug complexes. Single Mol 3:97-103.
10. Sischka, A., K. Toensing, R. Eckel, S. D. Wilking, N. Sewald, R. Ros, and D. Anselmetti. 2005. Molecular mechanisms and kinetics between DNA and DNA binding ligands. Biophys J 88:404-411.
11. Bennink, M. L., O. D. Scharer, R. Kanaar, K. Sakata-Sogawa, J. M. Schins, J. S. Kanger, B. G. de Grooth, and J. Greve. 1999. Single-molecule manipulation of double-stranded DNA using optical tweezers: Interaction studies of DNA with RecA and YOYO-1. Cytometry 36:200-208.
12. Vladescu, I. D., M. J. McCauley, I. Rouzina, and M. C. Williams. 2005. Mapping the phase diagram of single DNA molecule force-induced melting in the presence of ethidium. Phys Rev Lett 95:-.
13. Vladescu, I. D., M. J. McCauley, M. E. Nunez, I. Rouzina, and M. C. Williams. 2007. Quantifying force-dependent and zero-force DNA intercalation by single-molecule stretching. Nat Methods 4:517-522.
14. Glazer, A. N., and H. S. Rye. 1992. Stable Dye-DNA Intercalation Complexes as Reagents for High-Sensitivity Fluorescence Detection. Nature 359:859-861.
15. Rye, H. S., S. Yue, D. E. Wemmer, M. A. Quesada, R. P. Haugland, R. A. Mathies, and A. N. Glazer. 1992. Stable Fluorescent Complexes of Double-Stranded DNA with Bis-Intercalating Asymmetric Cyanine Dyes - Properties and Applications. Nucleic Acids Res 20:2803-2812.
16. Bianco, P. R., L. R. Brewer, M. Corzett, R. Balhorn, Y. Yeh, S. C. Kowalczykowski, and R. J. Baskin. 2001. Processive translocation and DNA unwinding by individual RecBCD enzyme molecules. Nature 409:374-378.

17. Ladoux, B., J. P. Quivy, P. Doyle, O. du Roure, G. Almouzni, and J. L. Viovy. 2000. Fast kinetics of chromatin assembly revealed by single-molecule videomicroscopy and scanning force microscopy. P Natl Acad Sci USA 97:14251-14256.
18. Gurrieri, S., K. S. Wells, I. D. Johnson, and C. Bustamante. 1997. Direct visualization of individual DNA molecules by fluorescence microscopy: Characterization of the factors affecting signal/background and optimization of imaging conditions using YOYO. Anal Biochem 249:44-53.
19. Akerman, B., and E. Tuite. 1996. Single- and double-strand photocleavage of DNA by YO, YOYO and TOTO. Nucleic Acids Res 24:1080-1090.
20. Waterman-Storer, C. M., A. Desai, J. C. Bulinski, and E. D. Salmon. 1998. Fluorescent speckle microscopy, a method to visualize the dynamics of protein assemblies in living cells. Curr Biol 8:1227-1230.
21. Marko, J. F., and E. D. Siggia. 1995. Stretching DNA. Macromolecules 28:8759-8770.
22. Smith, S. B., Y. J. Cui, and C. Bustamante. 1996. Overstretching B-DNA: The elastic response of individual double-stranded and single-stranded DNA molecules. Science 271:795-799.
23. Cluzel, P., A. Lebrun, C. Heller, R. Lavery, J. L. Viovy, D. Chatenay, and F. Caron. 1996. DNA: An extensible molecule. Science 271:792-794.
24. Larsson, A., C. Carlsson, and M. Jonsson. 1995. Characterization of the Binding of Yo to [Poly(Da-Dt)](2) and [Poly(Dg-Dc)](2), and of the Fluorescent Properties of Yo and Yoyo Complexed with the Polynucleotides and Double-Stranded DNA. Biopolymers 36:153-167.
25. Lepecq, J. B., M. Lebret, J. Barbet, and B. Roques. 1975. DNA Polyintercalating Drugs - DNA Binding of Diacridine Derivatives. P Natl Acad Sci USA 72:2915-2919.

Chapter 4

Force Spectroscopy and Fluorescence Microscopy of dsDNA-YOYO-1 Complexes: Implications for the Structure of dsDNA in the Overstretching Region

Abstract

When individual dsDNA molecules are stretched beyond their B-form contour length, they reveal a structural transition in which the molecule extends 1.7 times its contour length. The nature of this transition is a subject of debate. In the first model, the dsDNA helix unwinds and combined with the tilting of the basepairs (which remain intact), results in a stretched form of DNA (S-DNA). In the second model the basepairs break, resulting effectively in two single-strands, a process which is referred to as force-induced melting. Here a combination of optical tweezers force spectroscopy with fluorescence microscopy was used to provide some insights into the structure of dsDNA in the overstretching regime. Force extension curves of dsDNA in the presence of the intercalating fluorescent dye YOYO-1 show an overstretching region up to concentrations of 20 nM YOYO-1. Beyond this concentration the overstretching plateau could not be discerned anymore. The minimal influence of YOYO-1 on dsDNA in the low concentration range supports the use of YOYO-1 as a reporter for the structural properties of dsDNA. With fluorescence microscopy imaging of the complex during the stretching process an initial increase in intensity was observed and at the extension where the dsDNA started to overstretch the fluorescence intensity leveled off and ultimately decreased when stretched further into the overstretching region. Simultaneous force spectroscopy and fluorescence polarization microscopy revealed that the orientation of the dye molecules did not change significantly in the overstretching region (78.0° ±3.2°). These results presented here clearly suggest that the structure of overstretched dsDNA can be explained accurately by force induced melting.

The content of this chapter is based on:
Murade, C. U., V. Subramaniam, C. Otto, M. L. Bennink. 2010. Force spectroscopy and fluorescence microscopy of dsDNA-YOYO-1 complexes: implication for the structure of dsDNA in the overstretching region. Nucleic Acids Res. 2010 Feb 2 doi:10.1093/nar/gkq034

4.1
Introduction

The mechanical properties of single double-stranded DNA (torsionally unconstrained) molecules have been studied using various single molecule manipulation techniques such as magnetic tweezers, atomic force microscopy and optical tweezers (1-4). The force extension curve of the dsDNA obtained at physiological conditions shows a distinct overstretching plateau at about 65 pN, at which the molecule can be stretched to 1.7 times its contour length by changing the force only by 2-5 pN (4). The force-extension curve of the dsDNA up to 50 pN is accurately described by an extensible worm like chain model (5). The local structure of the dsDNA in this regime resembles that of B-DNA (Fig. 1A). The structure of the dsDNA in the overstretching region however is still a subject of debate (3-4, 6-7).

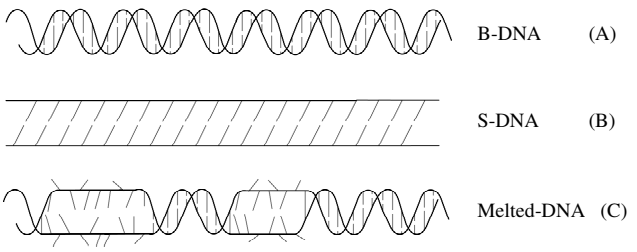

Fig. 1
Pictorial representations of different forms of dsDNA. (A) B-DNA which is the structure of the dsDNA below 50 pN. (B) S-DNA (stretched DNA) and (C) partially melted DNA are suggested structures of the dsDNA in the overstretching region.

A model presented by Cluzel *et al.* (3) and Smith *et al.* (4) describes the structure of the dsDNA in the overstretching region as a stretched ladder (Fig. 1B) in which the base pairs are tilted with respect to the helical axis. In this structure, named "S-DNA", the hydrogen bonds between the base pairs on either strand remain intact and are expected to break at much higher forces (above 120 pN) (8). A second model proposed by Rouzina and Bloomfield (6-7) describes the dsDNA as actually melting under the influence of force. In the overstretching region the hydrogen bonds between the base pairs break progressively as dsDNA is further stretched, resulting in regions of melted DNA separated by stretches of double helical DNA resembling the B-DNA structure (Fig. 1C). At this moment there are no direct experimental evidences for the S-DNA structure. Various modeling and simulation studies assuming this B-S transition in the DNA were not able to reproduce the features of the experimental force extension curves of dsDNA (3, 9). Experimental data on the mechanical properties of dsDNA as a function of various solution conditions such as

pH, ionic strength and temperature (10-12) and the interaction of overstretched dsDNA with glyoxal (13), and multicolor single molecule fluorescence imaging (14) support the force-induced melting hypothesis.

Here we have measured the mechanical properties and the total amount of fluorescence of single dsDNA-dye complexes as a function of the YOYO-1 concentration in the surrounding buffer using optical tweezers force spectroscopy combined with fluorescence microscopy. At 10 and 20 nM YOYO-1 the force extension behavior of the complex was only slightly different from that when no dye was added. This enabled the use of the fluorescent dyes at this concentration as a reporter for the structural properties of dsDNA. At concentrations of 40 nM and higher the characteristic overstretching plateau could not be discerned anymore, indicating a significant effect on the mechanical properties.

Simultaneously recorded fluorescence images of the single suspended complex while being stretched and relaxed were performed at concentrations of 10 and 100 nM YOYO-1. These data provided real-time information on the interaction of YOYO-1 with the dsDNA molecule under tension. In the case of 10 nM YOYO-1, as the molecule was stretched, the total amount of fluorescence initially showed an increase. When the molecule started to overstretch, the fluorescence started to flatten off, and even showed a slight decrease, as the molecule was stretched to the end of the overstretching plateau. At a 100 nM dye concentration, where the overstretching plateau could not be discerned, the total amount of the fluorescence was continuously increasing as the complex was stretched. Finally we performed simultaneous force spectroscopy and fluorescence polarization microscopy on the dsDNA-YOYO-1 complex at 10 nM YOYO-1, to get more insight into the orientation of the basepairs in the dsDNA during overstretching. The orientation of the YOYO-1 molecules with respect to the dsDNA helical axis remained constant (78º) when the dsDNA was stretched from the enthalpic stretching regime into the overstretching regime. From this we conclude that the orientation of the basepairs in the overstretched DNA is not significantly different from that in B-DNA. This final result is in contradiction with the assumption for S-DNA, which is that the basepairs are tilted. The fluorescence intensity changes measured during the extension and relaxation cycles suggest that the structure of the overstretched dsDNA can be explained by the melting of the dsDNA helix as induced by the force applied.

4.2
Materials and Methods

Force extension experiments on the dsDNA and dsDNA-YOYO-1 complex were performed using single beam optical tweezers as described in (15-16). Experiments were performed in a buffer solution containing 10 mM Tris-HCl, pH 7.5, 1 mM ethylenediaminetetraacetic acid (TE) supplemented with 150 mM NaCl and 0.05% NaN_3. For experiments with YOYO-1, the required concentration of dye is added to the above mentioned buffer. This buffer was bubbled with nitrogen gas for 1 hr to remove oxygen, to reduce the amount of quenching of the YOYO-1 dye and dye-induced photo damage of the dsDNA which causes dsDNA to break (17-18). Stretching and relaxing of the dsDNA was performed at 3 µm/s pulling speed in case no fluorescence images were acquired. When simultaneously fluorescence images were captured at 10 Hz (Fig. 2), the pulling speed was only 1 µm/s.

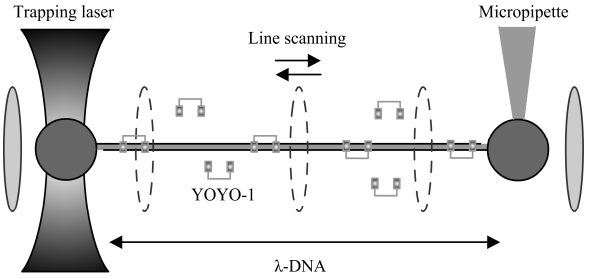

Fig. 2
Single λ-DNA molecule tethered between two 2.6 µm sized streptavidin coated polystyrene beads. One of these beads is placed on a micropipette (which can be moved with nanometer accuracy), while the second bead is held with the optical tweezers. YOYO-1 molecules which are present in the surrounding buffer bind the dsDNA through bisintercalation. Excitation of the dsDNA-YOYO-1 complex is achieved by scanning the dsDNA-dye complex with a line-shaped (0.3 x 3.5 µm) excitation beam (488 nm). Line frequency is 12.5 Hz.

For the fluorescence polarization experiments in order to get incident light with a polarization direction orthogonal to that of the laser, a half-wave plate was added in the excitation path before the scanning mirror. Emitted photons were separated into two polarization directions using a Wollaston prism in the detection path. Different transmission coefficients of the optical components of the instrument in all possible combinations of parallel and normal excitation and emission have been determined and taken into account. Fluorescence intensities were obtained from the images by integrating for every frame the light intensity in a fixed-width rectangle with a length equal to the dsDNA length. This rectangle completely enclosed the entire dsDNA molecule at all extensions. An identical rectangle was selected in a dark region, the total integrated intensity of which was used for

background-correction (16). The fluorescence images have been used to construct a kymograph as described in (19).

4.3
Results

4.3.1
Force spectroscopy of dsDNA-YOYO-1 complex

Fig. 3 presents examples of force extension curves of dsDNA in the presence of various concentrations of YOYO-1. The mechanical parameters were obtained by curve fitting the extensible worm like chain model (5) to the extension part of each curve (grey lines in Fig. 3B). The parameters resulting from this fit are presented in the Table 1. The contour length clearly shows an increase as the dye concentration in the surrounding buffer is increased. The force extension curve of the dsDNA without any dye shows a distinct overstretching plateau at about 65 pN, which is characteristic for dsDNA (4) (Fig 3A). At concentrations of 10 and 20 nM YOYO-1 the overstretching plateau is still discernable, but appeared at slightly higher forces as compared to the bare dsDNA: 72 (±3) pN and 80 (±4) pN respectively. Furthermore the slope of the overstretching region increases in the presence of YOYO-1, proportional to the concentration. In the presence of 40, 100, 200, 500 and 1000 nM YOYO-1, the force extension curve does not show any discernible overstretching region (Fig. 3B).

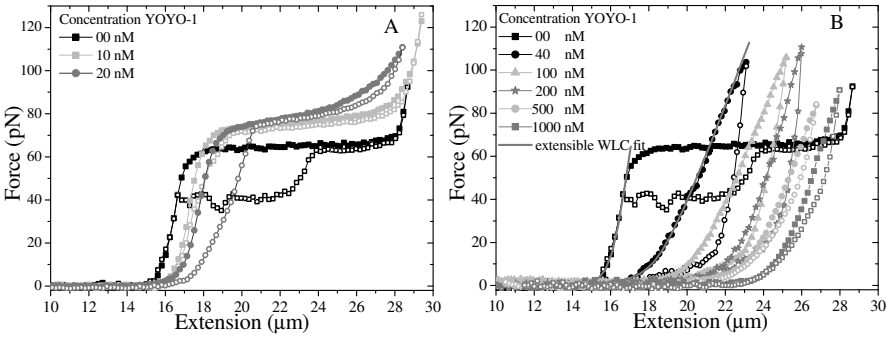

Fig. 3

Force extension curves of dsDNA molecules in the presence of various YOYO-1 dye concentrations in the surrounding buffer. Closed and open symbols represent the extension and relaxation part of the cycle respectively. The solid gray lines present the curve-fitted extensible WLC model (5) (for 0 and 40 nM). Pulling speeds are 3 µm/s.

Table 1 Apparent mechanical properties of dsDNA-YOYO-1 complexes at various concentrations of YOYO-1 molecules in the surrounding buffer. Parameters were obtained by curve-fitting the extensible worm like chain model (5) to the extension part of force extension relaxation curve.

Concentration of YOYO-1 (nM)	Persistence length (nm)	Contour length (µm)	Stretch modulus (pN)
0	52.0(±4.0)	16.40(±0.20)	1100(±100)
10	51.4(±4.0)	17.07(±0.30)	1075(±80)
20	42.0(±5.0)	17.56(±0.25)	965(±60)
40	20.7(±3.0)	19.05(±0.20)	470(±40)
100	16.6(±3.0)	21.43(±0.30)	570(±50)
200	12.8(±4.0)	22.89(±0.35)	783(±60)
500	14.9(±3.0)	24.67(±0.20)	786(±65)

4.3.2
Simultaneous force spectroscopy and fluorescence microscopy

In a next step we performed simultaneous force spectroscopy and fluorescence microscopy on the dsDNA-YOYO-1 complex in the presence of 10 and 100 nM YOYO-1 in the surrounding buffer. Fig. 4 presents the total fluorescence intensity versus the extension of the complex (A,B,C) along with the force versus extension curve (D,E,F). The total intensity of the complex in the presence of 100 nM YOYO-1 increases as the extension of the complex increases from 14 to 26 µm (Fig. 4A). This molecule is only stretched up to 80 pN, after which the complex broke, most probably due to dye-induced photocleavage (17-18). Figs. 4B and E present another molecule that was pulled up to 60 pN in the presence of 100 nM YOYO-1 also revealing the relaxation curve, also showing that the fluorescence increases proportional to the extension.

In the presence of 10 nM YOYO-1(Figs. 4C and F), a similar increase in total fluorescence intensity was observed from 17 to 20 µm (Fig. 4A). However, as the molecule started to overstretch, the increase in fluorescence intensity started to slow down, and eventually showed a reduction as the end of the overstretching plateau was reached. During the relaxation of the dsDNA-YOYO-1 complex the fluorescence intensity started increasing even beyond the maximum reached during the extension part of the cycle. When relaxed to about the start of the overstretching plateau, the intensity started decreasing.

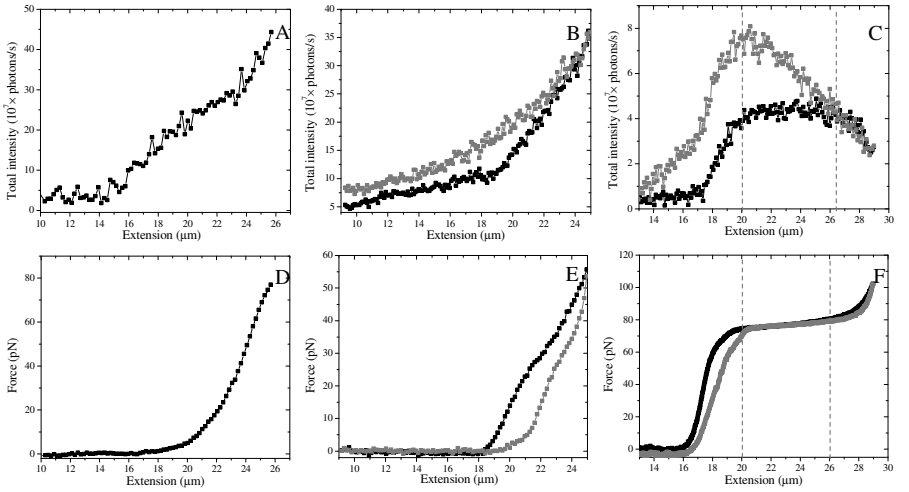

Fig. 4

Total fluorescence intensity of the dsDNA-YOYO-1 complex and the force as a function of the extension. Panel A, B and C present the total intensity of the dsDNA-YOYO-1 complex at 100, 100 and 10 nM YOYO-1 respectively. Panel D, E and F present the corresponding force extension curves of dsDNA respectively. The molecule in A and D did break during the stretching procedure, probably due to photo-induced damage. B and E presents the data on a molecule that, although stretched to only 60 pN, did not break and revealed a relaxation curve as well. Black and gray squares present the stretching and relaxation part of the force extension cycle. Area between two gray dotted lines marks the overstretching region (in C and F).

4.3.3
Simultaneous force spectroscopy and polarized fluorescence microscopy

Simultaneous force spectroscopy and fluorescence polarization microscopy was performed on the dsDNA-YOYO-1 complex in the presence of 10 nM YOYO-1. The polarized fluorescence intensity as function of the extension of the dsDNA-YOYO-1 (10 nM) complex is presented in the Fig. 5. I_{nn}, I_{np}, I_{pn} and I_{pp} are the intensities measured where first subscript refers to the polarization orientation of the excitation light (n=normal, p=parallel), and the second subscript refers to the polarization orientation of the emitted light. Orientations n and p are defined with respect to the helical axis of the dsDNA.

Fluorescence intensities I_{nn} and I_{np} (Fig. 5) both show a trend that is similar to the total intensity as a function of the extension plotted in Fig. 4C. The relative intensity however for I_{np} is about 3 to 4 times lower than that for I_{nn}. The fluorescence intensities I_{pn} and I_{pp} are much lower than the first two, and only show a slight increase at extensions from 26 to 28 μm.

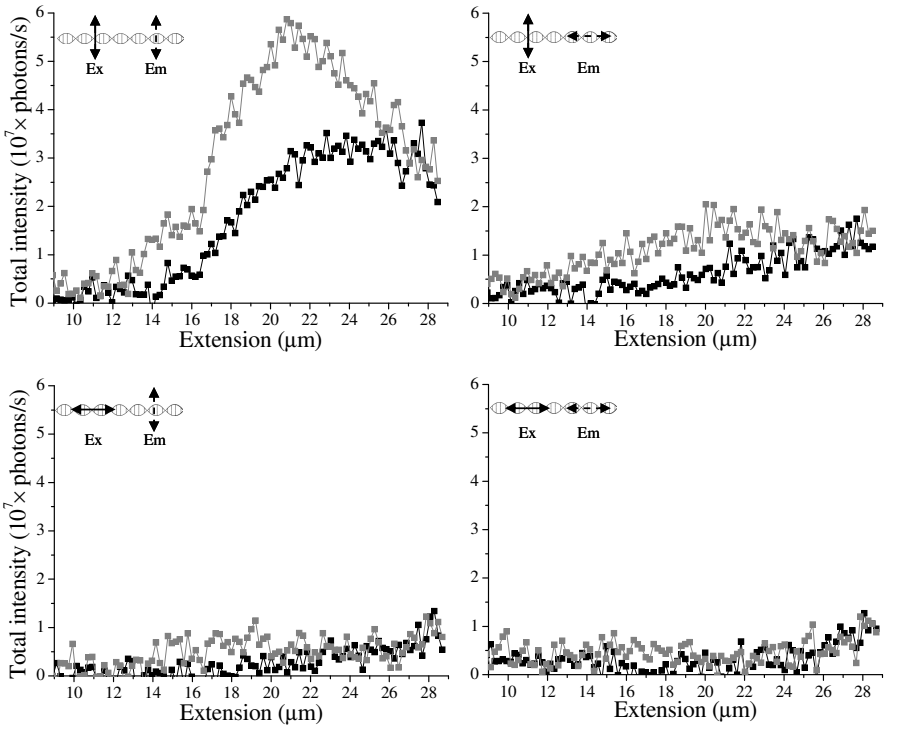

Fig. 5

Total fluorescence intensity of the dsDNA-YOYO-1 complex (at 10 nM YOYO-1) as function of extension, recorded at different polarization settings. Black and gray symbols represent extension and relaxation intensities respectively. Polarization orientation for excitation (Ex) and emission (Em) are indicated for each graph.

4.4
Discussion

4.4.1
Establishing YOYO-1 as dsDNA structural marker

In this study we aimed at using YOYO-1 as a reporter molecule for the structure of dsDNA in the overstretching region. YOYO-1 intercalates within double-stranded DNA (20-21) and changes its mechanical properties depending on the concentration of the dye used (15-16, 22). To use YOYO-1 molecules as markers for the structure of dsDNA, it is key to find a YOYO-1 concentration at which the structure of dsDNA is not significantly affected by the intercalation. Force extension and relaxation curves of the dsDNA-YOYO-1 complex at various concentrations of the dye are presented in Fig. 3 and mechanical parameters are presented in Table 1. At 10 nM YOYO-1 the mechanical parameters and therefore the force

extension curve of dsDNA-YOYO-1 complex are comparable to those of the dsDNA without any dye added. The overstretching region is clearly observable at 10 nM, and although at a slightly higher force (72 ± 3 pN), is similar to the plateau observed when no dye was added. At higher YOYO-1 concentrations (20 to 1000 nM) the mechanical parameters describing the force extension curve started deviating more from those obtained for bare dsDNA. Above 40 nM the overstretching region could not be observed anymore when the complex was stretched to 110 pN. Based on these data, 10 nM YOYO-1 concentration was used to carry out the experiments that are aimed at determining the structure of dsDNA in the overstretching region.

4.4.2
Structure of dsDNA in the overstretching region

As a first step to determine the dsDNA structure in the overstretching region, the total fluorescence intensity of the complex was measured while the complex was being stretched and relaxed. As the molecule was stretched at 10 nM YOYO-1, the total fluorescence intensity increased up to the start of overstretching transition. From this point on the total fluorescence intensity started leveling off, and eventually even decreased upon further extension (Fig. 4C). This result was different from that at a concentration of 100 nM in which the force extension curve revealed no overstretching region and the fluorescence intensity increased monotonically as a function of extension (Fig. 4A).

The increase in fluorescence intensity as the complex was stretched at 100 nM YOYO-1 was already observed in ((16), Chapter 3) and can be explained by assuming a force-dependent binding constant of the dye to the dsDNA. This means that as the force is increasing, the binding constant is increasing, and more YOYO-1 molecules actually bind to the dsDNA in order to restore the equilibrium. In the case of 10 nM YOYO-1 the fluorescence intensity initially is indeed increasing up to where the molecule starts to overstretch. In the overstretching plateau the increase in fluorescence starts to level off. If it is assumed that the number of molecules bound to the dsDNA-dye complex is proportional to the fluorescence observed, the conclusion must be that as the dsDNA enters the overstretching region, the number of molecules bound to the dsDNA reaches a certain limit, after which it remains constant. At some point at the end of the overstretching region the number of molecules bound even decreases a little. If the amount of fluorescence is indeed representative of the number of dye molecules bound to the dsDNA it is quite unexpected and hard to explain that the fluorescence intensity is actually increasing during the relaxation part in the overstretching region, making this explanation very unlikely.

An alternative explanation for this could be a change of the nano-environment of the intercalated YOYO-1 molecule, induced by the stretching, which can have an influence

on the fluorescence yield of the dye molecule. It has been generally accepted that the dsDNA goes through a structural change in the overstretching region but the exact nature of this transition and final structure is still a subject of debate (3-4, 6-7). The B-S transition model assumes that the inter-strand hydrogen bonds between the base pairs remain intact and that the inclination of basepairs changes in the overstretching region. The distance between the successive basepairs does not change significantly (23). The force-induced melting model assumes that, the inter-strand hydrogen bonds break progressively as the dsDNA is stretched further into the overstretching region. Lepecq and Paoletti (24) stated that inter-strand hydrogen bonding is a prerequisite for the intercalating dye molecule to enhance their fluorescent yield. That is, fluorescence enhancement of YOYO-1 molecules will reduce as the dsDNA is melting into ssDNA. An ethidium fluorescence assay has been developed by Johnson (25) to analyze the amount of denatured DNA based on this effect.

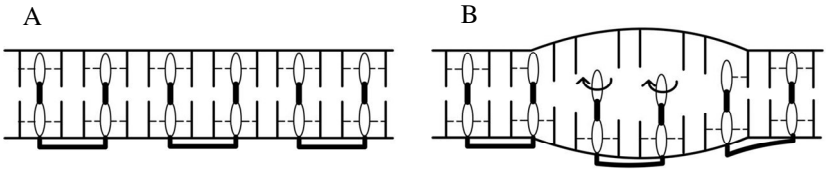

Fig. 6
Schematic picture of the YOYO-1 molecule intercalated in dsDNA. (A) YOYO-1 molecules intercalating the dsDNA where YO moieties interact with the adjacent basepairs. Interactions are indicated with dotted lines. (B) YOYO-1 molecules bound to the dsDNA that is partly melted. The center YOYO-1 molecule only interacts with one of the two strands, allowing the quinoline and benzoxazole moieties to rotate with respect to each other.

According to the force-induced melting model the inter-strand hydrogen bonds between the base pairs start to break, as the dsDNA molecule is stretched in the overstretching region. When the two strands separate, the ring complex of YO moiety will be exposed which will allow quinoline and benzoxazole moieties to rotate with respect to each other (as if free in solution). This means that although the dye molecule is still bound to a single stranded part of the DNA, it will hardly contribute to the fluorescence (26); schematically this is depicted in Fig. 6.

This interpretation is further supported by the fluorescence images of some dsDNA-YOYO-1 complexes (Fig. 7 and 8) in the presence of respectively 100 nM and 1 nM YOYO-1. Along the length of the molecule presented in Fig. 7 bright and dark regions within the dsDNA-YOYO-1 complex were observed when maintained at forces larger than 3.5 pN (Fig. 7A). The intensity along a line through the DNA molecule and next to it (background) is plotted in Fig. 7B at a force of 73 pN. At forces larger than 3.5 pN a clear dark region was observed in between two brighter regions. This non-fluorescent segment is most probably ssDNA, connecting the dsDNA at either end (bright segments).

Fig. 8 presents another example of a molecule that reveals a dark patch within the connecting polymer. The concentration of YOYO-1 in this experiment is only 1 nM, for which the force extension behavior is indistinguishable from that in case of no dye. To test the hypothesis that the connecting chain between the beads consists of partly double-stranded and partly single-stranded DNA, the force extension behavior of this complex was fitted with an expression in which part behaves as a FJC model (i.e. the ssDNA part) and part as a WLC model (i.e. dsDNA part)(13).

$$X(F) = (1 - f_a) \times X_{ds}(F) + f_a \times X_{ss}(F) \qquad (1)$$

f_a is the fraction of the contour length that is single-stranded. $X(F)$, $X_{ds}(F)$ and $X_{ss}(F)$ are extensions of the combined dsDNA+ssDNA, dsDNA and ssDNA as function of force respectively (13). Persistence length (L_p), contour length (L_0) and stretch modulus (S) values used for dsDNA are L_0 = 16.4 µm, L_p = 52 nm and S= 1100 pN (4). For the ssDNA values used are: L_0 = 27.16 µm, L_p = 0.75 nm, S = 800 pN (4). By curve fitting the force extension curve in Fig. 8 (circles) with Eq. 1, we determined the fraction of ssDNA (f_a) to be 0.40±0.04. The fluorescence image in Fig. 8 presents that of the DNA-YOYO-1 complex at 10 pN. The total extension of the complex is 18.2 µm. Fraction of ssDNA (f_a) was determined at 10 pN and extension of 18.20 µm using Eq. 1, fraction of ssDNA is 0.43, which is in agreement with the fraction of ssDNA derived from the force extension curve. The results presented in Fig. 7 and 8 clearly show that the YOYO-1 molecules bound to the ssDNA do not contribute to the total fluorescent intensity of the dsDNA-YOYO-1 complex.

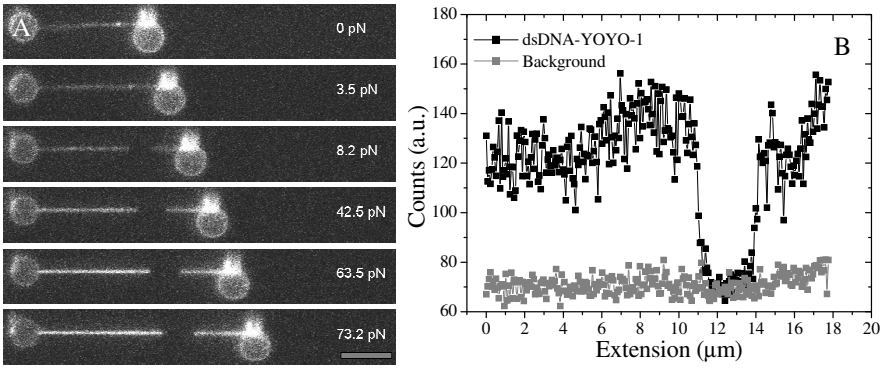

Fig. 7

(A) Fluorescence images of the dsDNA-YOYO-1 complex at different forces in the presence of 100 nM YOYO-1. Scale bar is 5 µm. (B) Fluorescence intensity of the dsDNA-YOYO-1 complex at 73.2 pN compared with the background signal.

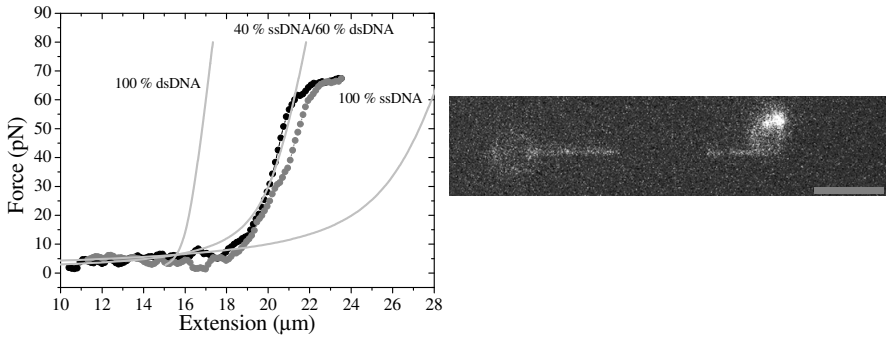

Fig. 8

Force extension curve of denatured DNA-YOYO-1 complex at 1 nM YOYO-1. Black and gray symbols present extension and relaxation respectively. Gray lines presents the calculated curve for 100% dsDNA, 100% ssDNA, and 40% ssDNA + 60% dsDNA, which best fitted the experimental data. Image panel presents the image of the combined ssDNA and dsDNA at 18.2 µm extension (10 pN), scale bar 5 µm.

We assume the fluorescence signal during the stretching cycle is leveling off (Fig. 4C) because double-stranded DNA is converted into single-stranded DNA, and not because fewer dye molecules bind to the DNA in the overstretching regime. This hypothesis furthermore explains the increased fluorescence observed during the relaxation cycle (Fig. 4C). The number of bound dye molecules kept increasing during the stretching part of the cycle, even though the fluorescence leveled off because of the change in nano-environment of the dye molecule. During the relaxation phase the increase in fluorescence can be explained by the fact that single-stranded DNA that has bound YOYO-1 is rehybridized to double-stranded DNA and as a result of that starts to fluoresce. In the presence of 100 nM YOYO-1 overstretching was not observed (Fig. 3B), presumably because the amount of YOYO-1 intercalated in the dsDNA is high enough to stabilize the DNA, preventing the melting of the dsDNA.

Fig. 9 presents the kymograph created from the sequence of fluorescence images recorded while stretching and relaxing a dsDNA-YOYO-1 in the presence of 10 nM YOYO-1. Clearly visible are dark and bright lines in the kymograph, indicating the single stranded/melted DNA segments and the double-stranded DNA segments respectively.

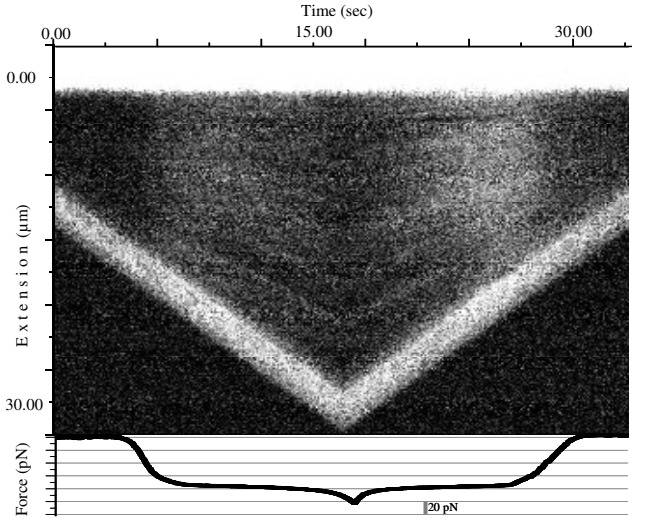

Fig. 9

Kymograph created from a sequence of fluorescence images recorded simultaneously while recording a force extension curve of dsDNA-YOYO-1 complex at 10 nM YOYO-1. The top axis is time, the left axis of the kymograph indicates the extension of the complex, and the lower axis represents the force on the complex. The two extremely bright lines in the kymograph represent the streptavidin coated polystyrene beads. The top bright line indicates bead in the trap and other bright line indicates bead on the micro pipette.

From the fluorescence polarization data presented in Fig. 5 the average orientation of the YOYO-1 molecules as function of extension using Eq. 2 (26) was determined. In the cylindrically symmetric sample like ours (dsDNA) I_{iso} is given by $I_{iso} = (I_n+2I_p)/3$. These results are presented in Fig. 10.

$$LD_r = \frac{I_p - I_n}{I_{iso}} = \frac{3}{2}(3\cos^2 \alpha_{eff} - 1) \qquad (2)$$

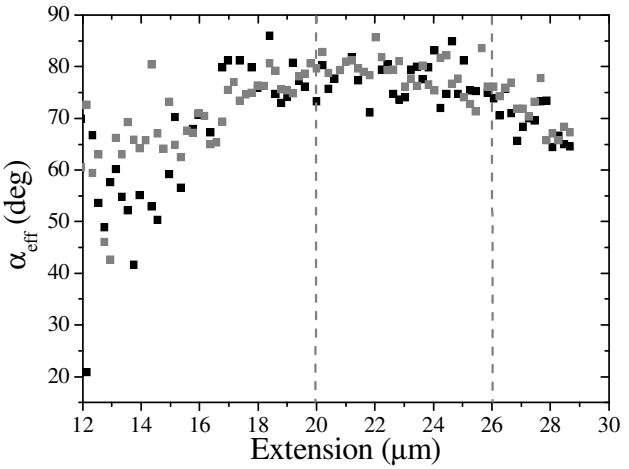

Fig. 10

Average orientation of YOYO-1 molecules with respective dsDNA helical axis as function of extension, calculated from the fluorescence polarization data recorded during the stretching of DNA-YOYO-1 in presence of 1 nM YOYO-1. Black and gray symbols present average (effective) angle while extension and relaxation of the complex respectively. Area between two dotted gray lines indicated the overstretching region.

As presented in Fig. 10 the effective orientation of the YOYO-1 molecules increases from ≈ 50° at an extension of 12 μm to ≈ 78° at 17 μm. Beyond this extension and during the overstretching region, this angle remains rather constant. The lower values obtained at extensions lower than 17 μm (F < 10 pN) show a lower angle and a greater variance, which can be explained by the fluctuations of the dsDNA molecule. The value obtained for the orientation of the YOYO-1 molecules with respective dsDNA helical axis at overstretching region 78.0°(±3.2) is in good agreement with earlier published results (15). The B-S transition model suggests that the base pairs in the overstretching region are starting to tilt with respect to the dsDNA helical axis, which is not consistent with the data in Fig. 10.

4.5
Conclusions

Combined optical tweezers and fluorescence microscopy has been used to study the structure of dsDNA in the overstretching region. In a first set of experiments force extension curves of the dsDNA in the presence of various (10 to 1000 nM) YOYO-1 concentrations were recorded, to determine the effect of YOYO-1 concentration on the mechanical properties of dsDNA (Fig. 3). At a concentration of 10 nM YOYO-1 the force extension behavior was similar to that of bare dsDNA, showing a clear overstretching plateau at 72 pN. At this concentration the dye molecules did not influence the dsDNA structure significantly, and could thus be used as faithful reporters of the dsDNA structure as it is being stretched. At higher concentrations the force extension behavior started to significantly deviate from those of the dsDNA in the absence of dye. At concentrations of 40 nM and higher for example the overstretching region could not be detected.

In a second set of experiments fluorescence microscopy images were recorded during the stretching and relaxation process at dye concentrations of 10 and 100 nM. The saturation and eventually slight decrease of the fluorescence intensity (at 10 nM) while the complex was being stretched, was explained by the fact that part of the dsDNA was converted to a single-stranded form (Fig. 4-5). This was further supported by fluorescent images that revealed some clear banding along the DNA molecule, indicative of single-stranded segments within the DNA (Fig. 7-9).

To assess the orientation of the basepairs within the dsDNA during stretching and relaxing, fluorescence polarization microscopy was applied in a third set of experiments. The average angle of the dye molecules remains rather constant throughout overstretching region (78.0° ±3.2) and has a value similar to that of B-DNA in the enthalpically stretched form.

From these data we conclude that the structure of overstretched dsDNA is best characterized by (i) a continuous conversion of double-stranded segments into single-stranded segments as the dsDNA is being stretched further and (ii) no significant tilting of the basepairs during the overstretching process. These characteristics are best described by the force-induced melting model, as suggested in (6-7, 10-14).

4.6
References

1. Gosse, C., and V. Croquette. 2002. Magnetic tweezers: micromanipulation and force measurement at the molecular level. Biophys J 82:3314-3329.
2. Rief, M., H. Clausen-Schaumann, and H. E. Gaub. 1999. Sequence-dependent mechanics of single DNA molecules. Nat Struct Biol 6:346-349.
3. Cluzel, P., A. Lebrun, C. Heller, R. Lavery, J. L. Viovy, D. Chatenay, and F. Caron. 1996. DNA: an extensible molecule. Science 271:792-794.
4. Smith, S. B., Y. Cui, and C. Bustamante. 1996. Overstretching B-DNA: the elastic response of individual double-stranded and single-stranded DNA molecules. Science 271:795-799.
5. Marko, J. F., and E. D. Siggia. 1995. Stretching DNA. Macromolecules 28:8759-8770.
6. Rouzina, I., and V. A. Bloomfield. 2001. Force-induced melting of the DNA double helix 1. Thermodynamic analysis. Biophys J 80:882-893.
7. Rouzina, I., and V. A. Bloomfield. 2001. Force-induced melting of the DNA double helix. 2. Effect of solution conditions. Biophys J 80:894-900.
8. Clausen-Schaumann, H., M. Rief, C. Tolksdorf, and H. E. Gaub. 2000. Mechanical Stability of Single DNA Molecules. Biophysical Journal 78:1997-2007.
9. Marko, J. F. 1998. DNA under high tension: Overstretching, undertwisting, and relaxation dynamics. Physical Review E 57:2134.
10. Williams, M. C., J. R. Wenner, I. Rouzina, and V. A. Bloomfield. 2001. Effect of pH on the overstretching transition of double-stranded DNA: evidence of force-induced DNA melting. Biophys J 80:874-881.
11. Wenner, J. R., M. C. Williams, I. Rouzina, and V. A. Bloomfield. 2002. Salt dependence of the elasticity and overstretching transition of single DNA molecules. Biophys J 82:3160-3169.
12. Williams, M. C., J. R. Wenner, I. Rouzina, and V. A. Bloomfield. 2001. Entropy and heat capacity of DNA melting from temperature dependence of single molecule stretching. Biophys J 80:1932-1939.
13. Shokri, L., M. J. McCauley, I. Rouzina, and M. C. Williams. 2008. DNA overstretching in the presence of glyoxal: structural evidence of force-induced DNA melting. Biophys J 95:1248-1255.
14. van Mameren, J., P. Gross, G. Farge, P. Hooijman, M. Modesti, M. Falkenberg, G. J. Wuite, and E. J. Peterman. 2009. Unraveling the structure of DNA during overstretching by using multicolor, single-molecule fluorescence imaging. Proc Natl Acad Sci U S A 106:18231-18236.
15. Bennink, M. L., O. D. Scharer, R. Kanaar, K. Sakata-Sogawa, J. M. Schins, J. S. Kanger, B. G. de Grooth, and J. Greve. 1999. Single-molecule manipulation of double-stranded DNA using optical tweezers: interaction studies of DNA with RecA and YOYO-1. Cytometry 36:200-208.
16. Murade, C. U., V. Subramaniam, C. Otto, and M. L. Bennink. 2009. Interaction of oxazole yellow dyes with DNA studied with hybrid optical tweezers and fluorescence microscopy. Biophys J 97:835-843.
17. Akerman, B., and E. Tuite. 1996. Single- and double-strand photocleavage of DNA by YO, YOYO and TOTO. Nucleic Acids Res 24:1080-1090.
18. Gurrieri, S., K. S. Wells, I. D. Johnson, and C. Bustamante. 1997. Direct visualization of individual DNA molecules by fluorescence microscopy: characterization of the factors affecting

signal/background and optimization of imaging conditions using YOYO. Anal Biochem 249:44-53.
19. Waterman-Storer, C. M., A. Desai, J. C. Bulinski, and E. D. Salmon. 1998. Fluorescent speckle microscopy, a method to visualize the dynamics of protein assemblies in living cells. Curr Biol 8:1227-1230.
20. Johansen, F., and J. P. Jacobsen. 1998. 1H NMR studies of the bis-intercalation of a homodimeric oxazole yellow dye in DNA oligonucleotides. J Biomol Struct Dyn 16:205-222.
21. Glazer, A. N., and H. S. Rye. 1992. Stable dye-DNA intercalation complexes as reagents for high-sensitivity fluorescence detection. Nature 359:859-861.
22. Sischka, A., K. Toensing, R. Eckel, S. D. Wilking, N. Sewald, R. Ros, and D. Anselmetti. 2005. Molecular mechanisms and kinetics between DNA and DNA binding ligands. Biophysical Journal 88:404-411.
23. Konrad, M. W., and J. I. Bolonick. 1996. Molecular Dynamics Simulation of DNA Stretching Is Consistent with the Tension Observed for Extension and Strand Separation and Predicts a Novel Ladder Structure. Journal of the American Chemical Society 118:10989-10994.
24. LePecq, J. B., and C. Paoletti. 1967. A fluorescent complex between ethidium bromide and nucleic acids. Physical-chemical characterization. J Mol Biol 27:87-106.
25. Johnson, D. 1975. A new method of DNA denaturation mapping. Nucleic Acids Res 2:2049-2054.
26. Larsson, A., C. Carlsson, and M. Jonsson. 1995. Characterization of the binding of YO to [poly(dA-dT)]2 and [poly(dG-dC)]2, and of the fluorescent properties of YO and YOYO complexed with the polynucleotides and double-stranded DNA. Biopolymers 36:153-167.

Chapter 5

Force-dependent binding kinetics of YO-1 and YOYO-1 with single dsDNA measured with optical tweezers force spectroscopy

Abstract

We have performed force extension and relaxation experiments on single λ-phage DNA molecules in the presence of various concentrations of YO-1 and YOYO-1 ranging from 100 to 2000 nM. From the force extension data of the dsDNA-dye complexes, the binding density as a function of concentration and applied force was determined. The binding density was higher as the dye concentration was increased. The data were subsequently sorted by force and curve-fitted with the McGhee-von Hippel binding isotherm to determine the binding constant and binding site size as a function of the applied force. From this analysis the binding constant of YO-1 and YOYO-1 was shown to increase as the applied force increased. Binding site size as function of force decreases for YO-1 whereas its constant for YOYO-1. The sum of the distance over which force is acting during binding and unbinding is lower for YOYO-1 (0.09 nm) compared to YO-1 (0.23 nm). Differences in the interaction of YOYO-1 and YO-1with dsDNA are explained by assuming different paths followed by these molecules while interacting with the dsDNA.

The content of this chapter is based on:
Murade, C. U., V. Subramaniam, C. Otto, M. L. Bennink. 2009. Interaction of oxazole yellow dyes with DNA studied with hybrid optical tweezers and fluorescence microscopy. Biophys. J. 97:835-843.

5.1
Introduction

Understanding the interaction of intercalating molecules such as YO-1 and YOYO-1 with double-stranded DNA (dsDNA) is of great significance (1-2). The molecules for example inhibit, upon binding to dsDNA, other DNA–protein interactions, which can have serious consequences for the operation of the living cell. This specific property of these intercalators makes them interesting candidates to be used in the development of anti-cancer drugs (3-5). In chapters 3 and 4 we have reported on the effect of mono- (YO-1) and bis-intercalating (YOYO-1) molecules on the mechanical properties of the dsDNA at 100 nM concentration. We have observed that the contour length of dsDNA increases as the YO-1 and YOYO-1 binds to it. Furthermore we have observed that the kinetics of YOYO-1 binding are relatively slow, such that the dsDNA-dye complex is not in equilibrium while it is stretched and relaxed at pulling rates of 3 μm/s. For YO-1 binding to dsDNA it was found to be in equilibrium, indicating faster kinetics.

Here we analyzed the force extension curves of dsDNA-YO-1 and dsDNA-YOYO-1 recorded at different dye concentrations in more detail. From these data we determined the binding density (fractional elongation) (6) as a function of the dye concentration and the applied force. Grouping the data points with the same force and curve-fitting these points with the McGhee-von Hippel binding isotherm (7) we were able to determine the binding constant and binding site size as function of the applied force for YO-1 and YOYO-1. The binding constant at zero force and the extension per intercalator (as define by Vladescu *et al.*) for YO-1 were $5.74 \cdot 10^5$ M^{-1} and 0.233 nm respectively, which are in good agreement with the values reported in literature (6) for ethidium ($4.6 \cdot 10^5$ M^{-1} mono intercalator). For YOYO-1 these values were $38.75 \cdot 10^5$ M^{-1} and 0.09 nm. The values obtained are smaller than that of reported in the literature $10^8 - 10^{10}$ M^{-1} and 0.884 nm respectively (8). The observed discrepancy in the expected value and obtained value of ΔX is addressed by assuming ΔX to be the sum of the distances over which the force is acting during binding and unbinding as appose to the assumption that ΔX is extension of the dsDNA per intercalator as reported in (6), and assuming that YOYO-1 and YO-1 follow different paths while interacting with dsDNA (chapter 3).

5.2
Materials and Methods

The optical tweezers instrument and the procedure of attaching a single λ-DNA molecule between two micron-sized beads have been described in detail in Chapter 2. In brief: An individual dsDNA molecule is suspended between two polystyrene beads, one of which is held in the optical trap and the other is immobilized on the tip of the glass micropipette using suction. Force spectroscopy is performed by moving the micropipette bead with respect to the optically trapped bead. Forces acting on the dsDNA are measured by determining the displacement of the trapped bead within the optical trap. After recording the force extension curve of an individual dsDNA molecule, buffer (10 mM Tris-HCl, pH 7.5, 1 mM ethylene – diaminetetraacetic acid (TE) supplemented with 150 mM NaCl and 0.05% NaN_3) containing various concentrations in the range of 100 to 2000 nM of YO-1 and YOYO-1 were flown in the flow cell. Force spectroscopy was performed at 3 μm/s pulling speed unless otherwise specified.

In order to determine the force-dependent binding constant of the dye binding to the dsDNA one needs to determine the dye binding density (ν) as a function of free dye concentration and the applied force. The binding density is defined as the ratio of the total number of bound dye molecules and the total number of available binding sites. Because both YO-1 and YOYO-1 are expected to cover multiple binding sites, the McGhee-von Hippel binding isotherm is used to determine the binding constant and the number of binding sites each ligands covers. The binding isotherm is given by Eq. 1(7).

$$\upsilon_F(C) = K_F \times C \times \frac{(1-n_F\upsilon_F)^{n_F}}{(1-n_F\upsilon_F+\upsilon_F)^{n_F-1}} \qquad (1)$$

Where $\nu_F(C)$ is the binding density of the dye on the dsDNA at force F as function of dye concentration. K_F is the binding constant as function of force, and n_F is binding site size in base pairs as function of force. C is the concentration of dye molecules in the surrounding buffer.

In chapter 3 we have observed a clear relationship between the increase in contour length of the dsDNA-dye complex, and the amount of fluorescence, revealing that the elongation is proportional to the amount of dye molecules bound and thus the binding density ν. The elongation of the dsDNA molecule in the presence of intercalating molecules at a specific concentration as a function of force can be defined in terms of fractional elongation γ(F,C). Fractional elongation of the dsDNA is defined as follows (6)

$$\gamma(F,C) = \frac{x_{complex}(F,C) - x_{DNA}(F)}{x_{DNA}(F)} \qquad (2)$$

Here $x_{complex}(F,C)$ and $x_{DNA}(F)$ represent the lengths of dsDNA at force F, respectively in the presence (at a certain concentration C) and the absence of intercalating molecules. The fractional elongation as a function of force at one particular dye concentration is determined from the force extension curves. In a next step by sorting these data upon force we are able to determine the fractional elongation as a function of concentration at a constant force (Fig. 2). The fractional elongation is converted to binding density and these curves are then curve-fitted with the McGhee-von Hippel binding isotherm (Eq. 1) (6-7) to obtain the binding constant (K) and binding site size (n) in base pairs.

5.3
Relation between fractional elongation and binding density

The fractional elongation can be rewritten as:

$$\gamma = \frac{x_{complex} - x_{DNA}}{x_{DNA}} = \frac{x_{DNA} + n \cdot \Delta x - x_{DNA}}{x_{DNA}} = \frac{n \cdot \Delta x}{x_{DNA}} = \frac{n \cdot \Delta x}{N \cdot x_{bp}} = \frac{\Delta x}{x_{bp}} \upsilon \qquad (3)$$

Where n is total number of dye molecules bound to the dsDNA and Δx is the elongation upon the insertion of one dye molecule. The length of the dsDNA molecule (x_{DNA}) is expressed as the number of basepairs (N) times the distance between two consecutive basepairs (x_{bp}). The ratio of the number of dyes bound (n) and the number of available binding sites (N, identical to the total number of basepairs) is the definition of the binding density. Each YO-1 molecule that intercalates the dsDNA causes an elongation equivalent to the distance between two basepairs (8). In this case $\Delta x = x_{bp}$ and therefore the fractional elongation is identical to binding density ($\gamma=\nu$). In the case of YOYO-1 the elongation equals the distance of 2 basepairs per inserted molecule. Δx equals therefore $2x_{bp}$ and $\gamma=2\nu$.

5.4
Results

5.4.1
Interaction of YO-1 with dsDNA

Force extension curves of dsDNA obtained in the absence and presence of 100, 200, 500, 1000 and 2000 nM YO-1 concentrations are presented in Fig. 1. The contour length of the dsDNA (at a particular force) increased with an increased dye concentration while the persistence length of the complex decreased (Table 1). The overstretching region, typical seen in force extension curves of bare dsDNA at about 65 pN force, was not observed at these concentrations for dsDNA-YO-1 complex. No hysteresis in the extension relaxation cycles was observed at these concentrations and a pulling rate of 3 µm/s, indicating that the complex was continuously in kinetic equilibrium while performing the force extension relaxation cycles.

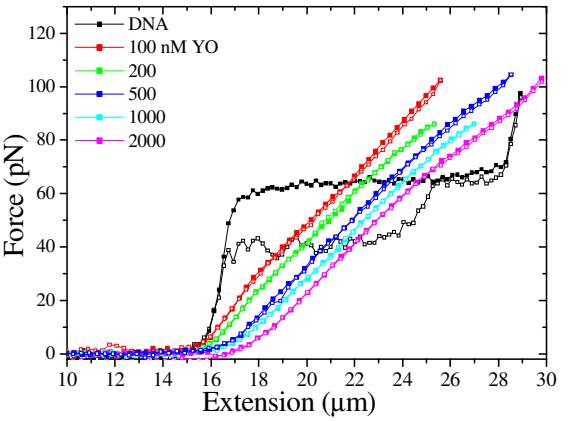

Fig. 1
Force extension curves of the λ-phage DNA in the absence and presence of YO-1 molecules at various concentrations of YO-1 in the surrounding buffer. Force extension curves were obtained at 3 µm/s pulling speed. Closed and open symbols present the extension and relaxation part of the cycle respectively.

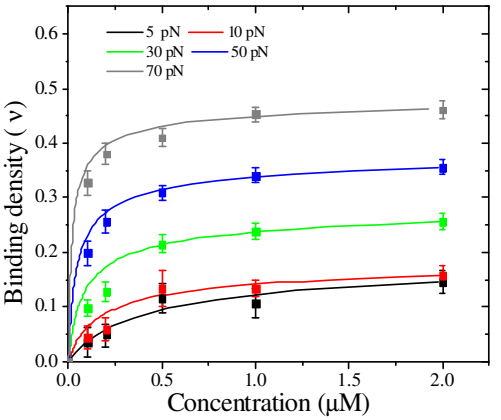

Fig. 2

Binding density (ν) as function of the free dye concentration at different forces for YO-1 binding to dsDNA. Solid lines represent the McGhee-von Hippel binding isotherm that was curve-fitted to the data (Eq. 1).

Table 1 Parameters obtained by curve-fitting the extension part of the force extension curve of dsDNA in the absence and presence of various concentrations of YO-1 molecules by EWLC fit (9).

Concentration YO-1 (nM)	Persistence length (nm)	Contour length (μm)	Stretch modulus (pN)
0	52.00	16.4	1100
100	48.00	17.2	587
200	46.10	17.3	457
500	28.20	17.6	187
1000	23.30	18.2	196
2000	19.90	18.5	200

The force extension curves of dsDNA obtained in the presence of different YO-1 concentrations (Fig. 1) were used to determine the binding densities as a function of both the applied force and the concentration of YO-1 using Eq. 2 and 3. The obtained binding densities were then sorted on applied force (Fig. 2). Data points presented in Fig. 2 are averages of at least 3 different force extension curves. For each force as presented in Fig. 2 we curve-fitted the binding density versus concentration curve with the McGhee-von

Hippel binding isotherm (Eq. 1) to determine the binding constant (K_F) and binding site size (n_F) as a function of the force. Results of these fits are presented in Fig. 3.

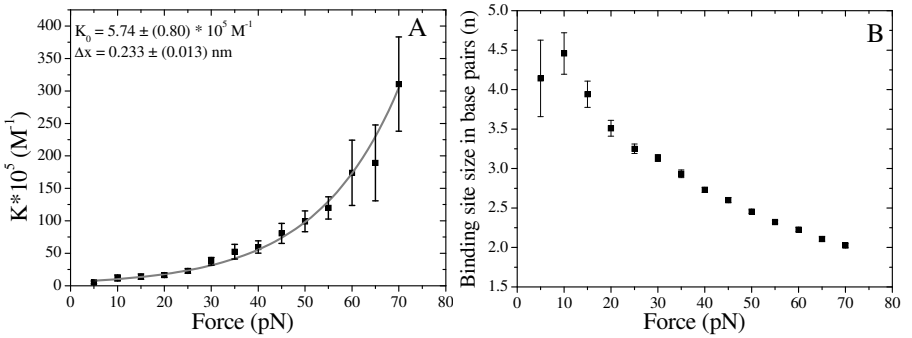

Fig. 3

Results of curve-fitting the data presented in Fig. 2 using the McGhee-von Hippel binding isotherm (Eq. 1). (A) Binding constant K as function of force. The continuous line is an exponential fit (Eq. 4) to the data. (B) Binding site size as function of force.

The binding constant can be expressed as a function of the kinetic rates of the binding and unbinding reactions:

$$K_F = \frac{k_1}{k_{-1}} = \frac{k_{1,0}\exp(-F\Delta x_1/k_BT)}{k_{-1,0}\exp(F\Delta x_{-1}/k_BT)} = K_0\exp(-F(\Delta x_1+\Delta x_{-1})/k_BT) = K_0\exp(-F\Delta X/k_BT) \qquad (4)$$

K_F is force dependent binding constant, K_0 is the zero force binding constant, F is applied force (pN), Δx is the extension of dsDNA per intercalator, k_B is Boltzmann constant and T is temperature. ΔX in this equation is the sum of the distances from the bound and unbound state to the transition state. In other words, it is the sum of the distances over which the force is acting from the binding and unbinding reaction.

From this derivation it is clear that the exponential force dependence of the K_F is a direct result from the force-dependence of the rate constants. The underlying principle is the reduction (in case of binding) or increase (in case of unbinding) of the energy barrier of the intermediate state, as a result of the externally applied force. Furthermore a change in the binding site size from 4.5 to 2.0 bp was obtained as the applied force changed from 10 to 70 pN. This reduction might be explained by the fact that the externally applied force causes the dsDNA to align and stretch, which effectively creates more binding sites which were not available at lower forces. From the curve-fit in Fig. 3A, we determined a binding

constant of YO-1 in the absence of an external force (K_0) of 5.74±(0.8)·10^5 M^{-1} and a ΔX of 0.233±(0.013) nm. This ΔX value obtained for YO-1 is in good agreement with the reported value obtained for ethidium (0.25 nm) which is another mono-intercalating dye molecule (6).

5.4.2
dsDNA-YOYO-1 equilibrium force extension curves

In Chapter 4 we have presented the force extension curves of the dsDNA-YOYO-1 complex in the presence of various concentrations of YOYO-1 (Fig. 4). From the hysteresis observed between the stretching and relaxation cycle, we concluded that the dsDNA-YOYO-1 is not in equilibrium while stretching and relaxing the molecule (chapter 3).

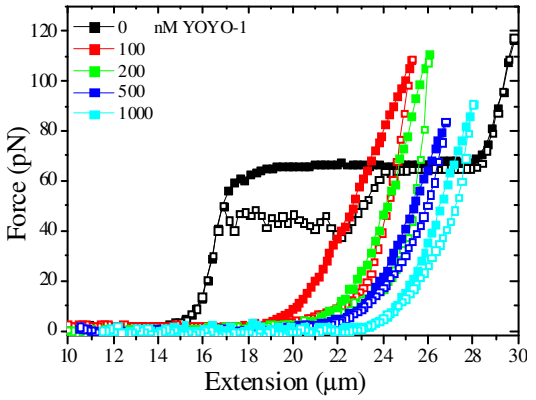

Fig. 4

Force extension curves of single λ-phage DNA molecules in the presence of various YOYO-1 concentrations. Force spectroscopy is performed at 3 μm/s pulling speed.

To determine the binding constant and binding site size as function of force, it is necessary to determine the force extension curves of the complex at thermodynamic equilibrium, not limited by the kinetics. These equilibrium force extension curves are obtained by pulling the dsDNA to different extensions in a stepwise manner, after which the system is left to restore its equilibrium. As soon as the preset extension is reached the force exerted by the complex drops exponentially to the equilibrium force (Fig. 5). The equilibrium forces attained by the complex were shown not to depend on the pulling speed

but only on the extension of the complex (chapter 3 Fig. 7A). Fig 5. shows the force relaxation curves as a function of time at different constant extensions and concentrations.

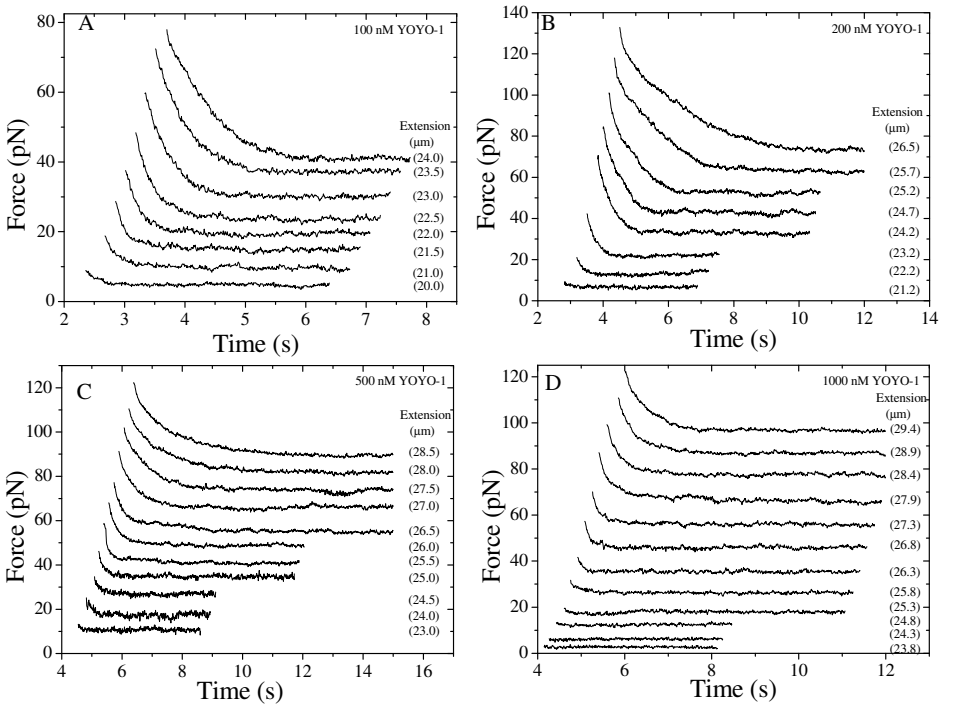

Fig. 5

Force relaxation curves recorded after pulling the dsDNA in the presence of various YOYO-1 concentrations to different preset extensions at 3μm/s pulling speed and allowed to reach to the equilibrium force. Panel A, B, C and D presents experiments performed in the presence of 100, 200, 500 and 1000 nM YOYO-1 respectively.

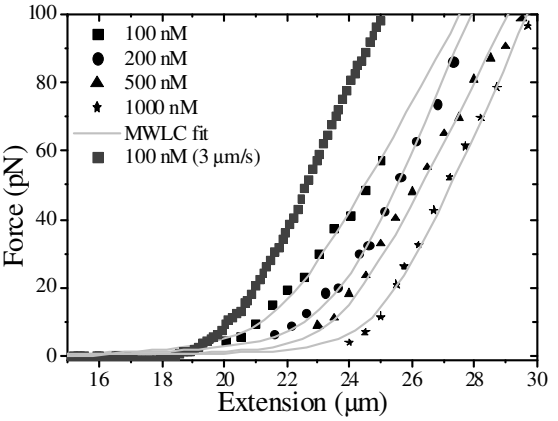

Fig. 6

Equilibrium force extension curves of the dsDNA-YOYO-1 complex at various YOYO-1 concentrations. The curves were obtained as mentioned in the main text. Obtained data points were curve fitted with extensible WLC model. Dark gray squares presents dsDNA-YOYO-1 complex in the presence of 100 nM YOYO-1 pulled at 3 µm/s which clearly indicates the difference in the equilibrium force extension curve and force extension curve obtained at 3 µm/s pulling speed.

The forces to which the complex equilibrates have been used to construct the equilibrium force extension curve of the dsDNA-YOYO-1 complex. This has been done for 100, 200, 500 and 1000 nM YOYO-1 (Fig. 6). By curve fitting the equilibrium force extension curve of the complex by the extensible WLC model (Table 2) (9) it was possible to obtain force values at intermediate extensions (Fig. 6).

Table 2 Parameters obtained by curve-fitting the equilibrium force extension curves of dsDNA-YOYO-1 complex (Fig. 6) by extensible WLC fit (9).

Concentration YOYO-1 (nM)	Persistence length (nm)	Contour length (µm)	Stretch modulus (pN)
0	52.00	16.4	1100
100	21.00	21.92	336
200	18.00	23.82	477
500	16.00	24.92	545
1000	16.00	26.24	635

After obtaining the equilibrium force extension curves for the dsDNA-YOYO-1 complex at different concentrations of YOYO-1 molecules, we determined the binding densities for dsDNA-YOYO-1 at different concentrations and forces using Eq. 2 and 3. The data were sorted on force and for each force the binding density was plotted as a function of concentration (Fig. 7). Data points presented in Fig. 7 are averages of at least 5 different force extension curves. Each curve was curve-fitted with the McGhee-von Hippel binding isotherm (Eq. 1) to determine the force dependent binding constant (K_F) and binding site size (n_F).

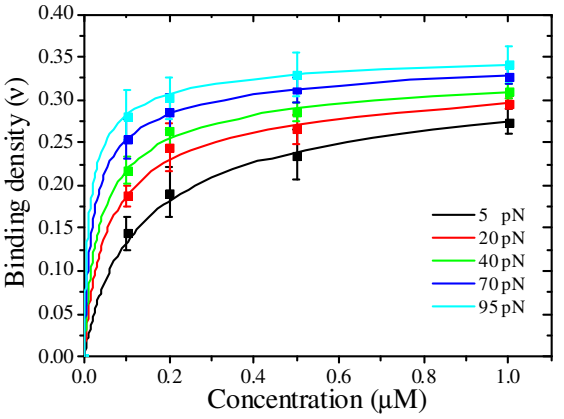

Fig. 7

Binding densities of dsDNA-YOYO-1 complex as function of concentration at different forces. Data points are curve fitted with McGhee-von Hippel binding isotherm (solid line, Eq. 1).

The binding constant and binding site size as function of force are presented in the Fig. 8. The binding site size does show a 3% change as function of applied force. The binding constant increases as function of applied force and curve-fitting the data in Fig. 8(A) with Eq. 4 resulted in a zero force binding constant $38.75\pm(1.28)\cdot 10^5$ M^{-1} and a ΔX of 0.09 nm.

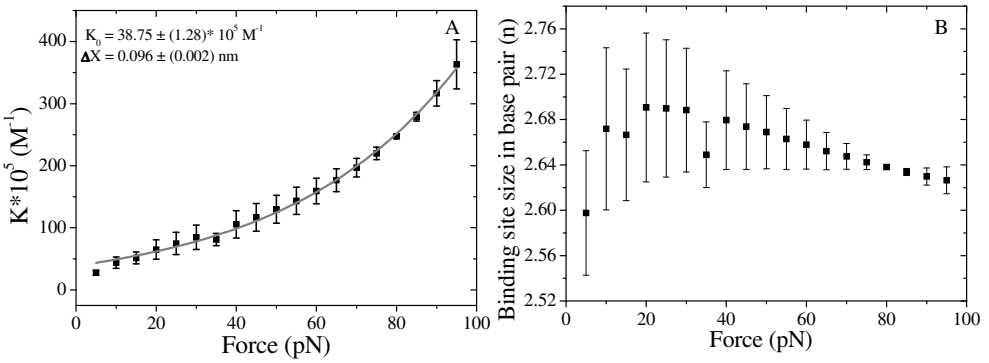

Fig. 8

(A) Binding constant K as function of force. The solid gray line is the curve-fit using Eq. 4. (B) Binding site size as function of force.

5.5

Discussion

In this chapter and chapter 3 we studied the interaction of the mono intercalator YO-1 with dsDNA at various concentrations of YO-1. The force extension curves did not show significant hysteresis between the stretch and relaxation cycle, suggesting that dsDNA-YO-1 complex is in equilibrium while performing the force measurements at these concentrations. Using the McGhee-von Hippel binding isotherm (7) we determined the binding constant and binding site size as function of applied force. Binding site size decreases from 4.5 to 2 bp whereas the binding constant increases from $1.18 \cdot 10^6$ to $3.11 \cdot 10^7$ M^{-1} as the applied force changes from 10 to 70 pN. Fitting the binding constant as a function of force with an exponential function, we have determined the zero force binding constant of YO-1 ($5.74 \cdot 10^5$ M^{-1}). Other mono-intercalating dye molecules such as ethidium ($5.8 \cdot 10^5$ M^{-1}) and TO ($32 \cdot 10^5$ M^{-1}) have comparable binding constants (6, 10). The ΔX value obtained for YO-1 is 0.233±(0.013) nm. This is in good agreement with ethidium (0.25 nm) and ruthenium (0.28 nm) molecules (6).

As reported in chapter 3, the interaction kinetics of the bis-intercalator YOYO-1 with dsDNA were found to be slower compared to YO-1. The equilibrium force extension curves for dsDNA-YOYO-1 complex have been determined by extending the complex in a stepwise manner and giving it time to reach its equilibrium. The extensions and corresponding forces that were reached were used to construct the equilibrium force extension curves. This would be equivalent to a force extension curve obtained with a pulling rate that is infinitely small. From these equilibrium force extension curves the binding constant and binding site size of YOYO-1 as a function of the applied force have

been determined. We observed that, the binding constant of YOYO-1 increases with force (Fig. 8A). The binding site size however does only reveal a 3% variation as a function of the force, which is quite different from that observed in the case of YO-1 (Fig. 8B). The zero force binding constant found for YOYO-1 is in the range of 10^6 M^{-1}, which is some orders of magnitude lower than values reported in the literature. Binding constant values for YOYO-1 are estimated to be in the range of 10^8 – 10^{10} M^{-1} (8, 11-12). The ΔX value obtained by fitting the binding constant as a function of force for YOYO-1 is 0.09 nm, which is 3 times smaller than that of YO-1. As derived in the Results section the ΔX is a sum of distances over which the force is acting in the binding and unbinding reaction. In the case of YO-1 the value for ΔX is 0.23 which is roughly the extension of the dsDNA due to the intercalation of one molecule. For YOYO-1 the extension of the dsDNA upon intercalation of one molecule is 0.884 nm (8). The ΔX value however found in the analysis is only 0.09 nm.

It is tempting to think that the ΔX that describes the force dependence of the binding constant is identical to the elongation of dsDNA upon intercalation of one dye molecule. This, however, is not correct. The ΔX value is the sum of the distances over which the force is acting during the binding and unbinding reaction, and depending on the precise shape of the energy landscape going from the bound to the unbound state and vice versa, this value can be much smaller. In the case of YO-1 the value is 0.23 nm, which is 68% of the length increase of the dsDNA upon intercalation. For YOYO-1 the value is 0.09, which is only 13% of the length increase. The fact that the value for YO-1 is about the same as for other mono-intercalators such as ethidium, supports the hypothesis that the different mono-intercalating agents bind in a similar manner, most probably in a one-step process, as proposed in Chapter 3. The low force dependence of the binding constant of YOYO-1 suggests that the binding does not occur in one single step, but in more than one step.

5.6 Conclusions

In this chapter the force extension curves of dsDNA in the presence of various concentrations of YO-1 have been recorded. For YOYO-1, since the kinetics of interaction are relatively slow with respect to the time of the experiment, equilibrium force extension curves have been measured. From these data the fractional elongation for both complexes and thus the binding densities were derived as a function of the dye concentration and the applied force. Grouping these data by force, the data was curve-fitted with the McGhee-von Hippel binding isotherm to determine the force dependent binding constant and binding site size. For YO-1 the binding site size decreased from 4.5 bp to 2 bp and the binding constant increased from $1.18 \cdot 10^6$ M^{-1} to $3.11 \cdot 10^7$ M^{-1} as force changes from 10 pN to 70

pN. The zero force binding constant for YO-1 is (5.74±(0.8)·10^5 M^{-1}) and extension of the dsDNA due to intercalation of single YO-1 molecules is 0.233 nm (ΔX). For YOYO-1 the binding site size was only 2.6 bp and varied not more than 3% with the same variation in force. The zero force binding constant was determined as 38.75±(1.28)·10^5 M^{-1}, which is many orders of magnitude lower than reported elsewhere (8, 11-12). Furthermore the dependence of the binding constant on the force was also lower than expected, resulting in a value for ΔX of only 0.09 nm, much lower than for YO-1. One possible way to explain the discrepancy in the data is to assume that YOYO-1 and YO-1 follows different paths while interacting with the dsDNA. dsDNA-YO-1 interaction is single step interaction where as dsDNA-YOYO-1 is a multiple step interaction.

5.7
References

1. Strekowski, L., and B. Wilson. 2007. Noncovalent interactions with DNA: an overview. Mutat Res 623:3-13.
2. Armitage, B. A. 2005. Cyanine Dye–DNA Interactions: Intercalation, Groove Binding, and Aggregation. 55-76.
3. Hurley, L. H. 2002. DNA and its associated processes as targets for cancer therapy. Nat Rev Cancer 2:188-200.
4. Waring, M. J. 1981. DNA modification and cancer. Annu Rev Biochem 50:159-192.
5. Leng, F., W. Priebe, and J. B. Chaires. 1998. Ultratight DNA binding of a new bisintercalating anthracycline antibiotic. Biochemistry 37:1743-1753.
6. Vladescu, I. D., M. J. McCauley, M. E. Nunez, I. Rouzina, and M. C. Williams. 2007. Quantifying force-dependent and zero-force DNA intercalation by single-molecule stretching. Nat Methods 4:517-522.
7. McGhee, J. D., and P. H. von Hippel. 1974. Theoretical aspects of DNA-protein interactions: co-operative and non-co-operative binding of large ligands to a one-dimensional homogeneous lattice. J Mol Biol 86:469-489.
8. Johansen, F., and J. P. Jacobsen. 1998. 1H NMR studies of the bis-intercalation of a homodimeric oxazole yellow dye in DNA oligonucleotides. J Biomol Struct Dyn 16:205-222.
9. Marko, J. F., and E. D. Siggia. 1995. Stretching DNA. Macromolecules 28:8759-8770.
10. Petty, J. T., J. A. Bordelon, and M. E. Robertson. 2000. Thermodynamic Characterization of the Association of Cyanine Dyes with DNA. The Journal of Physical Chemistry B 104:7221-7227.
11. Glazer, A. N., and H. S. Rye. 1992. Stable dye-DNA intercalation complexes as reagents for high-sensitivity fluorescence detection. Nature 359:859-861.
12. Larsson, A., C. Carlsson, and M. Jonsson. 1995. Characterization of the binding of YO to [poly(dA-dT)]2 and [poly(dG-dC)]2, and of the fluorescent properties of YO and YOYO complexed with the polynucleotides and double-stranded DNA. Biopolymers 36:153-167.

Chapter 6

Interaction of tri peptide *Lys-Trp-Lys* with dsDNA: a single molecule approach

Abstract

Many cellular processes involve interactions between DNA and protein molecules. Key here is the specificity of the interaction: the protein often needs to bind to a specific location in order to perform its biological function. The tri-peptide Lys-Trp-Lys is found in many protein molecules, and is hypothesized to be involved in the interaction with denatured parts of DNA. Here we report on single-molecule force spectroscopy experiments using optical tweezers on λ-DNA in the presence of Lys-Trp-Lys molecules at 150 mM and 10 mM NaCl. In quasi-physiological conditions (150 mM NaCl) in which the DNA adopts a stable double-helical structure in which most of the opposing bases are paired, there was no significant binding of Lys-Trp-Lys. However, at 10 mM NaCl, significant binding to the dsDNA molecule was observed, indicative of Lys-Trp-Lys molecules preferentially binding to partly destabilized dsDNA. At this lower NaCl concentration, binding densities of the Lys-Trp-Lys tripeptide to the dsDNA as a function of the applied stretching forces were determined from the recorded force extension curves of dsDNA-tripeptide complex at various concentrations of Lys-Trp-Lys. Values for the binding constant and the binding site size as a function of force were determined by curve fitting the binding densities as a function of the peptide concentration with the McGhee-von Hippel binding isotherm. The binding constant increases from 100 to 1200 M^{-1} and binding site size decreases from 5.4 to 3.8 bp as force increases from 10 to 50 pN.

6.1
Introduction

The interaction between dsDNA and proteins is at the center of most cellular processes, such as replication, transcription and DNA repair. During normal cell life the dsDNA is subjected to different types of induced and spontaneous chemical reactions that change its structure, which if not repaired can interfere with the aforementioned interactions and ultimately can lead to the loss of genetic information (1). Different proteins recognize their specific binding sites on the dsDNA by recognizing the sequence or the structure of the DNA (1-2). For example ultraviolet endonuclease recognizes denatured DNA sites (3) and single stranded binding proteins specifically bind to single stranded DNA (4). Interactions of protein molecules with DNA have been studied using single molecule techniques such as optical tweezers (4-5), to determine the various kinetic parameters such as association and dissociation constant as function of force and concentration of the protein molecules (4-5). The binding constants obtained are in the range of 10^6 to 10^{10} M^{-1} (4-7). In DNA-protein interactions the role of the aromatic amino acids (phenylalanine, histidine, tyrosine and tryptophan) present in proteins has been hypothesized to detect the denatured sites on the DNA molecules (via intercalation) and to specifically bind to the DNA creating a specific DNA-protein interaction. To study the interactions of aromatic amino acids with DNA small oligopeptides such as Lys-Trp-Lys have been used as model systems (8-10).

There are two different ways in which Lys-Trp-Lys interacts with the dsDNA. The first interaction is electrostatic in nature. At neutral pH the amino acid lysine (Lys) bears a positive charge and therefore the tripeptide interacts with the negatively charged backbone of the dsDNA. The second mode is a stacking interaction (intercalation) where the aromatic ring of the Trp inserts between two base pairs of the dsDNA (11). The interaction of Lys-Trp-Lys with dsDNA has been studied with bulk experimental techniques such as NMR and fluorescence (8-10, 12-14). It is reported that the binding constant of Lys-Trp-Lys is 4 to 5 orders of magnitude lower than that of other intercalating molecules such as ethidium ($4.6 \cdot 10^5$ M^{-1}) and YO-1 ($38.75 \cdot 10^5$ M^{-1}). The hypothesis is that the Lys-Trp-Lys tripeptide as part of the protein molecule is involved in the specific interaction of the protein with the denatured dsDNA site.

This chapter reports on the study of the interaction of Lys-Trp-Lys with a single λ-DNA molecule studied with force-measuring optical tweezers. The mechanical properties of the dsDNA in the presence of 100 μM Lys-Trp-Lys at 150 mM NaCl did not show any significant change from the case in the absence of peptide. This result indicates that there is no significant interaction (intercalation) between the dsDNA and the Lys-Trp-Lys at physiological conditions. Physiologically stable dsDNA was converted into partly denatured dsDNA (structurally destabilized DNA) by lowering the salt concentration from

150 to 10 mM and changing the pH from 7.5 to 6.5. In these conditions, a significant change in the mechanical properties of dsDNA in the presence of 100 µM Lys-Trp-Lys was observed. The contour length changed from 16.40 to 16.68 µm, the persistence length showed a reduction from 60 to 34 nm and the stretch modulus reduced from 800 to 340 pN. In a next set of experiments force extension curves of the dsDNA-Lys-Trp-Lys complex were recorded at various concentrations of Lys-Trp-Lys (100, 500 and 1000 µM) at 10 mM NaCl. The binding density of the Lys-Trp-Lys at different forces as function of concentration was determined. Curve-fitting the binding densities as a function of the peptide concentration at different forces with the McGhee-von Hippel binding isotherm (15) allowed the determination of the force-dependent binding constant and binding site size. The binding constant increases from 100 to 1200 M^{-1} and binding site size decreases from 5.4 to 3.8 bp as force increases from 10 to 50 pN.

6.2
Materials and Methods

The optical tweezers instrument used here to perform single molecule force spectroscopy of the single dsDNA and dsDNA-Lys-Trp-Lys complex has been described in detail in chapter 2 of this thesis. In brief, a single λ-DNA molecule was modified at both extremities with biotin to bind to two streptavidin-coated polystyrene beads (2.6 µm diameter). One of the beads is trapped with the help of the laser tweezers and a second bead is attached on tip of a glass micropipette (16). A buffer containing 150 mM NaCl, 10 mM Tris-HCl, pH 7.5, 1 mM EDTA and 0.01% NaN_3 was used (buffer 1). After attachment of the dsDNA between two beads, force spectroscopy was performed by moving the micropipette with respect to the optical trap to confirm that only one dsDNA was attached between the beads. Then the above-mentioned buffer supplemented with 100 µM Lys-Trp-Lys was flown in, and force spectroscopy was performed on the complex. In the second set of experiments another buffer (10 mM NaCl, 10 mM HEPES, pH 6.5, 1 mM EDTA and 0.01%NaN_3 with different concentrations of Lys-Trp-Lys ranging from 100 to 1000 µm) was used to perform force spectroscopy of the dsDNA-Lys-Trp-Lys complex at various tripeptide concentrations.

6.3
Results and Discussion

6.3.1
Interaction of Lys-Trp-Lys with dsDNA

Force extension and relaxation curves of the dsDNA in the presence and absence of Lys-Trp-Lys (100 µM) at 150 mM NaCl are presented in Fig. 1. The curve of the bare dsDNA shows the characteristic overstretching plateau at about 65 pN. Mechanical properties of the dsDNA with and without the tripeptide are obtained by curve-fitting the extension part of the force extension curves with the extensible WLC model (17). The results are presented in Table 1. The two force extension relaxation curves are very similar. This was further supported by the parameters resulting from the curve-fit, which were not significantly different in both cases.

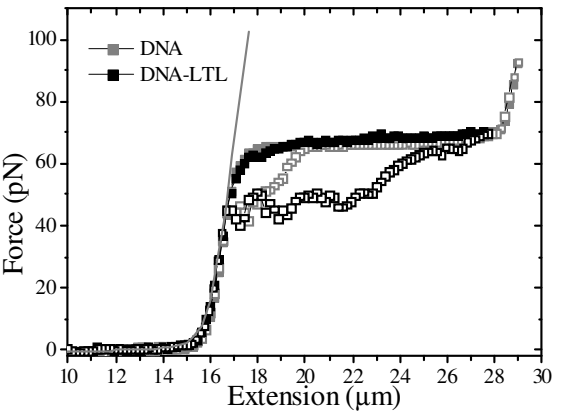

Fig. 1
Force extension curves of dsDNA in the presence (black symbols) and absence (gaey symbols) of 100 µM Lys-Trp-Lys. Both force extension curves are measured in the presence of 150 mM NaCl (buffer 1). Open and closed symbols present the extension and relaxation respectively. Gray solid line presents curve fitting of extension part of force extension curve by extensible WLC model. Force extension curves are obtained at 3 µm/s pulling speed.

The presence of Lys-Trp-Lys at a concentration of 100 µM in the surrounding buffer does not affect the mechanical properties of dsDNA in a significant manner in contrast to other intercalating molecules such as ethidium (18) and YO/YOYO (chapters 3-5 of this thesis). This indicates a low binding constant of the Lys-Trp-Lys molecule to the dsDNA under these conditions, relative to other intercalators.

Changing the pH (higher and lower than 7.5) of the buffer solution, increasing the temperature and lowering the salt concentration have a significant effect on the structural stability of the DNA (19-23). The force extension and relaxation curves of dsDNA in the presence of 10 mM NaCl were obtained and compared to curves recorded at 150 mM NaCl (Fig. 2). The extension part of the force extension curve is curve-fitted with the extensible WLC model to determine the various mechanical parameters (Table 1). The results extracted (contour length 16.4 μm, persistence length 60 nm and stretch modulus 800 pN) are in good agreement with published results (22). The lowering of the force at which the dsDNA starts to overstretch is a clear indicator of the structurally destabilized dsDNA (22). dsDNA molecules at 10 mM NaCl are extended up to only 26 μm extension, since the molecule or its linker has a tendency to break during the force extension relaxation experiment (22-23). Due to the lower stability of the dsDNA structure, it is very likely that the two single strands completely dissociate from one another and cause the molecule to fall apart.

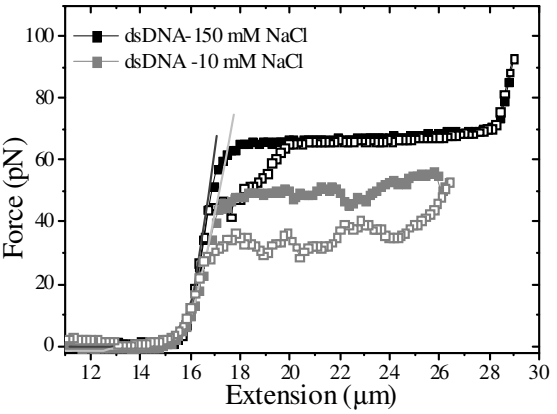

Fig. 2

Force extension relaxation curves of dsDNA in the presence of 150 mM (black symbols) and 10 mM NaCl (gray symbols). Open and closed symbols represent extension and relaxation respectively. Force spectroscopy is performed at 3 μm/s pulling speed. Solid lines represent the curve-fit to the extension part of force extension curve by extensible WLC model.

Table 1 Mechanical properties of dsDNA and dsDNA- Lys-Trp-Lys complex

dsDNA	Contour length (μm)	Persistence length (nm)	Stretch modulus (pN)
dsDNA (150 mM NaCl	16.40±0.20	52±4	1100±150
dsDNA + 100 μM Lys-Trp-Lys (150 mM NaCl	16.40±0.30	51±3	1050±200
dsDNA (10 mM NaCl)	16.40±0.20	60 ±4	800±100

6.3.2
Interaction of Lys-Trp-Lys with dsDNA at 10 mM NaCl

Force extension curves of dsDNA-Lys-Trp-Lys complex were recorded in the presence of the various Lys-Trp-Lys concentrations (100, 500 and 1000 μM) at 10 mM NaCl (Fig. 3). At all conditions tested a clear change in the mechanical properties of dsDNA-Lys-Trp-Lys complex was observed relative to bare dsDNA (Fig. 3). The extension part of the force extension curves was curve-fitted with an extensible WLC model (Fig. 3) and the results are presented in Table 2. The contour length of the dsDNA increased as function of Lys-Trp-Lys concentration in the buffer. If no peptide was added to the surrounding buffer the force extension curve showed a significant amount of hysteresis. This hysteresis is still present in the presence of 100 μM Lys-Trp-Lys but was observed to disappear at higher concentrations (500 and 1000 μM). The overstretching region for 100 μM Lys-Trp-Lys appeared at higher forces (70 pN) and tilted compared to the situation where no peptide was added (50 pN). At concentrations of 500 and 1000 μM no overstretching region was observed, probably partly because the complex has not been stretched up to a high force level. These changes in the mechanical properties are qualitatively very much similar to those seen when adding the intercalator ethidium (18) and YOYO-1 (chapter 5 of this thesis). dsDNA-Lys-Trp-Lys tends to break in the presence of 500 and 1000 μM Lys-Trp-Lys when stretched beyond 21 μm. Breaking of the complex is most probably due to denatured DNA and the ability of Lys-Trp-Lys to break the dsDNA (24-25).

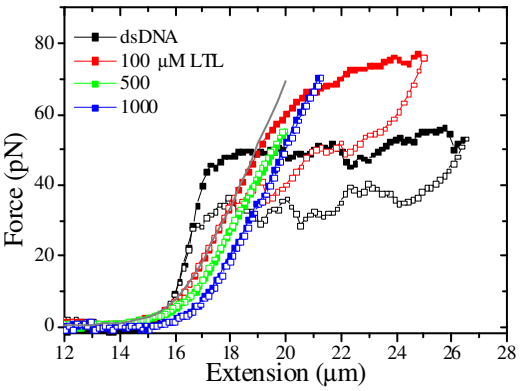

Fig. 3

Force extension curves of the dsDNA in the absence and in the presence various concentrations of Lys-Trp-Lys. Open and close symbols represent the extension and relaxation respectively. Force extension curves were obtained at 3 µm/s pulling speed. Gray line presents the curve-fit of extensible WLC model to the extension part of force extension curve. Experiments were performed in the presence of 10 mM NaCl.

Table 2 Mechanical properties of dsDNA and dsDNA- Lys-Trp-Lys complex at 10 mM NaCl

Lys-Trp-Lys concentration (µM)	Contour length (µm)	Persistence length (nm)	Stretch modulus (pN)
0	16.40 (±0.2)	60 (±4)	800 (±100)
100	16.68 (±0.20)	34 (±5)	340 (±70)
500	17.09 (±0.15)	25 (±3)	310 (±25)
1000	17.90 (±0.30)	20 (±2)	300 (±30)

6.3.3
Determining force dependent binding constants

The concentration-dependent force extension curves (Fig. 3) and binding density as function of concentration curves (Fig. 4) for Lys-Trp-Lys dsDNA complex are qualitatively similar to those presented for YO-1, YOYO-1 and ethidium (Chapter 6 of this thesis, (18)). From this it was concluded that the elongation of the dsDNA in terms of contour length is directly proportional to the number of molecules bound to the dsDNA.

The recorded force extension curves of dsDNA-Lys-Trp-Lys complex (Fig. 3) at various concentrations of Lys-Trp-Lys were used to determine the binding density of Lys-

Trp-Lys at different forces (please refer to chapter 5 of this thesis for the method used to determine the binding density). Fig. 4 shows the binding density as a function of concentration at different forces (data points are averaged over at least 4 molecules at each concentration). These data points are curve-fitted with the McGhee-von Hippel binding isotherm (Eq. 1, Eq. 2 in Ref. (18)) to determine the force dependent binding constant and binding site size.

$$\nu_F(C) = K_F \times C \times \frac{(1-n_F\nu_F)^{n_F}}{(1-n_F\nu_F+\nu_F)^{n_F-1}} \qquad (1)$$

Where $\nu_F(C)$ is the binding density of Lys-Trp-Lys as function of concentration of Lys-Trp-Lys molecules in the surrounding buffer and force, K_F is binding constant as function of force, and n_F is the binding site size in base pairs as function of force. In chapter 5 we have shown that this method provides reliable results for mono- intercalating molecules but not for bis-intercalating molecules. Lys-Trp-Lys is a mono- intercalating molecule (11, 13), so the analysis presented in chapter 5 can be used here to provide reliable results on the force-dependent binding constant and binding site size.

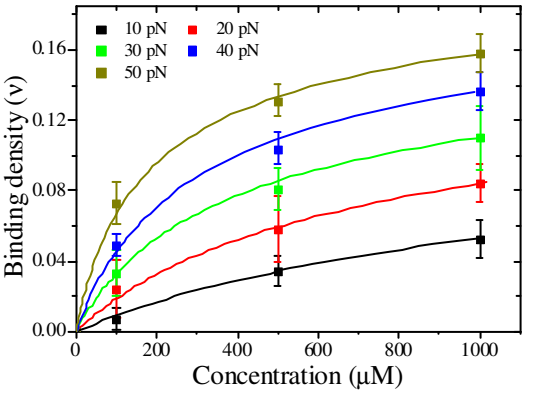

Fig. 4

Binding density of Lys-Trp-Lys to dsDNA as function its concentration in the buffer determined at different forces. For each force the data points are curve-fitted with the McGhee-von Hippel binding isotherm (Eq. 1).

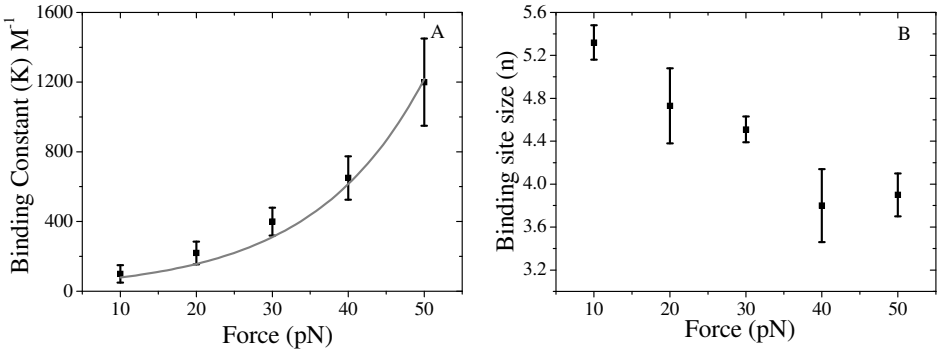

Fig. 5

(A) Binding constant as function of force. The solid gray line presents the curve-fit of Eq. 2. (B) Binding site size as function of force.

The binding constant for Lys-Trp-Lys to dsDNA as a function of force is presented in Fig. 5A. It increases exponentially with the applied force from 100±50 M^{-1} at 10 pN to 1200±250 M^{-1} at 50 pN. The exponential function (Eq. 2) was curve–fitted to the data points (Fig. 5A).

$$K_F = K_0 \times e^{F\Delta X / k_B T} \qquad (2)$$

where K_F is the force-dependent binding constant, K_0 is the zero force binding constant and ΔX is the sum of the distances over which force is acting during binding and unbinding. The zero force binding constant of Lys-Trp-Lys was found to be 40±(17) M^{-1}, which is in good agreement with the values reported in the literature of 7 and 50 M^{-1} (13, 26) obtained at 10 mM NaCl. ΔX is 0.28±(0.04) nm, which is similar to the distance between the basepairs. This value is in good agreement with ΔX values obtained for other mono-intercalators such as YO-1 (0.23 nm) and ethidium (0.28 nm) (18). Binding site size (in basepairs) decreases as function of applied force (Fig. 5B) from 5.3±0.16 bp at 10 pN to 3.9±0.2 bp at 50 pN. These results are in good agreement with our results with YO-1 (chapter 5 of this thesis).

6.4
Conclusions

The force extension curve of a dsDNA-Lys-Trp-Lys (100 μM) complex at 150 mM NaCl is similar to that of bare dsDNA, indicating that there is almost no interaction between the dsDNA and the tripeptide. This observation is in agreement with the results presented in the literature (8-10, 12-14). By changing the NaCl concentration from 150 mM to 10 nM in the buffer and changing pH from 7.5 to 6.5, the dsDNA structure is partly destabilized and a measurable interaction of Lys-Trp-Lys with dsDNA was observed. In these altered buffer conditions, the contour length of the dsDNA-tripeptide complex increased as function of the Lys-Trp-Lys concentration (Fig. 3 and Table 2). From this observation it was concluded that the Lys-Trp-Lys peptide has a larger binding affinity towards the dsDNA in partly denatured state relative to its physiologically native state. The enhanced binding of Lys-Trp-Lys to denatured dsDNA suggests that aromatic amino acids proteinmolecules play a role in detecting and interacting with denatured sites in the dsDNA.

Extracting the binding density as a function of the concentration at various forces and curve-fitting the McGhee-von Hippel binding isotherm to this data enabled the determination of the binding constant and binding site size of Lys-Trp-Lys as a function of force. The binding constant increased from 100±50 to 1200±250 M^{-1} as force changes from 10 to 50 pN. The binding site size decreases from 5.4 to 3.8 bp. The zero force binding constant of Lys-Trp-Lys is 40±(17) M^{-1} which is in agreement with the results presented in literature (9-10, 26). The distances over which the force (ΔX) is acting, which resulted from fitting the binding constant as a function of force, was 0.28±(0.03) nm, similar to values reported for intercalators such as ethidium (0.28 nm) and YO-1(0.23 nm).

6.5
References

1. Helene, C. 1985. Molecular mechanisms for the recognition of damaged DNA regions by peptides and proteins. Adv Biophys 20:177-186.
2. Werner, M. H., A. M. Gronenborn, and G. M. Clore. 1996. Intercalation, DNA kinking, and the control of transcription. Science 271:778-784.
3. Minton, K., M. Durphy, R. Taylor, and E. C. Friedberg. 1975. The ultraviolet endonuclease of bacteriophage T4. Further characterization. J Biol Chem 250:2823-2829.
4. Shokri, L., I. Rouzina, and M. C. Williams. 2009. Interaction of bacteriophage T4 and T7 single-stranded DNA-binding proteins with DNA. Phys Biol 6:025002.
5. Pant, K., R. L. Karpel, I. Rouzina, and M. C. Williams. 2005. Salt dependent binding of T4 gene 32 protein to single and double-stranded DNA: single molecule force spectroscopy measurements. J Mol Biol 349:317-330.
6. McCauley, M. J., J. Zimmerman, L. J. Maher, 3rd, and M. C. Williams. 2007. HMGB binding to DNA: single and double box motifs. J Mol Biol 374:993-1004.
7. Koch, S. J., A. Shundrovsky, B. C. Jantzen, and M. D. Wang. 2002. Probing protein-DNA interactions by unzipping a single DNA double helix. Biophys J 83:1098-1105.
8. Brun, F., J. J. Toulme, and C. Helene. 1975. Interactions of aromatic residues of proteins with nucleic acids. Fluorescence studies of the binding of oligopeptides containing tryptophan and tyrosine residues to polynucleotides. Biochemistry 14:558-563.
9. Dimicoli, J. L., and C. Helene. 1974. Interactions of aromatic residues of proteins with nucleic acids. I. Proton magnetic resonance studies of the binding of tryptophan-containing peptides to poly(adenylic acid) and deoxyribonucleic acid. Biochemistry 13:714-723.
10. Dimicoli, J. L., and C. Helene. 1974. Interactions of aromatic residues of proteins with nucleic acid. II. Proton magnetic resonance studies of the binding of tyramine and tyrosine-containing peptides to poly(adenylic acid) and deoxyribonucleic acid. Biochemistry 13:724-730.
11. Toulme, J. J., M. Charlier, and C. Helene. 1974. Specific recognition of single-stranded regions in ultraviolet-irradiated and heat-denatured DNA by tryptophan-containing peptides. Proc Natl Acad Sci U S A 71:3185-3188.
12. Toulme, F., C. Helene, R. P. Fuchs, and M. Daune. 1980. Binding of a tryptophan-containing peptide (lysyltryptophyllysine) to deoxyribonucleic acid modified by 2-(N-acetoxyacetylamino)fluorene. Biochemistry 19:870-875.
13. Sartorius, J., and H. J. Schneider. 1995. NMR-titrations with complexes between ds-DNA and indole derivatives including tryptophane containing peptides. FEBS Lett 374:387-392.
14. Behmoaras, T., J. J. Toulme, and C. Helene. 1981. Specific recognition of apurinic sites in DNA by a tryptophan-containing peptide. Proc Natl Acad Sci U S A 78:926-930.
15. McGhee, J. D., and P. H. von Hippel. 1974. Theoretical aspects of DNA-protein interactions: co-operative and non-co-operative binding of large ligands to a one-dimensional homogeneous lattice. J Mol Biol 86:469-489.
16. Bennink, M. L., O. D. Scharer, R. Kanaar, K. Sakata-Sogawa, J. M. Schins, J. S. Kanger, B. G. de Grooth, and J. Greve. 1999. Single-molecule manipulation of double-stranded DNA using optical tweezers: interaction studies of DNA with RecA and YOYO-1. Cytometry 36:200-208.

17. Marko, J. F., and E. D. Siggia. 1995. Stretching DNA. Macromolecules 28:8759-8770.
18. Vladescu, I. D., M. J. McCauley, M. E. Nunez, I. Rouzina, and M. C. Williams. 2007. Quantifying force-dependent and zero-force DNA intercalation by single-molecule stretching. Nat Methods 4:517-522.
19. Rouzina, I., and V. A. Bloomfield. 2001. Force-induced melting of the DNA double helix 1. Thermodynamic analysis. Biophys J 80:882-893.
20. Rouzina, I., and V. A. Bloomfield. 2001. Force-induced melting of the DNA double helix. 2. Effect of solution conditions. Biophys J 80:894-900.
21. Williams, M. C., J. R. Wenner, I. Rouzina, and V. A. Bloomfield. 2001. Effect of pH on the overstretching transition of double-stranded DNA: evidence of force-induced DNA melting. Biophys J 80:874-881.
22. Wenner, J. R., M. C. Williams, I. Rouzina, and V. A. Bloomfield. 2002. Salt dependence of the elasticity and overstretching transition of single DNA molecules. Biophys J 82:3160-3169.
23. Williams, M. C., J. R. Wenner, I. Rouzina, and V. A. Bloomfield. 2001. Entropy and heat capacity of DNA melting from temperature dependence of single molecule stretching. Biophys J 80:1932-1939.
24. Cheng, C. T., V. Lo, J. Chen, W. C. Chen, C. Y. Lin, H. C. Lin, C. H. Yang, and L. Sheh. 2001. Synthesis and DNA nicking studies of a novel cyclic peptide: cyclo[Lys-Trp-Lys-Ahx-]. Bioorg Med Chem 9:1493-1498.
25. Duker, N. J., and D. M. Hart. 1982. Cleavage of DNA at Apyrimidinic Sites by Lysyl-Tryptophyl-Alpha-Lysine. Biochemical and Biophysical Research Communications 105:1433-1439.
26. Toulme, J. J., and C. Helene. 1977. Specific recognition of single-stranded nucleic acids. Interaction of tryptophan-containing peptides with native, denatured, and ultraviolet-irradiated DNA. J Biol Chem 252:244-249.

Chapter 7

Conclusions and Outlook

Abstract

This chapter summarizes the main conclusions of the work presented in this thesis. An outlook on possible single molecule experiments which can be performed with combined optical tweezers and line scanning fluorescence microscopy is briefly discussed.

7.1
Final conclusions

Many biological processes in the living cell are the result of specific interactions between individual biomolecules, such as nucleic acids (DNA and RNA), proteins and lipids. In order to study these at the single molecule level an entire range of techniques have been developed or further refined, such as fluorescence microscopy (1), atomic force microscopy, optical tweezers and magnetic tweezers (2-4). In this thesis we set out to develop a method to study the interaction between dsDNA and protein molecules as a function of the force exerted on the dsDNA molecule. An essential requirement for this is to control the force and simultaneously probe the interaction(s) between the protein and dsDNA in a direct manner. To achieve this goal, we have integrated a force-measuring optical tweezers instrument with a line-scanning fluorescence microscope.

Force spectroscopy of the single dsDNA was performed by suspending end modified (biotin) dsDNA (λ-DNA) between two streptavidin-coated 2.6-μm polystyrene beads. One of the beads is attached to a glass micropipette and the second bead is optically trapped with optical tweezers. Force spectroscopy of the dsDNA was realized by moving the bead on the micropipette with respect to the trapped bead, so as to effectively stretch the molecule. Since the sample to be studied is a single dsDNA molecule decorated with fluorescently labeled proteins or dye molecules, and thus essentially linear, line-scanning fluorescence microscopy was chosen as the best option for imaging. Confocal fluorescence microscopy, although having a much better signal-to-noise ratio, was not chosen, because the instrument is technically much more complicated to construct and operate in this experimental context. Furthermore the amount of background fluorescence for these particular studies was expected to be low, since the suspended dsDNA molecule is held in the middle of a solution away from any surface that might add to background fluorescence. The other alternative is wide-field illumination, in which the entire field of view is excited. In comparison to this technique, which has the same signal-to-noise ratio, the use of a line-shaped beam offered more possibilities to illuminate particular parts of the dsDNA (5).

To test the performance of the combined optical tweezers and line-scanning fluorescence microscope instrument dsDNA was measured in the presence of YOYO-1. YOYO-1 is an intercalating fluorescent dye which is non-fluorescent when free in solution and is therefore a suitable test system. It is expected to change the mechanical properties as it binds to dsDNA and strongly emits fluorescence when bound (6-7).

Force spectroscopy experiments on dsDNA were performed with various concentrations of YO-1 and YOYO-1 dye present in the surrounding solutions. The data indicated clearly that the interaction of the mono-intercalating YO-1 molecules is very

distinct from that of bis-intercalating YOYO-1 molecules. The dsDNA-YO-1 complex was found to be in equilibrium while performing force spectroscopy in contrast to the case of YOYO-1. This observation was explained by assuming that YOYO-1 and YO-1 follow different binding mechanisms when interacting with the dsDNA. The oxazole yellow dye YO-1 binds to the dsDNA in one single step process where as YOYO-1 binding is thought to be a two-step process where the interaction of the positively charged linker of the YOYO-1 molecule with dsDNA is responsible for the observed non-equilibrium behavior in the dsDNA-YOYO-1 force spectroscopy data (7). Finally, we believe that the model presented here is broadly applicable to all mono- and bis-intercalating molecules.

Simultaneous force spectroscopy and fluorescence microscopy of the dsDNA-YOYO-1/YO-1 complex reveal that the interaction of YOYO-1/YO-1 (intercalating molecules) is force dependent (7). As the force on the dsDNA molecule increases, the total fluorescence intensity of the dsDNA/dye complexes increases in the presence of YOYO-1/YO-1. This study is the first visual proof of a long-standing assumption that the binding constant of intercalating molecules may be force dependent (6). Recently Vladescu *et al*. (8) described a method to determine the force dependent binding constant and the binding site size of the intercalating molecules. We have used this method to analyze our data and indeed observed that the binding constant of YOYO-1 and YO-1 increases exponentially as function of force acting on the dsDNA. The binding site size for YO-1 decreases as a function of force while the binding site size is constant for YOYO-1 as function of force. We believe that this result is due to the details of the mechanism of binding of YOYO-1 molecules to dsDNA, requiring additional research to elucidate the specifics of binding at the molecular level.

We further used our instrument to unravel the structure of the dsDNA in the overstretching region (9). The structure of the dsDNA in the overstretching region has been the subject of intense debate over the past few years. Simultaneous force spectroscopy and fluorescence (polarized) microscopy of the dsDNA-YOYO-1 complex at 10 nM YOYO-1 revealed that dsDNA undergoes melting (breaking of the hydrogen bonds) in the overstretching region rather than conversion from B to S DNA.

The results summarized in the previous sections show that we could indeed use the newly constructed instrument to study the interaction of dsDNA with fluorescent dye molecules in real time. As a next step towards studying protein-DNA interactions, we studied the interaction of Lys-Trp-Lys with dsDNA as a test system. It is assumed that the Lys-Trp-Lys motif in proteins facilitates the detection and anchoring of the proteins to denatured sites on dsDNA (10). Our single molecule experiments confirmed this assumption, - the interaction of Lys-Trp-Lys molecules with intact dsDNA is negligible whereas the interaction with denatured dsDNA was clearly observed. Finally we studied the

interaction of a fluorescently labeled EcoRI restriction enzyme with dsDNA. In this experiment it was possible to detect and localize one single EcoRI molecule bound to dsDNA.

In conclusion the combined optical tweezers and fluorescence microscope is able to perform high-resolution force spectroscopy data simultaneously with the recording of fluorescence images of single DNA-dye and DNA-protein complexes.

7.2 Outlook

In this section we discuss a selection of specific biophysical questions that the newly developed instrument could play a role in answering.

7.2.1 Chromatin

Within each human cell 2 meters of double-stranded DNA has to undergo an enormous compaction in length of a factor 10^5 to fit in the cell nucleus. The first step in this compaction process is the formation of nucleosomes. These complexes, ~ 11 nm in size are octamers of 4 different histone proteins (H2A, H2B, H3, H4) around which dsDNA is wrapping itself 1.7 times (146 bp) resulting in a 4-fold compaction (11). These nucleosome fibers are then in a next step further compacted into a higher order assembly known as the 30 nm fiber (12), resulting in further compaction. One fundamental question here is how protein molecules are able to access the compacted dsDNA for cellular processes such as transcription and replication. This means that the octamer has to undergo a certain conformational change to allow these processes that need access to the dsDNA template.

Nucleosome assembly and disassembly were studied using optical tweezers by Bennink *et al.* and Cui *et al.* (2, 13). Bennink *et al.* studied the force dependent assembly and unwrapping of nucleosomes. One fundamental question here is in which sequence histone molecules (H2A, H2B, H3, H4) actually bind to dsDNA and in what order the different histones are detached from the dsDNA? A related question is whether this process is cooperative?

One approach to shed some light on these questions is to study this system with the combined optical tweezers and line scanning fluorescence microscopy. Force spectroscopy will enable the detection of changes in the force upon association/dissociation of histones to the dsDNA, where as fluorescence microscopy will enable the detection and

precise spatial localization of the fluorescently labeled histone molecules on the dsDNA. This experiment will shade some light on the nature of the chromatin assembly and disassembly. Furthermore by using multiple fluorophores for the different histone molecules, one can even determine the sequence in which the different histone molecules are attaching and detaching from the dsDNA as a function of force. Such experiments will provide a more detailed insight into the interactions of dsDNA and histone proteins.

7.2.2
dsDNA-protein interaction

The pathway that a protein follows to detect its specific binding site on dsDNA is still enigmatic and is at the centre of dsDNA-protein interactions. Different mechanisms, such as sliding or hopping, have been suggested. Fundamental questions as these can be addressed using the new instrument. For example, with the help of optical tweezers one can precisely control the force acting on the dsDNA molecule and hence the length of the dsDNA. To observe the hopping of the protein molecules one has to hold the dsDNA with forces below 10 pN, and to observe the sliding nature one has to pull the dsDNA at least to its contour length. Furthermore one can study the dsDNA-protein interaction as a function of force. The structure of the overstretched dsDNA has been revealed to be a melted DNA (9, 14), suggesting further studies of the interaction of protein molecules with melted dsDNA to shed some light on the functional aspects of this structure of the dsDNA in DNA-protein interactions.

Another possible improvement in relation to this application would be the introduction of fluorescence spectroscopy into the existing instrument. We will be able to detect minute changes in the emission spectra of the protein/ligands interacting with dsDNA as function of force. These experiments can provide molecular details of these interactions.

In order to achieve a higher throughput in dsDNA-protein interaction experiments, it is advantageous to use a dual trap system (15) instead of a single trap and the glass micropipette. The use of the micropipette has a number of drawbacks such as being fragile and having other small particles attaching to it. The second improvement to increase the number of experiments per unit time would be to use a multichannel flowcell. This will allow to change the buffer at very short time scales (less than few seconds), which as a result of this will enable new types of experiments (16).

7.2.3
Development of new drugs

Drug molecules used in cancer chemotherapy interact with the dsDNA via intercalation (17). Intercalation of the drug molecules affects the interaction of protein molecules with the dsDNA and hence stops many cellular processes including dsDNA replication (18).

In this study the interaction between oxazole yellow dyes YO-1 and YOYO-1 and dsDNA have been studied, and at higher intensities it has been shown that the presence of the intercalating dye molecule can cause the dsDNA to locally photocleave. This observation opens a new way to think about developing anti-cancer drugs. Instead of having molecules that only intercalate and consequently interfere with the binding of proteins, it might be possible to use photoactivatable intercalating molecules, which not only will perturb the action of proteins by intercalation, but which might also photocleave the dsDNA as it is illuminated.

7.3
References

1. Roy, R., S. Hohng, and T. Ha. 2008. A practical guide to single-molecule FRET. Nat Methods 5:507-516.
2. Bennink, M. L., S. H. Leuba, G. H. Leno, J. Zlatanova, B. G. de Grooth, and J. Greve. 2001. Unfolding individual nucleosomes by stretching single chromatin fibers with optical tweezers. Nat Struct Biol 8:606-610.
3. Neuman, K. C., and A. Nagy. 2008. Single-molecule force spectroscopy: optical tweezers, magnetic tweezers and atomic force microscopy. Nat Methods 5:491-505.
4. Bennink, M. L., D. N. Nikova, K. O. van der Werf, and J. Greve. 2003. Dynamic imaging of single DNA-protein interactions using atomic force microscopy. Anal Chim Acta 479:3-15.
5. Sandison, D. R., and W. W. Webb. 1994. Background Rejection and Signal-to-Noise Optimization in Confocal and Alternative Fluorescence Microscopes. Appl Optics 33:603-615.
6. Bennink, M. L., O. D. Scharer, R. Kanaar, K. Sakata-Sogawa, J. M. Schins, J. S. Kanger, B. G. de Grooth, and J. Greve. 1999. Single-molecule manipulation of double-stranded DNA using optical tweezers: Interaction studies of DNA with RecA and YOYO-1. Cytometry 36:200-208.
7. Murade, C. U., V. Subramaniam, C. Otto, and M. L. Bennink. 2009. Interaction of Oxazole Yellow Dyes with DNA Studied with Hybrid Optical Tweezers and Fluorescence Microscopy. Biophys J 97:835-843.
8. Vladescu, I. D., M. J. McCauley, M. E. Nunez, I. Rouzina, and M. C. Williams. 2007. Quantifying force-dependent and zero-force DNA intercalation by single-molecule stretching. Nature Methods 4:517-522.
9. Murade, C. U., V. Subramaniam, C. Otto, and M. L. Bennink. 2010. Force spectroscopy and fluorescence microscopy of dsDNA-YOYO-1 complexes: implications for the structure of dsDNA in the overstretching region. Nucl. Acids Res.:gkq034.
10. Toulme, J. J., M. Charlier, and C. Helene. 1974. Specific recognition of single-stranded regions in ultraviolet-irradiated and heat-denatured DNA by tryptophan-containing peptides. Proc Natl Acad Sci U S A 71:3185-3188.
11. Kornberg, R. D., and Y. Lorch. 1999. Twenty-five years of the nucleosome, fundamental particle of the eukaryote chromosome. Cell 98:285-294.
12. Carruthers, L. M., and J. C. Hansen. 2000. The core histone N termini function independently of linker histones during chromatin condensation. J Biol Chem 275:37285-37290.
13. Cui, Y., and C. Bustamante. 2000. Pulling a single chromatin fiber reveals the forces that maintain its higher-order structure. Proc Natl Acad Sci U S A 97:127-132.
14. van Mameren, J., P. Gross, G. Farge, P. Hooijman, M. Modesti, M. Falkenberg, G. J. Wuite, and E. J. Peterman. 2009. Unraveling the structure of DNA during overstretching by using multicolor, single-molecule fluorescence imaging. Proc Natl Acad Sci U S A 106:18231-18236.
15. Moffitt, J. R., Y. R. Chemla, D. Izhaky, and C. Bustamante. 2006. Differential detection of dual traps improves the spatial resolution of optical tweezers. Proc Natl Acad Sci U S A 103:9006-9011.
16. van Mameren, J., E. J. Peterman, and G. J. Wuite. 2008. See me, feel me: methods to concurrently visualize and manipulate single DNA molecules and associated proteins. Nucleic Acids Res 36:4381-4389.

17. Hurley, L. H. 2002. DNA and its associated processes as targets for cancer therapy. Nat Rev Cancer 2:188-200.
18. Xu, C., M. Y. Losytskyy, V. B. Kovalska, D. V. Kryvorotenko, S. M. Yarmoluk, S. McClelland, and P. R. Bianco. 2007. Novel, monomeric cyanine dyes as reporters for DNA helicase activity. J Fluoresc 17:671-685.

Acknowledgements

I would like to express my sincere gratitude to all who have helped and supported me directly or indirectly to achieve this milestone in my life, in these most widely read pages of the thesis.

First and foremost, I would like to thank Prof. Dr. Vinod Subramaniam for giving me an opportunity to work in the BPE group. I would also like to thank him for all the support and the guidance and the strength he has provided me over last 5 years. I know, you will like to have this part as short as possible, so in short “jahapana tussi great ho”.

I am deeply grateful to my daily supervisor Dr. ir. Martin Bennink, I have learned so many things from you over the past 5 years (still learning). Thanks for keeping faith in me, and supporting me. I still remember the long discussions we had over different topics such as, our instrument then came the YOYO and YO experiments and the exciting results. You have really helped me not just in my research but also helped me how to put it in words. I really appreciate your keen observation.

I thank Dr. Cees Otto, for his guidance and the brainstorming discussion about experiments. You always put in energy in students and ask them to think out of box. I have learned how to look at the results critically and how to get interesting science out of ones results. Thank you Cees for supporting me for these long 5 years. I know that we have not yet finished, we need to finish some more manuscripts.

Dr. G. R. Kulkarni, Dr. Arum Banpurkar and Dr. Sudhir Husale were my first mentors who helped me in first place to start this journey. Without your help and guidance I could not have started this journey. Thank you very much. I had great time at University of Pune under you guidance.

At BPE group we have great team of technical staff; they helped and supported me over the last 4 years. I would like thank them all, especially to Kirsten for making my life easy in the chemical lab, Kees for all the help you provided while building hardware for my instrument, and it was really disappointing for me not having an opportunity to work with you on full-fledged project. Aufried you are too good at optics, and that’s what I learned from you, thank you very much for all that help and support.

Oh my god how I can forget Sylvia, I think she is the one who brings in huge energy and enthusiasm in the group, I would like to thank you Silvia for your great help in all kind of paper work, and cheering me up when ever there were problems.

I would like to take this opportunity to thank Prof. Dr. Frieder Mugele, who has supported me for last one and half year, its great opportunity to work with you Frieder. Working in PCF has helped me immensely on scientific and personal grounds. Thank you very much.

While working in the BPE group I was supported by many group members. I would like to take this opportunity to thank them all Mireille, Hans, Ine, Frans, Shashank, Marieke, Remco, Chien-Ching, Maryana, Christian Blum, Malte, Gabriel, Roy, Srirang, Kiran, Babu, Vinay, Raja, Bart, Jitin, Gabriel, Jurgen, Yanina and finally to my brother Thomaz, thank you for all your help.

After finishing my PhD work I moved to PCF group, where I received warm welcome from Dirk, Michel, Annelies, Mariska, Sissi, Omkar, Burak, Hao, Tarun, Dileep, Dieter, Gor, Jolet, Rielle, Huub, Joost, Daniel, Daniel Ebeling, Jung, Willam, these all people have helped me immensely. Thank you all for your help and openness.

My self and Meenakshi were lucky to have great group of Indian friends in Enschede, Supi-Anandita-Samhita, Jitu-Lavanya, Srivatsa, Sandeep-Jalja, Karina, Shrihari-Laxmi-Pujita, Dhaval-Hinal, Gigar-Phalguni, Mayur- Shradha, Ram-Veda, Ganesh, Ram (gaya Ram), Santoash, Andy, Anuragh, Ashavin. Especially I would like to thank Ravi-Madhavi (Girija) for their love and affection. Sameer-Uttara, Nilesh-Shewta you were great company. Vijay-Sangeeta thanks for your support and company. I would like to take this opportunity to thank Digu-Aabha for their great company and being my paranymph (Digu). Finally I would like to thank Pramodji-Vishakha for their everlasting support to both of us. They have always been by my side in all situations. And how can we forget Vibhor, he brought great joy in our lives with his smile and naughty things.

Last but not least, I would like to thank my family members Kaka, kaku and my sister Nama for their constant support and encouragement. I would like to thank Meenakshi for her constant support; this journey was not possible without your everlasting support and love. I am greatly indebted to my parents, Aai (Saptaphula) and Baba (Uttamrao) for their unconditional support and love. I dedicate my thesis to Aai, Baba, Meenakshi and my teachers who taught me throughout my academic career.

Chandrashekhar Uttamrao Murade
Enschede, June, 2010.

About the author

Chandrashekhar Uttamrao Murade was born on August 29th, 1980 in Hiwara Murade, India. After completing high school study, he received Bachelor of Science degree from Fergusson college, University of Pune in 2001. In the same year he joined Department of Physics at University of Pune to obtain Master of Science degree (Physics). He was awarded Master of Science degree in 2003 with first class. Later on he worked at Biophysical group at University of Pune under the supervision of Dr. G. R. Kulkarni and Dr. Arun Banpurkar.

In December 2004 he joined the Biophysical Engineering Group at the University of Twente, The Netherlands as PhD candidate under the supervision of Prof. Dr. V. Subramaniam, Dr. C. Otto and Dr. ir. M. L. Bennink on the topic probing dynamics of chromatin structure using force and fluorescence spectroscopy. This thesis is focused on the development of combined optical tweezers and line scanning fluorescence microscopy to obtain insights into DNA protein interactions at single molecular level. Results presented in this thesis also highlight the interaction of intercalating molecules with the DNA studied using combined optical tweezers and line scanning fluorescence microscopy.